CAPITAL UNIVERSITY OF SCIENCE AND TECHNOLOGY, ISLAMABAD

Range Extension of Subsonic Unpowered Gliding Vehicle

by

Ahmad Mahmood

A dissertation submitted in partial fulfillment for the degree of Doctor of Philosophy

in the

Faculty of Engineering
Department of Electrical Engineering

2024

Range Extension of Subsonic Unpowered Gliding Vehicle

By

Ahmad Mahmood

(DEE173001)

Dr. Ilker Ustoglu, Professor

Istanbul Technical University, Turkiye

(Foreign Evaluator 1)

Dr. Rini Akmeliawati, Associate Professor

The University of Adelaide, Australia

(Foreign Evaluator 2)

Dr. Fazal ur Rehman

(Dissertation Supervisor)

Dr. Noor Muhammad Khan

(Head, Department of Electrical Engineering)

Dr. Imtiaz Ahmad Taj

(Dean, Faculty of Engineering)

DEPARTMENT OF ELECTRICAL ENGINEERING

CAPITAL UNIVERSITY OF SCIENCE AND TECHNOLOGY

ISLAMABAD

2024

Dedicated to Mamma, Baba, Partner (HNA), and my children Saira, Yousaf, Hussain

CAPITAL UNIVERSITY OF SCIENCE & TECHNOLOGY
ISLAMABAD
Expressway, Kahuta Road, Zone-V, Islamabad
Phone:+92-51-111-555-666 Fax: +92-51-4486705
Email: info@cust.edu.pk Website: https://www.cust.edu.pk

CERTIFICATE OF APPROVAL

This is to certify that the research work presented in the dissertation, entitled "**Range Extension of Subsonic Unpowered Gliding Vehicle**" was conducted under the supervision of **Dr. Fazal ur Rehman**. No part of this dissertation has been submitted anywhere else for any other degree. This dissertation is submitted to the **Department of Electrical Engineering, Capital University of Science and Technology** in partial fulfillment of the requirements for the degree of Doctor in Philosophy in the field of **Electrical Engineering.** The open defence of the dissertation was conducted on **January 24, 2024**

Student Name : Ahmad Mahmood (DEE173001)

The Examination Committee unanimously agrees to award PhD degree in the mentioned field.

Examination Committee :

(a) External Examiner 1: Dr. Nadeem Shaukat
Professor
PIEAS, Islamabad

(b) External Examiner 2: Dr. Iftikhar Ahmed Rana
Associate Professor
SEECS, NUST, Islamabad

(c) Internal Examiner : Dr. Noor Muhammad Khan
Professor
CUST, Islamabad

Supervisor Name : Dr. Fazal ur Rehman
Professor
CUST, Islamabad

Name of HoD : Dr. Noor Muhammad Khan
Professor
CUST, Islamabad

Name of Dean : Dr. Imtiaz Ahmad Taj
Professor
CUST, Islamabad

AUTHOR'S DECLARATION

I, **Ahmad Mahmood** (Registration No. **DEE173001**), hereby state that my dissertation titled, "**Range Extension of Subsonic Unpowered Gliding Vehicle**" is my own work and has not been submitted previously by me for taking any degree from Capital University of Science and Technology, Islamabad or anywhere else in the country/ world.

At any time, if my statement is found to be incorrect even after my graduation, the University has the right to withdraw my PhD Degree.

(Ahmad Mahmood)

Dated: 24 January, 2024

Registration No : DEE173001

PLAGIARISM UNDERTAKING

I solemnly declare that research work presented in the dissertation titled "**Range Extension of Subsonic Unpowered Gliding Vehicle**" is solely my research work with no significant contribution from any other person. Small contribution/ help wherever taken has been duly acknowledged and that complete dissertation has been written by me.

I understand the zero-tolerance policy of the HEC and Capital University of Science and Technology towards plagiarism. Therefore, I as an author of the above titled dissertation declare that no portion of my dissertation has been plagiarized and any material used as reference is properly referred/ cited.

I undertake that if I am found guilty of any formal plagiarism in the above titled dissertation even after award of PhD Degree, the University reserves the right to withdraw/ revoke my PhD degree and that HEC and the University have the right to publish my name on the HEC/ University Website on which names of students are placed who submitted plagiarized dissertation.

(**Ahmad Mahmood**)

Dated: 24 January, 2024

Registration No : DEE173001

List of Publications

It is certified that following publication(s) have been made out of the research work that has been carried out for this dissertation:-

1. **Ahmad Mahmood**, Fazal ur Rehman, and Aamer Iqbal Bhatti. "Trajectory Optimization of a Subsonic Unpowered Gliding Vehicle Using Control Vector Parameterization." *Drones* 6.11 (2022): 360, doi.org/10.3390/drones6110360

2. **Ahmad Mahmood**, Fazal ur Rehman, and Aamer Iqbal Bhatti. "Range Guidance for Subsonic Unpowered Gliding Vehicle using Integral Action based Sliding Mode Control, International Journal of Dynamics and Control (2023): 1-11, doi.org/10.1007/s40435-023-01229-y

(Ahmad Mahmood)
Registration No: DEE173001

Acknowledgement

First of all, I would like to express my humble gratitude to ALLAH Almighty, The Most Gracious, The Dispenser of Grace, for His blessings and for giving me the strength to accomplish this endeavor, and providing people who are always standing in my support. He blessed me with the knowledge, courage, and ability to complete my research work and dissertation. This whole endeavor would not have been possible without the immeasurable blessings of the Almighty ALLAH. He has helped me through so many rough and tough times that I have lost count. I can only express my acceptance that He is my Creator, and I am His creation. Only He knows what is good and bad for me. Thanks, and regards to the Holy Prophet MUHAMMAD (P.B.U.H), the last messenger of ALLAH, whose whole life is the perfect model for all human beings and Whose teachings are the source of guidance in all disciplines of practical life, that makes me focused and humble.

I am indebted to all my teachers whose teachings have brought me to this stage. Certainly, it's a pleasant obligation to thank my supervisor Prof. Dr. Fazal ur Rehman for his valuable guidance, strong encouragement, and kind support towards my study and research. I have not only learned from his insight, and deep technical knowledge, but a lot of things from him as a person as well. It has been a real honor for me to work under his supervision and to attend his lectures and talks. I am much obliged to my co-supervisor, Prof. Dr. Amer Iqbal Bhatti for his patience, motivation, enthusiasm, and immense knowledge, which paved a way for me to explore my abilities and skills. Without his support, it would not have been possible to complete my Ph.D. His cheerful and brotherly approach was a source of inspiration for me during the frustrating periods of my Ph.D. You have shown me the path of research addiction, and where I am today is mainly because of you.

I am also highly obliged to Dr. Bilal Ahmed Siddique, Dr. Mateen Qazi, and Dr. Imran Mir for providing me with the necessary background knowledge of the aerodynamic domain. I would especially like to thank my childhood friends Zahid, Shahroz, Hasan, Salman, Luqman, and Ammar whose precious company

always helped me out of depression during dissertation. I am also indebted to my classmates Aamir Khalil, Saad Alvi, and Rana Fazail for listening to my heart. I would also like to thank the entire CASPR group for their continuous and timely support, valuable suggestions, and comments. In particular, I acknowledge the suggestions of Zohaib Latif, Faheem Manzoor, Faheem Gulzar, Abrar Hashmi, Sidra, and Hafiz Yasir Naeem.

I would like to thank Higher Education Commission (HEC) Pakistan for financial support to complete my Ph.D. Finally, I would like to give special thanks to my uncle Abdul Hameed for accommodating me during my Ph.D and I will always remember the amazing gathering of my uncle Shehzad.

(Ahmad Mahmood)

Abstract

Unpowered gliding vehicles perform gliding flight with a limited glide range by using mechanically stored energy provided by a platform such as a drone or aircraft. Additionally, unpowered gliding vehicles are distinguished by their intended use, fuselage, geometry of aerodynamic surfaces, and Mach number. For this study, a Subsonic Unpowered Gliding Vehicle (SUGV) is selected to maximize the gliding range. When the SUGV is released from the carrier platform after obtaining the dispersion points, it starts gliding with a loitering state due to the flight transition, and after covering some range the gliding vehicle due to its inherent stability starts a steady gliding flight. By choosing an appropriate optimization method, the range is maximized with a damped and stable gliding flight. It is worth noting that the range maximization problem is also an endurance problem, and the final time in this optimal problem is also free. Therefore, to solve this sort of problem, a time-scaling approach has already been proposed and effectively implemented, however, the employment of this approach introduces an extra variable handled as the optimal control input or optimal variable, increasing the complexity of the dynamic optimization problem.

To address this issue, the halting constraint idea has been updated for the maximum stoppable time. Then, to achieve damped and steady gliding flight, a non-uniform exponential spacing-based Control Vector Parameterization (CVP) is proposed, and this CVP has close spacing at the beginning of the time vector and large spacing at the end of the time vector. To test the effectiveness of the proposed CVP with damped and steady gliding flight, it is compared with uncontrolled flight (maximum elevator deflection) and classical uniform CVP. While longitudinal dynamics of SUGV are considered and three different cases depending on the number of nodes are also evaluated to obtain the maximum gliding range. Simulations show that the SUGV successfully achieves a range of 856m with the proposed non-uniform CVP by handling damped and stable gliding flight. Furthermore, the proposed CVP approach demonstrates superiority over GPOPS based

on the hp-adaptive Gaussian quadrature collocation approach with a horizontal range of 330 m.

In the second major part of this study, a range guidance and control methodology is developed to attain the intended range of SUGV. The proposed range guidance, on the other hand, is dependent on the measured angle of attack and dispersion points. Terminal error due to non-smooth range guidance command and saturation effect is measured, and to reduce these problems, an Integral Action Sliding Mode Control (IA SMC) is proposed. SMC has a drawback of chattering, and to mitigate this problem, a atan based strong exponential reaching law is employed. To observe the terminal error, smooth guidance command, and less saturation, a comparison is conducted between the proposed control scheme and the PID SMC scheme. Range guidance and control is also validated for two cases 120 km and 125 km and quantitative analysis in the form of root mean square error, the energy consumption of range guidance law, and terminal error is performed to assess the effectiveness of the IA SMC for both cases, and the IA SMC outperformed the PID SMC with a terminal error of 0.29 m.

Contents

List of Figures

List of Tables

Abbreviations

BCI	Boundary Control Iteration
CV	Control Vector
CVP	Control Vector Parametrization
CVI	Control Vector Iteration
DCM	Direction Cosine Matrix
DoF	Degree of Freedom
GR	Glide Ratio
IVP	Initial Value Problem
IA	Integral Action
ISV	Integral Square Value
KKT	Karush-Kuhn-Tucker
LF	Load Factor
NLP	Non Linear Programming
PMP	Pontryagin Minimum Principle
PCHIP	Piecewise Cubic Hermite Interpolating Polynomial
PID	Proportional Integral Derivative
QP	Quadratic Programming
RMSE	Root Mean Square Value
SUGV	Subsonic Unpowered Gliding Vehicle
SQP	Sequential Quadratic Programming
SMC	Sliding Mode Control
TPBVP	Two Point Value Boundary Problem
UGV	Unpowered Gliding Vehicle

Symbols

α^*, γ^*	Angle of attack and glide path angle at $(L/D)_{max}$ ratio
X_e, Y_e, Z_e	Inertial axis system
X_b, Y_b, Z_b	Body axis system
X_s, Y_s, Z_s	Stability axis system
X_w, Y_w, Z_w	Wind axis system
V, β, α	Airspeed, side slip angle and angle of attack along X_w-axis, Y_w-axis and Z_w-axis
P, Q, R	Roll, pitch, yaw rates along x-axis, y-axis and z-axis
ϕ, θ, ψ	Roll,pitch and yaw angles along x-axis, y-axis and z-axis
L, Y, D	Drag, side and lift forces along x-axis, y-axis and z-axis
l, M, N	Roll,pitch and yaw moments along x-axis, y-axis and z-axis
F_x^{gw}, F_y^{gw}, F_z^{gw}	gravitational force components along x-axis, y-axis and z-axis
ρ	Air density
C_{L_α}, C_{M_α}	Lift and pitching moment coefficients w.r.t angle of attack
C_{L_Q}, C_{M_Q}	Lift and pitching moment coefficients w.r.t pitch rate
$C_{L_{\delta_e}}$, $C_{D_{\delta_e}}$ $C_{M_{\delta_e}}$	Lift, drag and pitching elevator coefficients w.r.t elevator deflection
$\mathcal{J}$	Cost function
$\mathcal{L}$	Lagrange function
λ	Co-states
$\mathcal{H}$	Hamiltonian function
$\mathfrak{W}$	Adapting rate
$\mathfrak{B}$	Time scaling parameter
t_0	Initial time

t_m	Maximum stoppable time
S_m	Stopping manifold
t_s	Stopping time
δ_e	Elevator deflection
d_e	Subinterval size for uniform subintervals
μ_o	Lower bound of exponential curve
t_0	Initial time
Υ	Interval size of logarithmic vector
ℓ	Logarithmic vector
T_{exp}	Exponential time vector
χ	Exponential spacing factor for non-uniform CVP
$\mathcal{D}_j$	Derivative of nodal control variable
C^k	Step size in QP subproblem
d^k	Search direction in QP subproblem
H_k	Hessian of the Lagrangian
u_{eq}	Equivalent control for SMC
u_{dis}	Discontinue control for SMC
S_s	Sliding surface
$\eth$	Glide ratio between dispersion points and range
θ_c	Range guidance command pitch angle
R_g	Intended range
∂_{θ_c}	Filtered command of integral action
$S_{S_{IA}}$	Integral action based sliding surface
$\tilde{C}_1$, $\tilde{C}_2$	Designing parameter of integral action based sliding surface
$\tilde{U}$	Range guidance law
ϱ	Quadratic Lyapunov candidate function
Λ_1, Λ_2, Λ_3	Designing parameters of integral action SMC
$\tilde{U}_{ISV}$	Integral square value of range guidance law for energy consumption

Chapter 1

Introduction

1.1 Background

Such an air vehicle capable of flying by using the dynamic reaction of the wind against its lifting surfaces as wings and tails and whose flight does not depend on a power source such as an engine or booster is known as an Unpowered Gliding Vehicle (UGV) [1].

With improvements in aerial technology, air vehicles have been developed as powered (active) or unpowered (passive) [2, 3]. Active flight is a very expensive concept to move a unit of mass per unit of distance, although it requires a much higher power output than passive flight [4]. A UGV only performs mechanical work in the form of actuation to produce lift force L greater than or equal to weight and drag force D less than airspeed to keep the wings down on a horizontal plane [5, 6].

Since UGVs do not generate any mechanical energy (potential plus kinetic) but they use stored energy which is stored by the carrier platform. Therefore, the performance of a UGV depends on the mechanically stored energy and this performance can be studied through the relationship between L and D forces [7, 8].

The Glide Ratio (GR) is one of the most important parameters for the unpowered flight which helps to determine how much the UGV descends for forward motion.

The GR is the ratio of lift to drag forces and these forces are directly proportional to their respective coefficients through the proportionality constant.

The effective GR is like that.

$$GR = \frac{L}{D} = \frac{u}{w} = \frac{1}{\tan\gamma} \tag{1.1}$$

where u and w are forward speed and downward speed. However, this relationship is limited to wing-level steady flight [9], and this condition is not necessarily present during flight. GR is also characterized in terms of speed ratio, as the ratio of the forward speed u to the downward speed w. It is alternatively written as $(1/\tan\gamma)$, where γ is the glide angle. The GR relationship for an unpowered gliding vehicle can be assessed from Fig.1.1.

The transition between level flight, gliding flight, and parachuting flight (flight for terminal guidance) is conventionally taken to occur at the 45 deg of γ [10], and, nevertheless, L and D contribute equally to support the weight of the air vehicle throughout the flight.

The UGV performs gliding flight if $L/D > 1$, and parachute flight if $L/D < 1$. While the parachute condition only applies when the target is to be neutralized with maximum damage, Fig.1.1 visualizes the concept of gliding and parachuting. When the equilibrium speed V approaches, the glide path flattens until the vertical force F equals the W.

The resulting force F may be decomposed into D rearward along the glide path and L perpendicular to it. In parachuting, the area supporting the weight is small, the lift is small relative to the combined drag of the fuselage. Therefore, the overall GR is lower, resulting in a correspondingly faster glide path.

The Load Factor (LF), which guarantees the maintenance of the wing-level steady flight during gliding flight, is another crucial parameter. It is a ratio between the L and the weight W. It is worth noting that during cruise flight, LF has a value of one and is related as

$$LF = \frac{L}{W} \tag{1.2}$$

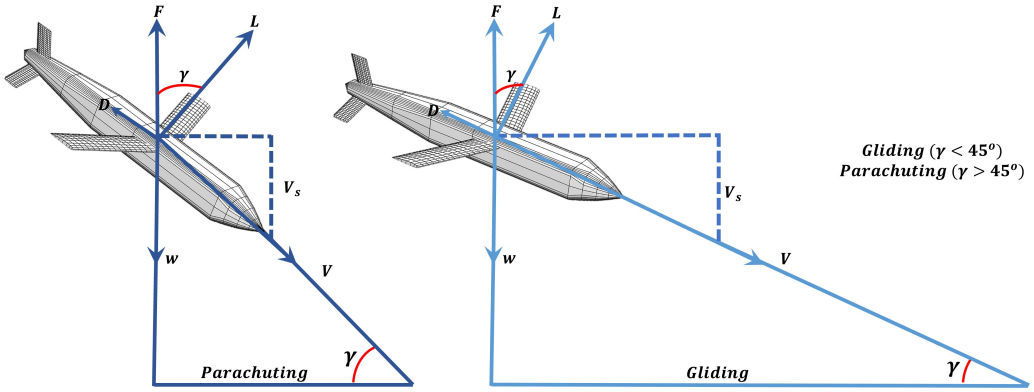

FIGURE 1.1: Glide ratio and Glide angle

This relation, nevertheless, is not applicable during gliding flight to maintain the wing-level steady flight. From Fig. 1.1, it can be inferred that to achieve the wing-level steady flight, the resultant force F should be equal to the weight, and it is demonstrated as

$$LF = \frac{F}{W} = \frac{\sqrt{L^2 + D^2}}{W} \tag{1.3}$$

While from LF, the flight variability can be figured during gliding flight as

- Pull up condition if $LF > 1$
- Wing-level steady gliding flight if $LF = 1$
- Falling condition for unpowered flight if $LF < 1$

1.2 Types of Unpowered Gliding Vehicle

Operational deployment of UGVs is always challenging due to their endurance and range limitations. In an effort to overcome the limitations of range, aerodynamic efficiency, geometric configurations are commonly adopted. UGVs are classified mostly on the basis of geometric configurations (Morphing wings [11, 12], fixed wings [13, 14], position and size of wings and tail), maneuverability, ability to

withstand compressibility effects and heating flux. Compressibility effects cause dynamic pressures that affect airspeed reduction and unstable gliding flight [15].

When the dynamic stress is divided by the modulus of elasticity the resulting quantity is a dimensionless quantity equal to one-half of the square of the free-stream Mach number [15]. Simply put, the ratio between the current speed of a body and the speed of light is the Mach number. So UGVs can be easily characterized on the basis of Mach number, airspeed regime as listed in the Table. 1.1.

Re-entry gliding vehicle, Re-useable launch vehicle and Inter Continental Ballistic missile (ICBM) are example of hypersonic UGVs. These vehicles have a high spectrum of angle of attack α , for example, 20 deg to 45 deg [1, 16]. Most of these UGVs are designed for routine operations without a thrust source.

Engine failure in aircraft or fighter jets is another situation that can force to perform gliding in subsonic regime with the spectrum of α with 10 deg to 15 deg [17, 18]. Joint direct attack munition [19], Joint stand-off weapon [20], gun launched artillery [21], are also type of Subsonic UGV (SUGV). Ground launched gliders such as Small Diameter Gliding Bomb [22] utilizes booster to achieve specific altitude, after gaining the predefined altitude, booster is separated and starts gliding.

TABLE 1.1: Airspeed regime

Regime	Mach	Speed (ms^{-1})
Subsonic	<0.8	<270
Transonic	0.8-1.2	270-410
Supersonic	1.2-5.0	410-1700
Hypersonic	>5.0	>1700

These days, a wing adaptation kit or range extension kit is mounted on the general-purpose bomb (MK-series) to modify the bomb into a glider [23]. The main desired objectives of SUGV are 'long range' and 'accuracy' and these objectives relate to trajectory optimization and terminal guidance for accuracy.

1.3 Motivation

Note that the SUGV is unpowered and therefore has a short stand-off distance (horizontal range). Some other factors on which the stand-off distance reduction depends are the geometric configuration of the fuselage, headwind, descent rate, and dispersion points (initial altitude, initial airspeed, and initial angle of attack). Glide ratio, glide path angle, and mechanically stored energy can be manipulated in an optimal way to overcome these factors and enhance the stand-off distance of SUGV. Endurance (time of flight) is another aspect that affects maximizing stand-off distance, and dealing with endurance means dealing with glide ratio, in other words, if the glide ratio is high, then SUGV will fly further, cover more stand-off distance, and require long endurance.

While physical constraints such as heating rate and dynamic pressure are not necessary for SUGV to achieve optimum stand-off distance as these constraints avoid structural damage which rarely occurs. Therefore, some motivations for enhancing the stand-off distance of SUGV are itemized below.

- Geometric configuration: the geometric configuration of the SUGV is also responsible for enhancing the stand-off distance through proper selection of the SUGV geometry resulting in reduced drag. By reducing the drag, the glide ratio increased which ensures the enhancement in the stand-off distance. Aspect ratio, wing sweep angle, wing area, fuselage shape, control surface placement, and payload integration are major parameters that have the ability to manipulate the stand-off distance of SUGV. A higher wing aspect ratio, meaning longer and narrower wings, can provide a higher lift-to-drag ratio (L/D) and result in a more efficient glide, thereby extending the stand-off distance and reducing the induced drag. A very common example of payload integration into the fuselage of a SUGV is the Joint stand-off weapon. Payload integration affects static and dynamic stability as well as the center of gravity, which, in turn, affects stand-off distance performance.

- Mechanically stored energy: the SUGV derives mechanical energy from its carrier platform in the form of kinetic and potential energy. The initial launch velocity determines the kinetic energy of the SUGV. A higher initial speed can increase the stand-off distance, but the choice of launch platform can limit this requirement. Managing stored energy, including initial altitude and velocity, is key to achieving maximum stand-off distance. This involves optimizing the tradeoff between stand-off distance and stored energy through the glide ratio [24, 25]

- Steady wing level glide: in this gliding condition, the force resulting from lift and drag is equal to the weight of the SUGV. This means that the SUGV performs a gliding flight in steady descent at a constant glide angle. By achieving and maintaining this condition, the stand-off distance performance of the SUGV can be enhanced.

- Stability: The stability of the SUGV also plays an important role in maintaining wing level steady glide flight and can be maintained by the pitching moment. The relationship between the pitching moment and the angle of attack ensures that the SUGV is stable and controllable during its gliding flight. This includes shaping the wing and tail surfaces as well as control surfaces such as elevators to provide stability and control. To achieve fast stability, there must be a steeper slope between the pitching moment and the angle of attack [15]. If the SUGV has fast stability, then after launching from the carrier platform, it will stabilize itself more quickly, and eventually achieve the wing-level glide flight to increase the stand-off distance.

1.4 Research Objectives

This research is carried out to investigate the damped and steady gliding flight, and to increase the stand-off distance (maximize the range) of the SUGV. Therefore, the following points are highlighted on the main objectives of this research work.

- To avoid the time scaling approach, modified the optimal problem by specifying the height as a stopping constraint for maximum stoppable time.
- Develop a non-uniform control vector parameterization approach for the optimization problem.
- Develop a range guidance scheme dependant on dispersion points and angle of attack.
- Design an integral action based sliding mode controller to track the range guidance command.

1.5 Thesis Contributions

The main contributions of this thesis are the glide range maximization of SUGV and the development of a nonlinear closed-loop control system based on range guidance for SUGV. The following individual contributions lead to these goals.

1.5.1 Open Loop Range Maximization

(a) The optimization problem is formulated with height as the stopping constraint for the stoppable time.

(b) The maximum range is yielded by achieving damped and steady gliding flight through non-uniform control vector parameterization.

(c) A comparison of non-uniform CVP between uncontrolled flight and uniform CVP has been investigated.

(d) Finally, the non-uniform CVP is compared with the hp-adaptive Gaussian quadrature collocation based GPOPS tool.

The above contributions resulted in the publication of the following journal:

- **Mahmood A**, Rehman F.u and Bhatti A.I. "Trajectory optimization of a subsonic unpowered gliding vehicle using control vector parameterization". Drones 2022; 6(11): 360. doi.org/10.3390/drones6110360

1.5.2 Range Guidance Scheme

(a) A range guidance scheme based on dispersion points (dropping parameters from an aircraft or fixed-wing UAV) and angle of attack is proposed to attain the intended range.

(b) To mitigate the saturation effects and produce a smooth range guidance command, an Integral Action based Sliding Mode Control (IA SMC) approach is employed for the nonlinear SUGV.

(c) To reduce the chattering effect in SMC, a atan based strong exponential reaching law is implemented. Then, a comparison between PID-based SMC (PID SMC) and (IA SMC) has been simulated and studied.

The contributions mentioned above have been collected in the following journal publication:

- **Mahmood A**, Fazal ur Rehman, and Aamer Iqbal Bhatti. "Range Guidance for Subsonic Unpowered Gliding Vehicle using Integral Action based Sliding Mode Control", International Journal of dynamics and control (2023): 1-11. doi.org/10.1007/s40435-023-01229-y

1.6 Thesis Structure

- Chapter 2 accounts for the literature review related to range maximization approaches and range guidance and control. Gap analysis is then described to guide the research direction and problem formulation.

- In chapter 3, the 6-DoF model of SUGV has been explained in detail. After explaining the different axis systems, the transition relation from one system to another is also explained. Then, the force equations, moment equations, kinematic equations, and position equations are defined in the wind axis frame of reference. The nonlinear 6-DoF model of SUGV is decoupled into longitudinal and lateral models, and the longitudinal model is selected for further study.

- Chapter 4 is devoted to the description of the range maximization problem of SUGV. A comprehensive explanation of the types of optimization is presented. Then, a dynamic optimization problem is formulated to maximize the range of SUGV. A new formulation of non-uniform CVP is then explained and at the end of the chapter, a comparison between the range maximization outcomes for the uncontrolled gliding flight, uniform CVP, and non-uniform CVP range based on three different cases of nodes is discussed. Moreover, a comparative study between non-uniform CVP and hp-adaptive Gaussian quadrature collocation-based GPOPS tool is also presented.

- In chapter 5, a range guidance approach is developed for the desired range based on dispersion points and angle of attack and then, the IA SMC controller is employed to track the range guidance signal. To verify the superiority of the IA SMC controller through simulation, it is compared with the PID SMC controller in two different cases, and numerical analysis is also performed at the end of this chapter.

- Finally, in chapter 6, the thesis is summarized and future recommendations are made.

Chapter 2

Literature Review

For vehicles such as airplanes, missiles, bombs, gliders, or ground-launched artillery, there is always a gap in terms of optimal fuel consumption, optimal utilization of stored energy, optimal endurance, optimal path following, avoiding no-fly zones, optimal guidance, optimal terminal guidance, and optimal glide range. Extending the glide range of aero vehicles is an ambitious and challenging task.

This chapter deals with a comprehensive survey of range maximization of unpowered gliding vehicles by considering various approaches that contribute to increasing gliding range. Maximum endurance, the geometric configuration of the aerodynamic surfaces and fuselage, and types of the cost function are various approaches studied to maximize the gliding range.

Further, a literature survey is conducted based on optimization methods and then on range guidance and control approaches. Then, based on the observations from the literature survey, a gap analysis is presented that describes the research direction and formulation of the research problem.

The structure of this chapter is as follows: section 2.1 illustrates the optimal range approaches based on a performance measure, endurance, and optimal geometric configuration of aerodynamic surfaces. Section 2.2 presents a survey based on optimization methods for range maximization. A range guidance and control survey for the UGV range is given in section 2.3. The analysis of the gap in range

extension is investigated in section 2.4 and finally, a summary of this chapter is presented in the last section 2.6.

2.1 Optimal Range Approaches for UGV

As mentioned in the previous chapter UGVs have no source of power so improving the range is an interesting and complex task. While optimal strategies are classified into indirect and direct methods [26], and UGV range trajectory is optimized by applying one of these methods using performance measures such as maximum glide range [27], maximum endurance [28], maximum horizontal range [29], or maximum glide ratio [30].

While path constraints such as load factor to achieve wing-level steady gliding flight, dynamic pressure to avoid structural damage, and heating flux to avoid melting damage are often used to optimize glide trajectory, and some terminal constraints are also imposed to achieve stopping goals such as target engagement and velocity impact.

2.1.1 Glide Range or Horizontal Range Approach

The glide range or horizontal range is used as a performance index for maximizing the range. The range is one of the most important tactical indicators, and many missions require a long final range as well as an end time to be determined. Lena et al. [31] maximized the range of a guided bomb by considering the horizontal range as a cost function as well as the free final time by applying the Homotopy method.

In [32], the range maximization problem is solved by dynamic programming using the horizontal range as a performance index. A numerical approach using the second-order gradient method and the single-perturbation method for the initial conditions of an unpowered gliding vehicle is exerted to compute the optimal range problem in [27, 33, 34]. Qiu et al. [35] addressed the problem of the partial

GV's maximum downrange by considering the booster-separated gliding vehicle. By considering the Legendre–Gauss–Radau collocation points, the nonlinear optimization issue was converted into a nonlinear programming problem. Then, to optimize the downrange, a pseudospectral technique with adaptive mesh refinement was used.

Zhang et al. [24] released an investigation of the maximum gliding range based on the flight path angle for SUGVs. They also established an inverse relationship between the lift/drag ratio and dynamic pressure to calculate the optimum lift/drag ratio responsible for the maximum glide range. To optimize the gliding trajectory of a gun-launched unpowered gliding weapon, the hp-adaptive pseudospectral technique, a trajectory optimization approach, was studied in [36].

Using the Radau pseudospectral approach, Yuan et al. [37] explored the maximum glide range of a glide-guided bomb. In this work, the principle of covector mapping is applied to compute the optimal gliding trajectory. Yang et al. [38] assessed an optimal glide scheme in a maximum range manner (Mayer form of horizontal range) using the Adaptive Radau Pseudospectral method in the GPOPS tool applied to a point mass model of an airdropped mine. Wang [39] focused on the optimal design for gliding trajectory with maximum L/D ratio. The trajectory in the presence of a maximum L/D ratio is shown as a parameter optimization problem and solved by the direct shooting method.

Yu et al. [40] addressed the problem of oscillations in the glide phase reducing the optimal glide range. The authors proposed a suppression scheme based on feedback control to control the glide range. If the total loss of thrust occurs during flight, a powered aircraft converts to a glider, which can use kinetic and potential energy only. For this reason, an optimal approach is needed for enhancing the glide range in cases of the total loss of thrust.

Shapira et al. [41] introduced the singular perturbation theory to optimize the range by taking timescale separation and dynamic effects into consideration. They also used a dichotomic basis method to build an indirect solution for optimum control over two timescales. Considering an engine failure scenario, Feng et al.

[42] paid attention to increasing the gliding range as well as endurance through the FALCON tool. Ben Asher et al. [29] put into action a pseudo-spectral technique based on GPOPS and DIDO tools to optimize the glide range trajectory taking into account the effects of initial condition variation on the engine cutoff scenario.

Segal et al. [43] released a glide range maximization algorithm for engine-out aircraft that ensured a constant heading and velocity during descent flight. They also developed a relationship for the maximum glide speed that depends on the speed of the aircraft in the presence of still air.

2.1.2 Endurance Approach

Endurance means how much time the gliding vehicle uses to perform gliding flights or stay in the air, and it also participates in maximizing the standoff distance of the gliding vehicle. In [44], the authors adopted a control parameterization method to solve the maximum endurance problem. Walton [28] borrowed a simplified model of a ground launch gliding vehicle to maximize endurance, providing a comparison of two different numerical approaches to the endurance problem and the maximum range of a gliding vehicle. Vinh et al. [45, 46] presented an optimal endurance solution to obtain the stand-off distance between the aircraft and the target through Pontryagin's principle. The authors also applied a point mass model with bank angle as the control variable with maximum load factor and maximum lift coefficients as constraints. The main objective of these investigations is to study the effect of release point on stand-off distance and endurance. In [47], the perturbations in the initial conditions are investigated employing analytical solutions to examine the effect of tolerance on the gliding range.

2.1.3 Aerodynamic Surfaces Configuration Approach

The main objectives of the aero configuration are first to create an aero configuration with a high L/D ratio to maximize range and second to develop controllability and stability characteristics resulting in steady gliding flight. Precise geometry in

the configuration of wings, tails, and fins also helps to increase stand-off distance. Furthermore, an unpowered aerodynamic model is designed for maximum glide range using empirical and non-empirical methodologies.

Elsherbiny et al. [23, 48] published a solution for optimal aerodynamic lifting surfaces to extend gliding range using a hybrid optimization algorithm integrated with missile DATCOM. In [49], a particle swarm optimization approach is used in conjunction with missile DATCOM to optimize the shape, fin size, and position of the control surfaces for a given projectile's gliding range.

In [50], a range extension of gliding indirect munition is optimized by lifting surfaces resulting in optimal L/D ratio and trim angles. In [51], the geometry of the actuators and flight dynamics have been optimized to evaluate the long range of the guided projectile.

In [52], to improve the range of the guided bomb, two different scenarios of the tail cross fins stretch out model and fins folded model is executed. Kivaj et al. [53] considered a multidisciplinary conceptual design optimization approach with genetic algorithms focused on optimizing the position of aero surfaces and the geometry of guided projectiles resulting in increased range.

2.2 Optimization based Approach

Numerical dynamic optimization is classified into indirect and direct methods. In the indirect method, the optimal problem is transformed into a two-point boundary value problem and then solved using a variational calculus approach.

In the direct method, the optimization problem is discretized and then converted to a nonlinear programming approach [54] and a detailed classification is presented in Chapter 4.

In this section, the range of UGVs based on indirect and direct methods is presented.

2.2.1 Indirect Method

A homotopy scheme (already found a gliding trajectory based on the optimal L/D ratio for comparison), has been employed to compare with the outcome of maximum principle to obtain maximum gliding range in [31]. Kim et al. [55] studied the effects of fin deployment and autopilot delay on achieving the maximum range, and the authors developed a two-stage Hamiltonian function to solve a variational calculus problem.

In [27, 33], to study the effect of initial altitude and velocity on the range maximization problem, a two-point boundary value problem is formulated and then the necessary conditions are calculated individually by the second-order gradient method, and the singular perturbation method.

Vinh et al. [45] obtained the optimal subsonic gliding flight solution of an unpowered gliding vehicle in a horizontal plane by applying Pontryagin's principle. In some optimization problems, the optimal control during the formulation procedure faces a singular arc (Hamiltonian depends on the control in a linear manner) problem.

Rivas et al. [56] studied the maximum glide range problem by considering the singular arc problem. Burich et al. [57] published a new concept to overcome the drawback of the indirect method in which the initial conditions of the co-states introduce complexity and insensitivity. They transform the range maximization problem into a direct form, and an indirect approach is then considered to obtain the maximum glide range.

2.2.2 Direct Method

The direct method is further classified into control vector and combined state and control vector discretization [54]. A study on range maximization based on quasi-equilibrium glide condition is carried out, and also the effect of the increasing number of nodes on the maximum range is investigated in [58]. Jiao et al. [32]

solve the maximum range problem using a direct method in which they transform the control vector into cubic polynomials to avoid discontinuities. Feng et al. [42] used the FALCON tool to obtain the optimal gliding trajectory. This tool transforms the optimization problem into nonlinear programming and then uses the primal-dual interior point algorithm with a filter line search method.

Guo et al. [36] chose the Hp-Adaptive Pseudospectral Method to maximize the gliding range in which the optimal control problem is modeled as a nonlinear programming problem by parameterizing the state and control using global polynomials (Chebyshev or Lagrange polynomials), and collocating the differential equations using nodes obtained from a Gaussian distribution. Yan-bo et al. [37] performed glide trajectory optimization by incorporating the Radau Pseudo-spectral Method, a global collocation method based on Chebyshev polynomials.

In [59], a Chebyshev Pseudospectral Method is utilized to perform the glide trajectory optimization in a windy environment. Qui et al. [35] performed the optimization to achieve maximum range and employed the Legendre–Gauss–Radau collocation approach to transforming the infinite-dimensional problem into the finite problem, and adaptive mesh refinement pseudospectral method is then used to optimize the control vector intervals. In [24], a GPOPS tool that solves dynamic optimality problems by the hp-adaptive pseudospectral method is used to obtain the maximum range of SUGV.

Yang et al. [38] optimized an optimal glide scheme of an airdropped mine in a maximum range manner using the Adaptive Radau Pseudospectral method through the GPOPS tool. A Control Vector Parameterization (CVP) method based on a Gaussian distribution of time nodes is applied in [60], and then the downrange is optimized based on the resulting CVP.

The range maximization problem is also related to the time maximization problem because there is no estimate of the terminal time when the unpowered gliding vehicle will complete its gliding flight. So to overcome this problem, Zang et al. [24] put into action an enhancing parametrization method, and in this method, the time scale is converted to a specific scale that ranges from zero to one, and

then a CVP approach is utilized to achieve the maximum glide range. Teo et al. [61] solve the problem of maximizing the range of a gun-launched projectile, and to solve this problem, they transformed the infinite-dimensional problem into a finite-dimensional problem through CVP.

Liu et al. [62] developed a constraint handling approach for a hypersonic gliding vehicle, and then the authors employed a classical control vector parametrization approach to optimize the maximum downrange of the gliding vehicle. In [39], a control parametrization with a multiple shooting approach is considered to optimize the gliding range of an unpowered gliding vehicle.

Liu [63] employed an adaptive control arc length based trajectory optimization methodology that combines the CVP method with a Gauss time grid distribution and an adaptive time grid refinement procedure to increase the downrange performance of a hypersonic GV after the re-entry phase.

To increase the hypersonic UGV range, Hui et al. [64] combined the conventional CVP approach with an improved sparrow search algorithm and a time-scaling approach. They also used the golden sine update strategy, and tent chaotic sequence mapping to obtain the initial guess efficiency and optimality.

2.3 Range Guidance and Control

Offline optimization means solving as much of the problem as possible on the computer and then using the best results to track through the appropriate controller. In the glide phase of a hypersonic vehicle, the glide path angle γ^* at $(L/D)_{max}$ in the quasi-steady equilibrium condition is named the commanded glide path angle and it is derived by assuming that dynamic pressure during flight remains constant.

A feedback controller for the α^* and γ^* is represented as [65]

$$\alpha = \alpha^* - \mathcal{K}_\gamma(\gamma - \gamma^*) \tag{2.1}$$

where the angle of attack is α^* at $(L/D)_{max}$ and this guidance law is mostly employed in the hypersonic range guidance [24, 40, 58]. A dynamic pressure tracking guidance scheme for a hypersonic vehicle is studied in [66]. The main goal of this study is to reproduce the offline optimal trajectory in real-time and the authors extended the concept of a feedback controller (2.1) suitable for adjusting the dynamic pressure since the dynamic pressure becomes an important factor, especially for hypersonic gliding vehicles. In [51], a quasi-equilibrium glide condition in a predictor-corrector guidance algorithm is applied to eliminate the phugoid oscillations during mid-course guidance, and an altitude-based acceleration law is developed to extend the gliding range.

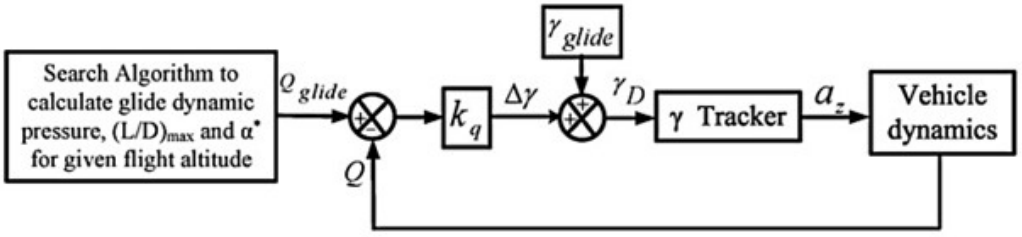

FIGURE 2.1: Optimal dynamic pressure tracking [66].

Fok et al. [67] designed a dynamic pressure based feedback controller and the main objective of this controller is to maintain the desired dynamic pressure set point to increase the gliding range. Feng et al. [42] developed an optimal range guidance model based on a $\mathcal{L}_1$ adaptive altitude controller, and then the offline computed optimal glide trajectory is exerted to track the altitude. Mir et al. [68] designed a feedback control scheme, computed the trim profile with constant dynamic pressure, and then used a gain-scheduled LQR controller to obtain the SUGV gliding range.

Phillips et al. [69] developed an optimal guidance rule for a gun-launched subsonic gliding vehicle that ensures maximum glide range and maximum flight time based on a time-to-go strategy, and then the model predictive control scheme is applied to control the gliding flight and ensuring the terminal guidance. Intelligent technologies grouped under the banner of artificial intelligence have begun to demonstrate promising outcomes in the optimization sector.

In [70], a neural network-based optimal glide control approach is developed which ensures maximum glide range during engine off scenario. Reinforcement learning (RL) is the process of learning based on trials and improving the choice of actions (control input) to maximize the cumulative reward (cost function). To determine the best strategy that maximizes the cumulative reward from interactions with the environment (maybe a dynamical system), the agent (controller) updates the policy (control law) for each time step on behalf of the observations (trajectories) and reward, and Fig.2.2 shows the implementation of RL.

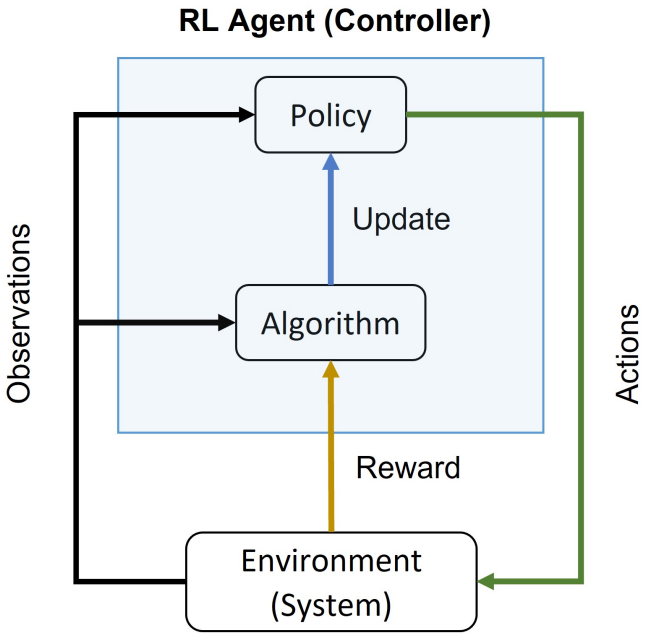

FIGURE 2.2: Implementation of RL.

Din et al. [71–74] exerted the RL approach to achieve the maximum range of subsonic UAV by modifying the RL algorithms such as DDPG, TRPO, PPO, and MRL.

2.4 Gap Analysis

Much of the research on extending glide range has been concerned with hypersonic UGVs. On the other hand, SUGVs have limited research on glide range extension and do not have to face the glide range maximization problems of hypersonic

UGVs, as their structure, fuselage, and control surfaces are designed to operate in the subsonic spectrum.

When the SUGV achieves the desired dispersion points and is released from the carrier platform, the horizontal component of the drag force is less than or equal to the horizontal component of the airspeed. At the same time, the vertical component of the lift force is larger than the vertical component of the drag force which adds more altitude to the initial altitude and this increase may lead to the collision of the SUGV with the carrier platform. After gaining some altitude, the vertical component of the drag force becomes greater than the vertical component of the lift force, and at the same time, the horizontal component of the drag force becomes greater than the horizontal component of airspeed, thus the SUGV goes nose down. This is unstable glide phase, and is repeated until the SUGV enters the stable glide phase. An unstable glide phase causes a reduction in glide range because mechanically stored energy is mostly consumed in this phase to stabilize the gliding flight, and to overcome this, constraint on airspeed and load factor as control variable are used to maximize the glide range in [75] but this approach could not completely stabilize this phase. A stable glide phase is ensured by the pitching moment inherent to the SUGV's fuselage through the control surfaces and geometric configuration. Consequently, handling of unstable glide phase requires dealing with the short period mode (fast states in longitudinal mode) as fast pitching moment stabilization can be obtained from the pitch rate and nose alignment can be obtained from the angle of attack. So by imposing constraints on load factor and short period mode, damped and steady gliding flight can be achieved that eliminates the unstable glide phase and increases the gliding range or horizontal range.

A closed-loop range guidance scheme is another approach by which the intended glide range or horizontal range of the SUGV can be achieved. In this approach, the controller ensures the states of the SUGV to track the range guidance command and this controller can be an intelligent controller or a linear/nonlinear controller. Intelligent controllers such as RL controller [71–74] are used to achieve the glide range of SUGV but the performance of RL controller depends on the design of

the reward function which behaves as an optimal function. The control scheme presented in [68] is based on a constant pressure-based trim profile which is further considered to linearize the SUGV model and employ a closed-loop approach to stabilize the states and such that the SUGV performs gliding flight based on constant pressure. During steady glide flight, the SUGV tries to maintain a constant glide path angle, which means that the ratio of height decrease to horizontal distance increase remains constant. A range guidance scheme based on dispersion points and angle of attack can be designed to achieve the desired horizontal range through a closed-loop approach by selecting the appropriate controller. The dispersion points are responsible for the glide path angle with respect to the intended horizontal range in this range guidance.

2.5 Problem Statement

As discussed in section 2.4, an unstable glide phase can cause a collision of SUGV with the release platform and a reduction in glide range. Furthermore, the development of range guidance to achieve the required horizontal range through a closed-loop scheme. Thus, the main objective of this research work is twofold:

1. Formulate an optimization problem capable of handling unstable gliding flight as well as maximizing the gliding range. Additionally impose a short period mode constraint and load factor constraint to achieve steady gliding flight.

2. Develop range guidance based on the dispersion points and angle of attack to achieve the intended horizontal range of the SUGV through a suitable nonlinear controller in the presence of nominal environment.

2.6 Summary

In this chapter, a detailed literature review on the range extension of unpowered gliding vehicles is presented. After presenting the literature survey, the research direction is extracted from the gap analysis. According to the survey, there is a need to mitigate the instability in the early phase of the glide trajectory, and via this range may be expanded, and it is also observed that the most optimal trajectory tracking-based feedback control schemes are developed. Consequently, there is a need to develop an intended range-based closed-loop control scheme that is easy to implement and eliminates instability problems.

In the next chapter, the system description about SUGV is presented.

Chapter 3

System Description

This chapter begins by discussing the axis systems used in deriving the equations of motion for an Unpowered Gliding Vehicle (UGV). The equations of motion for a rigid UGV are then derived from Newton's second law. Following that, kinematic equations and position equations are reviewed and incorporated into the equations of motion to construct a complete set of nonlinear UGV dynamic equations. Eventually, the longitudinal dynamic model is stated in terms of the UGV's states and physical properties.

Section 3.1 describes the different axis systems necessary to construct the UGV dynamic model. Section 3.2 covers the UGV 6-DoF model. Section 3.3 presents the longitudinal dynamic equations of the UGV, while Section 3.4 provides a summary of this chapter.

3.1 Introduction

While studying the motion of any aero-vehicle, its stability needs to be thoroughly investigated, and a complete study of the aero-vehicle can be done by analyzing its stability. The major themes of the study are how effectively an aero-vehicle can fly and how it can be steered. The capacity of an object to recover to its equilibrium state after being disrupted is referred to as stability. Static and dynamic stability

are two aspects of aero-vehicle stability. The reluctance of an aero-vehicle to return to an equilibrium condition in the face of disruption is referred to as static stability. If time is involved in the stability, the stability is transformed into dynamic stability. When the motion of an aero-vehicle after being perturbed diminishes over time and attains an equilibrium state known as dynamic stability. In addition to static stability, an aero-vehicle must be dynamically stable. The stability factor is critical in understanding the dynamic properties of an aero-vehicle and devising controls. The flying qualities of any aero-vehicle depend on the performance of the controller and the opinion of the pilot. It is therefore important to understand the relationship between flight characteristics with the equations of motion of any aero-vehicle. Additionally, before formulating the equations of motion for an aero-vehicle, it is crucial to have a basic understanding of the various frames of reference and coordinate systems. The need for suitable coordinate systems arises when the position and velocity of the aero-vehicle with respect to the ground are to be navigated and when the position and velocity with respect to the environment are required for the performance of the aero-vehicle.

3.1.1 Coordinate Systems

To construct the 6-DoF equations of motion, it is critical to ensure that all necessary information is required in the relevant axis system. The static aero coefficient data is usually obtained in the body axis whereas the dynamic aero coefficient data is obtained in the stability axis. Furthermore, the orientation on which the 6-DoF model is based differs from the orientation on the ground. So for these reasons, the coordinate transformation is required.

In physics, a frame of reference refers to a coordinate system or set of axes within which the position, orientation, and other properties of object can be measured, or it can refer to an observational frame that describes the state of motion of an observer. It can refer to both an observational reference frame and its associated coordinate system as a single unit. Also, all coordinate systems have the common property of being right-handed and orthogonal.

3.1.1.1 Inertial Axis

A frame of reference in which an object moves along a straight path with a constant velocity while not being acted upon by forces is called an inertial frame of reference (Galilean frame of reference).

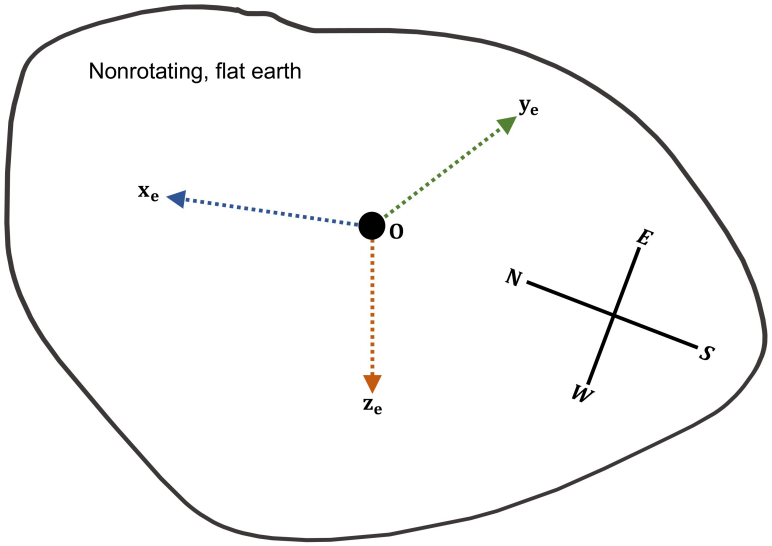

FIGURE 3.1: Inertial frame of reference

Consequently, an object accelerates concerning an inertial frame only when a physical force, either external or internal, is applied, and the object then continues to move according to Newton's first law of motion. Newton's first law asserts that unless forced to alter its condition by the action of an external force, an object will stay at rest or in uniform motion in a straight line.

So, all inertial frames are moving in a constant, rectilinear motion with regard to one another and are not accelerating. For the inertial frame, the Earth is assumed to be non-rotating and flat because the range of flight is small and the angular rotation of the Earth is smaller than the normal angular rotation of an aero-vehicle.

An inertial axis system with the origin at a convenient point on the Earth's surface, $F_I(OX_eY_eZ_e)$, is chosen and shown in Fig. 3.1. The axis system is right-handed with the positive Z_e pointing towards the center of the earth. X_e is perpendicular to Z_e and is positive to the north, and Y_e is perpendicular to the X_eZ_e -plane and is positive to the east.

3.1.1.2 Body Axis

A frame of reference relative to the structure of the body is known as the body axis. In this axis system, the origin fixes (center of gravity) with respect to the body but the axes are free to rotate and It is a right handed reference frame. Body axis system is important for describing the dynamic equations of an aero-vehicle and is shown in Fig. 3.2. X_b axis is in the plane of symmetry of the aero-vehicle and is positive in the forward direction.

Z_b axis is also in plane of symmetry and perpendicular to X_b axis and positive in downward direction. Y_b axis is perpendicular to the X_bZ_b plane and positive to the right starboard wing. X_b, Y_b, and Z_b are also known as the roll axis, pitch axis, and yaw axis, respectively. Since all inertial laws are valid in the inertial frame of reference and to compute the dynamic equations of the aero-vehicle in the body frame of reference, a transformation is necessary to specify the orientation of the body axis system to the inertial axis system.

This is usually accomplished by employing a set of three Euler angles, which define an ordered set of rotations from one axis system to another. This method yields a Direction Cosine Matrix (DCM) [76], which can produce equations relating to different flight angles. the rotational sequence is as follows:

$$TM_\psi = \begin{bmatrix} C_\psi & S_\psi & 0 \\ -S_\psi & C_\psi & 0 \\ 0 & 0 & 1 \end{bmatrix} \tag{3.1}$$

$$TM_\theta = \begin{bmatrix} C_\theta & 0 & -S_\theta \\ 0 & 1 & 0 \\ S_\theta & 0 & C_\theta \end{bmatrix} \tag{3.2}$$

$$TM_\phi = \begin{bmatrix} 1 & 0 & 0 \\ 0 & C_\phi & S_\phi \\ 0 & -S_\phi & C_\phi \end{bmatrix} \tag{3.3}$$

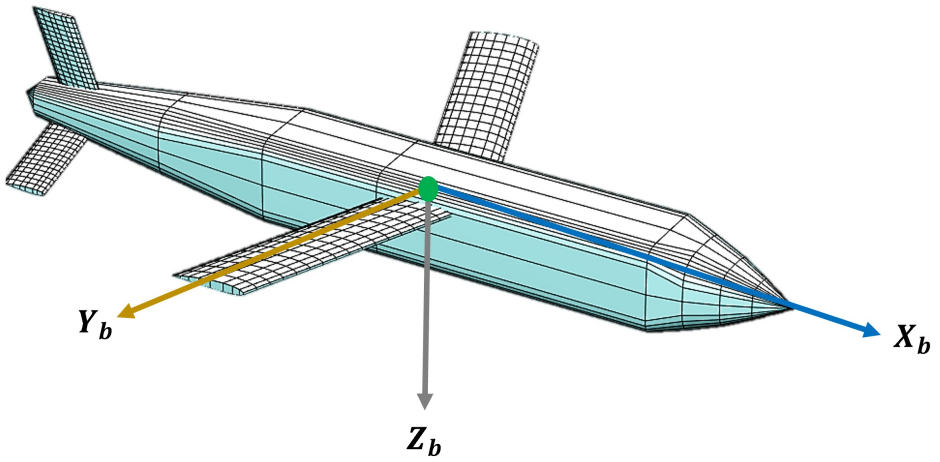

FIGURE 3.2: Body axis

where S and C are subscript of 'sin' and 'cos'. The rotational sequence is encapsulated as

- The right-handed rotation of the Z_b axis produces ψ.
- In the result of Z_b axis rotation, the new Y_b axis is obtained, which is then rotated to generate θ
- A new X_b axis, in the result of Y_b axis rotation, is rotated to obtain ϕ.

The conversion from inertial to body-fixed reference frame and vice versa is obtained by the following matrix multiplication.

$$DCM = TM_{\psi}TM_{\theta}TM_{\phi} \tag{3.4}$$

3.1.1.3 Stability Axis

It is a unique axis system that is influenced by the angle of attack. The X_b of the aero-vehicle is usually not coincident with the relative wind, and this difference creates an angle called the angle of attack α. The stability axis system is therefore used to associate X_b with the relative wind. Basically, the body axis system is rotated about the Y_b to accommodate α. Additionally, This is a right-handed system in which X_s is aligned with the relative wind in steady flight, Y_s identical

to Y_b, and Z_s is perpendicular to the $X_s Y_b$ plan. It is important to keep in mind that if α is zero then this is a real body-axis system.

A pictorial illustration of the stability axis system is shown in Fig. 3.3. The relation of the change of the stability axis to a body axis is also expressed in this way.

$$\begin{bmatrix} X_s \\ Y_s \\ Z_s \end{bmatrix} = \begin{bmatrix} C_\alpha & 0 & S_\alpha \\ 0 & 1 & 0 \\ -S_\alpha & 0 & C_\alpha \end{bmatrix} \begin{bmatrix} X_b \\ Y_b \\ Z_b \end{bmatrix} \tag{3.5}$$

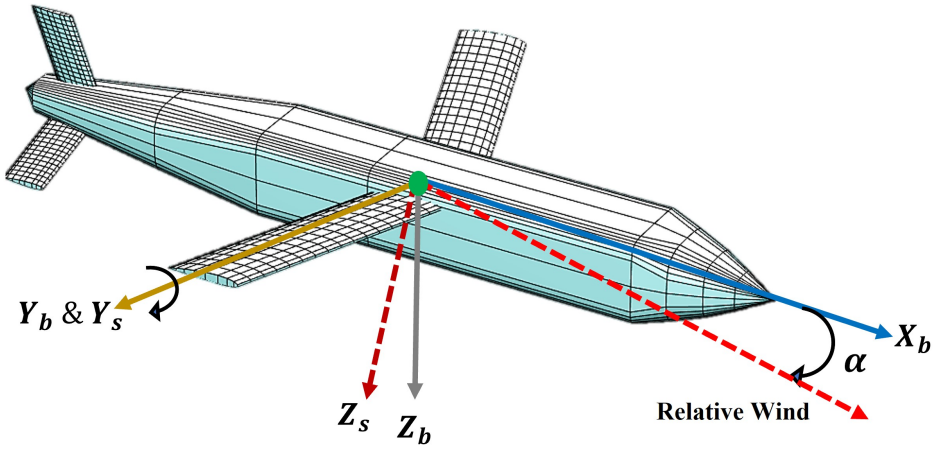

FIGURE 3.3: Stability axis

3.1.1.4 Wind Axis

The wind axis system is significant in determining the aero coefficients and aero forces, and it is also affected by the sideslip angle. The angle difference between the relative wind and the plane of symmetry of an aero-vehicle is known as sideslip angle β, and it is positive when the relative wind is from the right side of the plane of symmetry.

β is measured in the wind axis, although Z_w stays the same as Z_s. X_w is along the relative wind and Y_w is chosen in such a way to follow a right-hand rotation trend. Z_w is rotated around the symmetry plane to accommodate β. It is worth mentioning that when β is zero, the wind axis and stability axis coincide. Only

in this situation, Y_w coincident with Y_s and Y_b, is normal to the X_bZ_b. Fig. 3.4 depicts a graphical representation of the wind axis system. A stability axis to wind axis and a body axis to wind axis change are also expressed in this way

$$\begin{bmatrix} X_w \\ Y_w \\ Z_w \end{bmatrix} = \begin{bmatrix} C_\beta & S_\beta & 0 \\ -S_\beta & C_\beta & 0 \\ 0 & 0 & 1 \end{bmatrix} \begin{bmatrix} X_s \\ Y_s \\ Z_s \end{bmatrix} \tag{3.6}$$

$$\begin{bmatrix} X_w \\ Y_w \\ Z_w \end{bmatrix} = \begin{bmatrix} C_\alpha C_\beta & S_\beta & S_\alpha C_\beta \\ -C_\alpha S_\beta & C_\beta & -S_\alpha S_\beta \\ -S_\alpha & 0 & C_\alpha \end{bmatrix} \begin{bmatrix} X_b \\ Y_b \\ Z_b \end{bmatrix} \tag{3.7}$$

The transformation of the body axis to the wind axis is outlined as:

- A right-handed rotation about the Y_b axis, to align X_b with the relative wind, resulting in a stability axis.
- A right-handed rotation about the new Z_s axis to match the symmetry plane with the relative wind yields the wind axis.

3.2 Construction of Equations of Motion

After defining the various axis systems and transformation relationships, the equations of motion for the SUGV can be derived from Newton's second law of motion. The sum of all external forces acting on a body must be equal to the time rate of change of its linear momentum, and the sum of all external moments must be equal to the time rate of change of its angular momentum, as stated by Newton's second law of motion, where the time rate of change is with respect to the inertial space. During a frame of reference shift, the rate of change of the vector varies when viewed from the reference axis system.

When two or more axis systems rotate relative to each other, the Coriolis equation needs. So the Coriolis equation is defined as the motion of an object P as seen

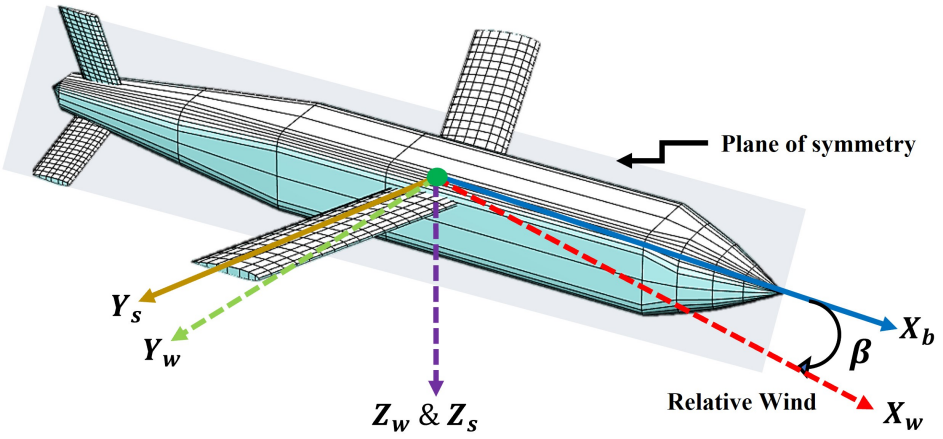

FIGURE 3.4: Wind axis

from a frame of reference A is equal to its motion as seen from a moving frame of reference B , plus the motion resulting from the relative angular velocity of the moving frame with respect to the reference frame [77].

So the statement of Coriolis equation can be written as

$$\dot{R}_B = \dot{R}_A + \omega_A \times R_A \tag{3.8}$$

where $\dot{R}_A$ is the velocity vector as seen from the moving frame and $\dot{R}_B$ is the moving reference frame.

3.2.1 Force Equations

Newton's second law for linear motion is written as

$$\frac{d}{dt}(mv)|_I = \sum F \tag{3.9}$$

where m is the constant mass and Earth is the inertial frame of reference. v and F are the vectors of velocity and acting forces, respectively. After using the Coriolis equation (3.8) and applying the transformation from the body to the wind axis (3.7), a general force equation relationship is given as

$$\dot{u}_w + \omega_w \times u_w = \frac{F_w}{m} \tag{3.10}$$

where u_w and ω_w are the linear velocity and angular velocity components in the wind axis along the X_w, Y_w and Z_w axes, respectively.

F_w is the sum of the aerodynamic forces and gravity forces in the wind axis along the X, Y and Z axes, respectively. So after solving (3.10) by complex calculations, the force equations in the wind axis for SUGV are written as follows.

$$\dot{V} = -\frac{D}{m} + F_w^{gx} \tag{3.11}$$

$$\dot{\beta} = \frac{Y}{mV} - R + \frac{F_w^{gy}}{V} \tag{3.12}$$

$$\dot{\alpha} = -\frac{L}{mVC_\beta} + \frac{Q}{C_\beta} + \frac{F_w^{gz}}{VC_\beta} \tag{3.13}$$

where F_w^{gx}, F_w^{gy} and F_w^{gz} are expressed as

$$\begin{aligned} F_w^{gx} &= g * (S_\beta S_\phi C_\theta - C_\alpha C_\beta S_\theta + S_\alpha C_\beta C_\phi C_\theta) \\ F_w^{gy} &= g * (C_\alpha S_\beta S_\theta + C_\beta S_\phi C_\theta - S_\alpha S_\beta C_\phi C_\theta) \\ F_w^{gz} &= g * (S_\alpha S_\theta + C_\alpha C_\phi C_\theta) \end{aligned} \tag{3.14}$$

States of force equations, aerodynamic forces, and gravitational forces are all characterized as

- V is the airspeed, β is the sideslip angle along the Y_w axis, and α is the angle of attack along the Z_w axis.
- D is the drag force along the X_w axis, Y is the side force along the Y_w axis and L is the lift along the Z_w axis.
- Gravitational forces (F_w^{gx}, F_w^{gy}, F_w^{gz}) are in the wind axis.

3.2.2 Moment Equations

For angular motion, Newton's second law is stated as follows.

$$\frac{d}{dt}(H)|_I = \sum M_A \tag{3.15}$$

where H is the angular momentum of the SUGV defined as $H = I_B * \omega_B$ and I_B is the moment of inertia of the SUGV about the body axis. In our case, the SUGV is assumed to be symmetric about the $X_b Z_b$ plane then the products of inertia, I_{xy}, and I_{yz} are zero.

$$I_B = \begin{bmatrix} I_{xx} & I_{xy} & I_{xz} \\ I_{xy} & I_{yy} & I_{yz} \\ I_{xz} & I_{yz} & I_{zz} \end{bmatrix} \tag{3.16}$$

So after employing the Coriolis equation (3.8), the moment equations along the X, Y and Z axes are written as

$$\wp \dot{P} = I_{zz} l + I_{xz} N + PQ I_{xz}(I_{xx} - I_{yy} + I_{zz}) - QR(I_{xz}^2 + I_{zz}^2 - I_{yy} I_{zz}) \tag{3.17}$$

$$I_{yy} \dot{Q} = M + PR(I_{zz} - I_{xx}) - I_{xz}(P^2 - R^2) \tag{3.18}$$

$$\wp \dot{R} = I_{xz} l + I_{xx} N - QR I_{xz}(I_{xx} - I_{yy} + I_{zz}) - PQ(I_{xz}^2 + I_{xx}^2 - I_{xx} I_{yy}) \tag{3.19}$$

where $\wp$ is $(I_{xx} I_{zz} - I_{xz}^2)$, and It is worth noting that all gravitational moments are zero because the force of gravity acts on the CG of the SUGV.

The angular rates and moments are itemized as follows

- P, Q and R are the rolling rate along the X_b axis, the pitch rate along the Y_b axis and the yaw rate along the Z_b axis, respectively.
- l, M and N are the rolling moment along the X_b axis, the pitch moment along the Y_b axis and the yaw moment along the Z_b axis, respectively.
- All gravitational moments (l_g, M_g, N_g) are zero.

3.2.3 Kinematic Equations

The equations of motion are derived in the moving body axis system. But unfortunately, the orientation of the SUGV is represented in the fixed body axis system. So to relate the angular velocities to the axes of a fixed body, a relation

is written in terms of the Euler angular rates as follows

$$\dot{\phi} = P + QS_{\phi}T_{\theta} + RC_{\phi}T_{\theta} \tag{3.20}$$

$$\dot{\theta} = QC_{\phi} - RS_{\phi} \tag{3.21}$$

$$\dot{\psi} = Q\frac{S_{\phi}}{C_{\theta}} + R\frac{C_{\phi}}{C_{\theta}} \tag{3.22}$$

where T is the subscript of 'tan' and the Euler angles are defined as

- ϕ is a roll angle along the X_b axis.
- θ is a pitch angle along the Y_b axis.
- ψ is a yaw angle along the Z_b axis.

3.2.4 Position Equations

The equation of the position of SUGV in the wind axis system are described as follows

$$\dot{P}_N = V(C_{\alpha}C_{\beta}C_{\theta}C_{\psi} + S_{\beta}(C_{\psi}S_{\theta}S_{\phi} - S_{\psi}C_{\phi}) + S_{\alpha}C_{\beta}(C_{\psi}S_{\theta}C_{\phi} + S_{\psi}S_{\phi})) \tag{3.23}$$

$$\dot{P}_E = V(C_{\alpha}C_{\beta}C_{\theta}S_{\psi} + S_{\beta}(S_{\psi}S_{\theta}S_{\phi} + C_{\psi}C_{\phi}) + S_{\alpha}C_{\beta}(S_{\psi}S_{\theta}C_{\phi} - C_{\psi}S_{\phi})) \tag{3.24}$$

$$\dot{h} = V(C_{\alpha}C_{\beta}S_{\theta} - S_{\beta}C_{\theta}S_{\phi} - S_{\alpha}C_{\beta}C_{\theta}C_{\phi}) \tag{3.25}$$

The states of the position equation are summarized as follows

- P_N represents the horizontal distance, also known as the range.
- P_E represents latitude, commonly known as side distance.
- P_N denotes the vertical distance or height measured up to ground level.

3.3 Longitudinal Equations of Motion

To compute control derivatives and stability derivatives, each aero-vehicle is split into four aerodynamic surfaces: wings, tailplane, fin, and fuselage. Any aero-vehicle's aerodynamic study is separated into two parts: symmetric flow (longitudinal) analysis and asymmetric flow (lateral) analysis. Because of the symmetric plan, the lateral motion during longitudinal motion is assumed to be zero. During lateral motion, there remains an opportunity for aerodynamic interfaces between the various surfaces of the aero-vehicle.

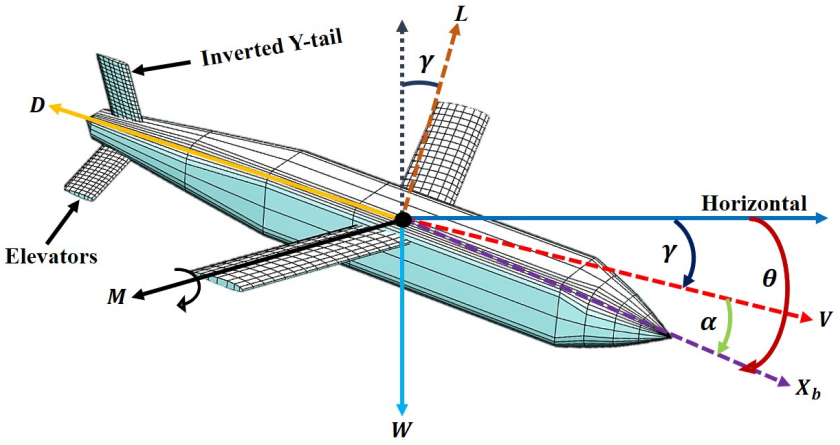

FIGURE 3.5: Longitudinal model

This means that all aerodynamic coefficients have some effect. However, the effects of the lateral coefficients are smaller than the longitudinal ones and hence can be assumed zero [15]. These assumptions lead to an aerodynamic analysis to the dynamics into a longitudinal and lateral aerodynamic dynamics.

Since the model of 3-DoF motion in longitudinal is significantly simpler than the model of 6-DoF motion and it is also useful to explore the equations of motion under wings-level steady-state flight conditions. Figure 3.5 depicts a longitudinal model with aero forces and pitching moment during unpowered gliding flight based on the preceding discussion. The following is an explanation of the longitudinal dynamical model of SUGV.

$$m\dot{V} = -D - W(S_\theta C_\alpha - C_\theta S_\alpha) \tag{3.26}$$

$$m\dot{\alpha} = -\frac{L}{V} + \frac{W}{V}(C_\theta C_\alpha + S_\theta S_\alpha) + mQ \tag{3.27}$$

$$\dot{Q} = \frac{M}{I_y} \tag{3.28}$$

$$\dot{\theta} = Q \tag{3.29}$$

$$\dot{R} = V(C_\theta C_\alpha + S_\theta S_\alpha) \tag{3.30}$$

$$\dot{h} = V(S_\theta C_\alpha - C_\theta S_\alpha) \tag{3.31}$$

3.3.1 Aerodynamic Forces, Moment and Coefficients

The continuity principle of incompressible flow and the Bernoulli equation are the fundamental building blocks for calculating aerodynamic forces, and these forces are also dependent on dynamic pressure. The lift L and drag D forces are usually calculated in the wind axis, and the pitching moment M is computed in the body axis, and shown as

$$\begin{aligned} L &= 0.5\rho V^2 S C_L \\ D &= 0.5\rho V^2 S C_D \\ M &= 0.5\rho V^2 S \bar{C} C_M \end{aligned} \tag{3.32}$$

where C_L, C_D and C_M are the aerodynamic coefficients, S is the wing surface area, $\bar{C}$ is the aerodynamic chord of the wing, ρ is the air density function of the altitude [15].

$$\rho = 1.222 - 1.15e^{-4}h + 3.18e^{-9}h^2 \tag{3.33}$$

It is important to note that the relation of ρ in (3.33) is valid for 11 km to 0 km altitude. The lifting effect of the fuselage is often neglected because it is usually much smaller than that of the wing.

Although the tailplane's lift effect is frequently insignificant, even when compared to the wing, it is still taken into account in the model analysis because of its profound impact on the pitching moment coefficient. The impact of drag on the tailplane, on the other hand, is ignored since it is minor in comparison to the wing

and fuselage. Airflow parallel to the symmetric plan shows that the fin produces no lift force and its drag force is neglected for the same reason as that of the tailplane. The preceding debate can be summed up as follows.

- Lift force is produced by the wing and tailplane.
- Wing and fuselage produce drag force.

During longitudinal motion, lateral aerodynamic coefficients are assumed to be zero due to the symmetric plan. Additionally, an aero-vehicle typically has a flexible structure and can be damaged by the effects of high dynamic stresses. Therefore, it is important to calculate the aerodynamic coefficients, in practice, as functions of altitude, Mach, and the aerodynamic angles [15].

Deflection of the control surfaces changes the coefficients and consequently changes the camber of the wing, which changes the drag, lift, and pitching moment. A few assumptions are considered before defining the aerodynamic coefficients as follows

- The coefficients are not affected by the zero angle of attack.
- The coefficients are independent of the aerodynamic angle of attack rates.

Then drag C_D , lift C_L , and pitching moment C_M coefficients are defined as

$$\begin{aligned} C_L &= C_{L_\alpha}\alpha + \frac{C_{L_Q}Q\bar{C}}{2V} + C_{L_{\delta_e}}\delta_e \\ C_D &= \frac{C_L^2}{2\pi eAR} + C_{D_{\delta_e}}\delta_e \\ C_M &= C_{M_\alpha}\alpha + \frac{C_{M_Q}Q\bar{C}}{2V} + C_{M_{\delta_e}}\delta_e \end{aligned} \tag{3.34}$$

where $C_{L_{\delta_e}}$, $C_{D_{\delta_e}}$ and $C_{M_{\delta_e}}$ stand for the partial derivative of lift, drag, and pitching moment with respect to the elevator deflection δ_e. C_{L_α} and C_{M_α} point out the partial derivative of lift and pitching moment with respect to α, respectively. C_{L_Q} and C_{M_Q} are the partial derivative of lift and pitching moment with respect to Q, respectively. Moreover, e is the Oswald efficiency number, and AR is the aspect ratio of the SUGV.

3.4 Summary

In this chapter, the inertial axis system, body axis system, stability axis system and wind axis system with transformation relations are described. A transformation relation between two moving frames of references is also defined, known as the Coriolis equation. Then, a 6-DoF mathematical model, Newton's second law based relation for linear and angular motions, orientation-based equations, and position-based equations are written for gliding vehicle. After that, a decoupled nonlinear longitudinal model for a SUGV with aerodynamic forces and aerodynamic coefficients is presented which is considered for further study.

Chapter 4

Trajectory Optimization of SUGV

In many aero gliding vehicles, achieving the maximum gliding range is a challenging task. This chapter describes the maximum range problem of SUGV. When the SUGV starts gliding at the given dispersion points, it eventually strikes the ground after some distance, and height is considered as a stopping constraint in this general condition. To avoid the time-scaling approach for the free time optimal problem, the maximum stoppable time with a stopping constraint is addressed to attain the maximum glide range.

This problem can be chosen as an optimal gliding range problem which can be solved by direct methods. After being released from dispersion points, the SUGV has to face fluctuating gliding flight because of the flight phase transition that causes gliding range reduction.

To achieve a damped and steady gliding flight while maximizing the gliding range, A non-uniform Control Vector Parameterization (CVP) approach is proposed that uses the notion of exponential spacing for the time vector. When compared with the maximum step (uncontrolled flight) input and conventional uniform CVP approach, simulations of the proposed non-uniform CVP approach demonstrate that the SUGV exhibits superior damping and steady gliding flight, with a maximum gliding range. To observe the effect of control nodes by considering the proposed CVP approach, three different cases for range maximization are also illustrated.

The architecture of this chapter is outlined as follows: Introduction to optimization and its types are described in section 4.1. Problem formulation with maximum stoppable time in section 4.2 is narrated. Uniform CVP and proposed non-uniform CVP are explained in section 4.3. The results of three cases are discussed in section 4.4 and a comparative analysis is also elucidated. Finally, section 4.5 sums up the chapter.

4.1 Introduction

One of the challenges of engineering is to accomplish tasks optimally with minimum energy and resources. Because of the unpredictable nature of things, the term optimal has a very vague and complex meaning. Controlling sophisticated dynamic systems, such as limiting the miss distance between a gliding weapon and its stationary target, on the other hand, is a difficult challenge. As a result, the method or strategy used to tackle one job is not always appropriate for subsequent ones.

Yet, for a given system or process, an accurate characterization of the needs, available resources, and the physical restrictions on specific capacity (constraints) allows engineers to feel more confident in identifying the best, most advantageous, most helpful, or optimal solution. Practical realization of the optimal solution is the next step that engineers have to accomplish. During implementation, the engineers frequently confront several hurdles that force them to come up with the closest or best solution.

This can be achieved by updating or rejecting some user demands without sacrificing generality. During the entire optimization process, the main objective of the problem is to satisfy a goal function, cost function, target function, performance measure or performance index, and the optimal problem can easily be transformed into a minimal problem and vice versa. In the field of mathematics, the method of solving an optimization problem is called 'programming' and the numerous forms

of programming that are suboptimal regions of optimization vary dependent on the cost function and constraints. Some basic programming approaches are defined as

Linear Programming: It is the process of solving optimization problem involving a linear cost function and linear constraints and is represented as follows:

$$\begin{aligned} \mathcal{J} &= min\ \tilde{\mathcal{P}}^T x \\ \text{s.t. } & ax = b, \\ & x \leq 0 \end{aligned} \tag{4.1}$$

where $\mathcal{J}$ is a linear cost function, $\tilde{\mathcal{P}} \in \Re^{m \times n}$ is constant vector and $x \in \Re^n$ is the design variable vector, $a \in \Re^{m \times n}$ and $b \in \Re^m$. All constraints remain linearly independent. To ensure that all constraints continue to be linearly independent, it is assumed that the matrix a is of full rank.

Quadratic Programming: If in (4.1) the quadratic cost function has linear constraints, the optimization problem is transferred to quadratic programming and is written as follows:

$$\begin{aligned} \mathcal{J} &= min\ 0.5 x^T \tilde{\mathcal{P}} x + \tilde{\mathcal{Q}} x + \tilde{\mathcal{R}} \\ \text{s.t. } & ax = b, \\ & x \leq 0 \end{aligned} \tag{4.2}$$

where $\tilde{\mathcal{P}} \in \Re^{n \times n}$ is a symmetric strictly positive semi-definite matrix, $\tilde{\mathcal{Q}} \in \Re^n$, $\tilde{\mathcal{R}} \in \Re$. It is worth noting that a quadratic programming problem is always convex.

If the inequality constraints are convex in nature, this method of programming is known as Quadratically Constrained Quadratic Programming.

4.1.1 Classification of Optimization

Before attempting to solve the optimization issue, it is critical to determine the effect of time, which plays a crucial role in categorising the optimization problem

as static or dynamic. The problem is addressed as a dynamic optimization problem if the optimal solution is found in time space.

4.1.1.1 Static optimization

The main focus of static optimization is on optimal physical structural design and optimal value measurements. Another concern of static optimization is to control a plant or system at a steady state, which means that the states of the system do not vary with time, and in this case, the system is described by algebraic equations and is solved by ordinary calculus, Lagrange multiplier, linear and nonlinear programming techniques. The outcomes of static optimization are calculated using the search method or optimality criteria method as shown in Fig.4.1.

Optimality criteria are conditions that a function must meet at its minimum point, and optimization methods that assist in finding a solution to satisfy the optimality criteria are sometimes referred to as optimality criteria methods.

The design space for the optimal solution is traversed numerically in search methods, and this search begins with an initial estimate of the optimum design for the problem. If the initial optimum design does not meet the optimality criteria, it is updated iteratively until the optimality criteria are met. To solve the static

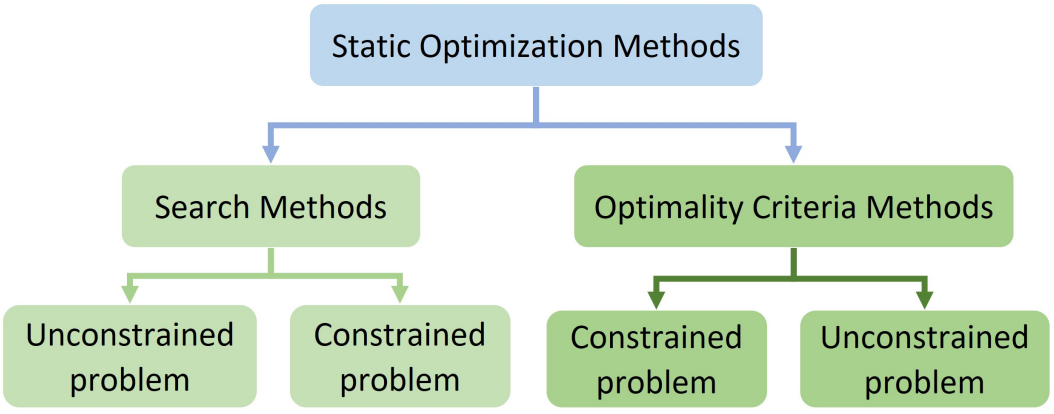

FIGURE 4.1: Classification of static optimization methods.

optimization problem, consider a target function $\mathcal{F}$ of several design variables $x_1, ..., x_n$ under the constraints of the form $\mathcal{G}_i(x_1, ..., x_n) = 0$, $\tilde{\mathcal{G}}_i(x_1, ..., x_n) < 0$,

and $\hat{\mathcal{G}}_i(x_1, ..., x_n) > 0$ for $i = 1, ..., \mathsf{T}$, the Lagrange multiplier approach is particularly useful for solving the static optimum problem. Instead of minimizing the function $\mathcal{F}$ with respect to the independent variables $x_1, ..., x_n$ over the constraints $\mathcal{G}_i, \tilde{\mathcal{G}}_i$, and $\hat{\mathcal{G}}_i$, an augmented function $\mathcal{L}$ with respect to its Lagrange multipliers (the basic idea is to transform a constrained problem in such a way that the derived test for an unconstrained problem can still be applied) is solved.

$$\mathcal{L} = \mathcal{F}(x_1, ..., x_n) + \sum_{i=1}^{\mathsf{T}} \lambda_i \mathcal{G}_i + \sum_{i=1}^{\mathsf{T}} \tilde{\lambda}_i \tilde{\mathcal{G}}_i + \sum_{i=1}^{\mathsf{T}} \hat{\lambda}_i \hat{\mathcal{G}}_i \tag{4.3}$$

It is wise to note that the value of the Lagrange multiplier for each constraint depends on the functional form for the constraint. According to the notion of Lagrange multipliers, inequality constraints must be turned into equality constraints, and to do this, extra variables in the form of $\leq$ constraints, known as slack variables, are introduced.

Since the values of slack variables at the feasible point is either negative or zero. For inequality constraints of the form $\geq$, variables are introduced and referred to as surplus variables having a value of either positive or zero at the feasible point. Slack and surplus variables, known as synthetic variables, behave as additional unknowns that must be determined as a part of the solution to the optimization problem.

At the optimum point, if the slack S_l or surplus S_p variable is positive, the corresponding constraint is inactive and if S_l or S_p is zero, the constraint is active. It is worth mentioning that synthetic variables will be treated as a quadratic term if a numerical technique is employed otherwise variables will not use the quadratic term for linear programming to avoid nonlinearity.

The necessary conditions for a stable optimization problem with equality and inequality constraints written in standard form are commonly known as the "Fritz-John" or "Karush-Kuhn-Tucker" (KKT) conditions [78].

KKT Optimality Conditions are summarised as follows:
Let x^* be a regular point of the feasible set that is a local minimum for $\mathcal{F}(x)$,

subject to $\mathcal{G}_i(x) = 0; i = 1 \text{ to } a$; $\tilde{\mathcal{G}}_j(x) \leq 0; j = 1 \text{ to } b$; $\hat{\mathcal{G}}_k(x) \geq 0; k = 1 \text{ to } c$.

Then there are Lagrange multipliers λ (a-vector), $\tilde{\lambda}$ (b-vector), $\hat{\lambda}$ (c-vector) such that the Lagrangian function is stationary with respect to x_i, λ, $\tilde{\lambda}$, $\hat{\lambda}$, S_{l_j} (b-vector) and S_{p_k} (c-vector) at the x^*.

- The Lagrangian function for the problem written in standard form is

$$\mathcal{L} = \mathcal{F}(x) + \sum_{i=1}^{a} \lambda_i \mathcal{G}_i(x) + \sum_{j=1}^{b} \tilde{\lambda}_i(\tilde{\mathcal{G}}_i(x) + S_{l_j}^2) + \sum_{k=1}^{c} \hat{\lambda}_i(\hat{\mathcal{G}}_i(x) - S_{p_k}^2)$$

- Gradient conditions:

$$\frac{\partial \mathcal{L}}{\partial x_e} = \frac{\partial \mathcal{F}}{\partial x_e} + \sum_{i=1}^{a} \lambda_i^* \frac{\partial \mathcal{G}_i}{\partial x_e} + \sum_{i=1}^{b} \tilde{\lambda}_i^* \frac{\partial \tilde{\mathcal{G}}_i}{\partial x_e} + \sum_{i=1}^{c} \hat{\lambda}_i^* \frac{\partial \hat{\mathcal{G}}_i}{\partial x_e}; \quad e = 1 \ to \ f$$

$$\begin{aligned} \frac{\partial \mathcal{L}}{\partial \lambda} &= 0 \Rightarrow \mathcal{G}_i(x^*) = 0; \quad i = 1 \ to \ a \\ \frac{\partial \mathcal{L}}{\partial \tilde{\lambda}} &= 0 \Rightarrow (\tilde{\mathcal{G}}_j(x^*) + S_{l_j}^2) = 0; \quad j = 1 \ to \ b \\ \frac{\partial \mathcal{L}}{\partial \hat{\lambda}} &= 0 \Rightarrow (\hat{\mathcal{G}}_k(x^*) - S_{p_k}^2) = 0; \quad k = 1 \ to \ c \end{aligned}$$

- Feasibility check for inequalities:

$$\begin{aligned} S_{l_j}^2 &\geq 0; \quad j = 1 \ to \ b \\ S_{p_k}^2 &\leq 0; \quad k = 1 \ to \ c \end{aligned}$$

- Switching conditions:

$$\begin{aligned} \frac{\partial \mathcal{L}}{S_{l_j}} &= 0 \Rightarrow 2\tilde{\lambda}_j^* S_{l_j} = 0; \quad j = 1 \ to \ b \\ \frac{\partial \mathcal{L}}{S_{p_k}} &= 0 \Rightarrow 2\hat{\lambda}_j^* S_{p_k} = 0; \quad k = 1 \ to \ c \end{aligned}$$

- Nonnegativity of Lagrange multipliers for inequalities:

$$\begin{aligned} \tilde{\lambda} &\geq 0; \quad j = 1 \ to \ b \\ \hat{\lambda} &\geq 0; \quad k = 1 \ to \ c \end{aligned}$$

- Regularity check: The gradients of active constraints must be linearly independent. In this scenario, the Lagrange multipliers for the constraints are unique.

Example: [78] The tank is closed at both ends and is required to have volume V. The radius R and height H are selected as design variables. It is desired to design the tank having minimum surface area A.

$$\textbf{Optimal Problem} = \begin{cases} \mathcal{F}_A = 2\pi R(R+H) \\ s.t.\ G = \pi R^2 H - V = 0 \end{cases}$$

where R and H are design variables.

Solution:

$$\mathcal{L} = 2\pi R(R+H) + \lambda(\pi R^2 H - V)$$

$$\frac{\partial \mathcal{L}}{\partial R} = 2\pi(R(2+\lambda H) + H) = 0$$

$$\frac{\partial \mathcal{L}}{\partial H} = \pi R(2+\lambda R) = 0$$

$$\frac{\partial \mathcal{L}}{\partial \lambda} = \pi R^2 H - V = 0$$

Note that there are three equations with three unknowns (R, H and λ) and solved by the elimination process, giving the optimal solution as

$$\mathcal{F}_A^\star = 3\left(\frac{V}{2\pi}\right)^{0.67}; \quad R^\star = \left(\frac{V}{2\pi}\right)^{0.33}; \quad H^\star = \left(\frac{4V}{\pi}\right)^{0.33}; \quad \lambda^\star = -\frac{1}{\pi R^\star}$$

4.1.1.2 Dynamic optimization

Dynamic optimization is associated with the control of a plant or system under dynamic conditions, which implies that the system's trajectories vary over time, and therefore time is incorporated into the system's description and optimization. The plant is then characterized by a differential or difference equation. Dynamic programming, variational calculus, the Pontregian principle, and search techniques

are popular methods for dealing with dynamic optimization problems. Before delving into the specifics of dynamic optimization, it is necessary to understand the distinction between the terminology trajectory optimization and optimal control. In the realm of dynamic optimization, these two concepts are often used interchangeably. In the situation of trajectory optimization, where the system's inputs do not directly accommodate the provided performance index (pure function of states), it is intended to establish such values of these inputs that result in such trajectories that optimize the performance index.

On the other hand, in the case of optimal control, system inputs are fed into the cost function, with the aim of discovering the exact input and trajectory that optimizes a specified performance index. While a trajectory optimization is a function optimization problem and optimal control is a functional optimization problem [79]. However, in both cases the inputs are functions of time. Analytical and numerical approaches are used to solve dynamic optimization issues, and numerical methods are further subdivided into indirect methods [80], direct methods [81], and dynamic programming [82], and classification is expressed in Fig.4.2.

In the indirect method (i.e. optimize then discretize), the calculus of variations is employed to derive the first order necessary conditions of the dynamic optimization problem. The indirect approach leads to first evaluating the necessary conditions, and then trying to solve the boundary value problem by solving the system of differential equations, and when the necessary conditions are satisfied, it results in candidate optimal trajectories called extremals [83].

Each computed extremal is then analyzed to determine whether it is a local minimum, maximum, or saddle point, and the local minimum solution with the lowest cost is preferred. Pontregin's minimum principle is an example of an indirect method that solves a two point boundary value problem. Nevertheless, the indirect method has the disadvantages of complex computations and high sensitivity to the initial conditions of the dynamic system, which restricts its application.

In the direct method (i.e. discretize then optimize), the control variables (shooting or multiple shooting) or control and state variables (global collocation or local

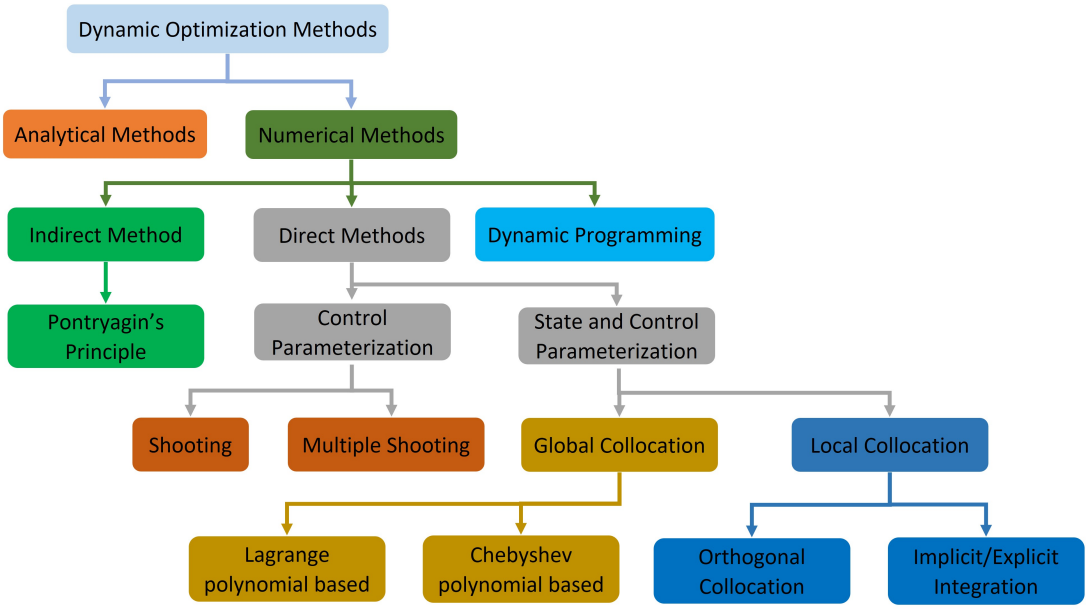

FIGURE 4.2: Classification of dynamic optimization methods.

collocation) of an optimal control problem are discretized into equal or unequal configurations and the problem is then modeled as a nonlinear optimization problem or Nonlinear Programming problem (NLP). The NLP is then solved using gradient-based techniques to arrive at the optimum.

The main advantage of the direct method is that it transforms an infinite-dimensional optimization problem into a finite-dimensional optimization problem, the necessary conditions are avoided, and the parameterized variables are directly calibrated to optimize the performance index.

The shooting method is based on estimating the value of the unknown boundary condition at one end of the interval. Whereas an initial value problem is solved to obtain a solution at the other end of a predetermined interval. Although the shooting method is easy to put into action and it is ineffective when the dynamic system is ill-defined or stiff, especially when the optimal control problem is sensitive and complicated [84].

To combat this limitation of the shooting method, multiple shooting method is employed, particularly breaking the time vector into additional sub-intervals and applying the shooting method to each of these intervals [85]. The class of collocation methods [86] is most robust against boundary value problems and rapidly

converging ones, where piecewise polynomials are implemented to parametrize the state and control variables, and means of root-finding techniques are utilized to solve a dynamic system.

While dynamic programming utilizes the concept of multistage decision-making problems, and it follows Bellman's optimality principle [87] to solve the optimization problem of any complex dynamical system.

Optimal Control

Determining the control vector profile $[u(t), \forall\, t_0 \leq t \leq t_f]$ of a given dynamic system that drives the states from their initial conditions $x(t_0)$ to their final conditions $x(t_f)$, while simultaneously maximizing or minimizing the objective functional $\mathcal{J}$ is defined as an optimal control problem, and the resulting control vector that executes the state profile $[x(t), \forall\, t_0 \leq t \leq t_f]$ is referred to as an optimal trajectory. A cost function or cost functional can be defined as follows:

- The objective functional indicates the costs or benefits of the dynamic system to prevent or achieve a desired physical state.
- The cost function quantifies the penalty that a dynamic system remunerates as a result of deviation from the ideal physical state.
- A cost function can also indicate the time it takes to transition from the state's beginning to final values.
- A positive cost might be interpreted as a negative benefit, and vice versa.

Typically, the objective of optimal control is to identify the control history $[u(t)$ $\forall\, t_0 \leq t \leq t_f]$ that minimizes the cost function, however, another method to represent the same problem is to strive to maximize the cost function with the opposite sign.

The objective function can generally be defined in three different forms that are easily interchangeable. The cost function with only terminal penalties, proposed

in 1890, is the Mayer cost function written in (4.4) and can be visualized in Fig.4.3.

$$\mathcal{J} = \mathcal{O}[x_{t_f}, t_f] \tag{4.4}$$

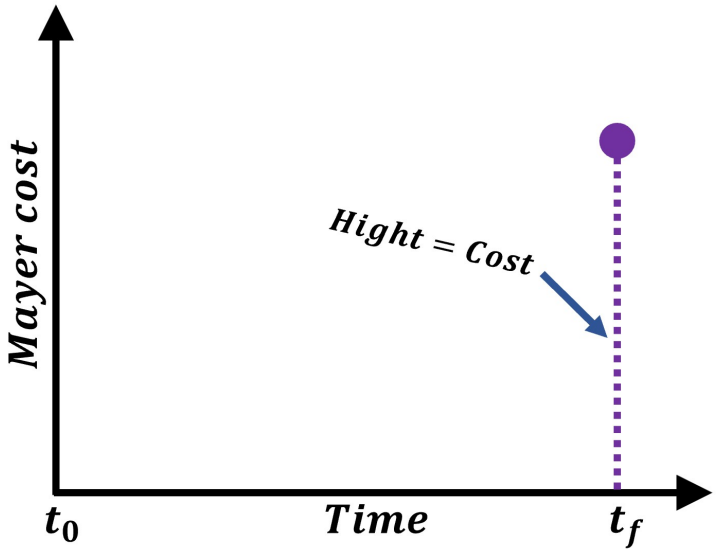

FIGURE 4.3: Mayer cost function

A cost function that incurs a penalty during the running time, proposed in 1780, is known as the Lagrange cost function denoted in (4.5) and is graphically illustrated in Fig.4.4.

$$\mathcal{J} = \int_{t_0}^{t_f} \mathfrak{O}(x(t), u(t), t)dt \tag{4.5}$$

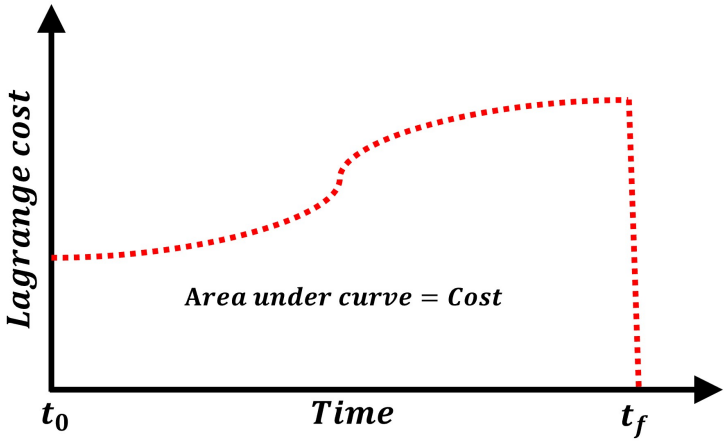

FIGURE 4.4: Lagrange cost function

A cost function based on the combination of terminal and running costs proposed in 1900 is known as the Bolza cost function in (4.6) and is shown diagrammatically in Fig.4.4.

$$\mathcal{J} = \mathcal{O}[x_{t_f}, t_f] + \int_{t_0}^{t_f} \mathfrak{O}(x(t), u(t), t)dt \tag{4.6}$$

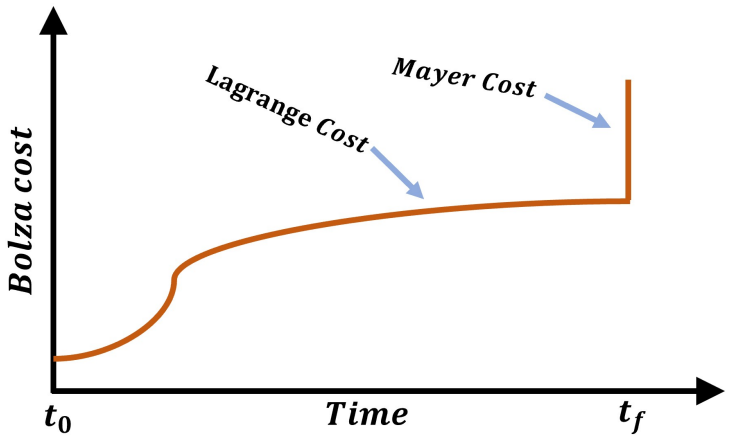

FIGURE 4.5: Bolza cost function

Here t represents the independent time variable, t_0 and t_f denote the initial and final time of the process, respectively, and $x(t) \in \Re^{n^x}$ is a vector of state variables, $u(t) \in \Re^{n^u}$ denotes a vector of control variables that need to be optimized. $\mathcal{J}$, $\mathcal{O}$ and $\mathfrak{O}$ are then real-valued functions (functionals) while $\mathcal{O} : \Re^{n^x} \times \Re \to \Re$ and $\mathfrak{O} : \Re^{n^x} \times \Re^{n^u} \times [t_0 \ t_f] \to \Re$.

Physical constraints of the dynamic system or design specifications of the optimization problem may affect the choice of the cost function. Optimal control tasks can generally be identified by fixed, free, initial, terminal, time, and/or state.

The initial time and states are usually fixed because it is a natural phenomenon whether or not each system has stored energy at the beginning (initial time) of the process. Nonetheless, a schematic depiction of the typical optimal control tasks is presented in Figs.4.6, 4.7, 4.8 and 4.9. Using any objective function (Mayer, Lagrange, Bolza), optimal control problems are elaborated in terms of typical tasks such as terminal problem, minimum time problem, and quadratic problem.

- Control effort problem

$$\mathcal{J} = \int_{t_0}^{t_f} u^2 \, dt \tag{4.7}$$

The main objective of this problem is to minimize or maximize the control effort (energy or load on the actuator) required to drive from an initial state x_{t_0} to a specified x_{t_f} or an unspecified state $x_{t_{f(free)}}$ in a known t_f or unknown time $t_{f(free)}$ and can be visualized in Figs. 4.6 and 4.7.

- Minimum time problem

$$\mathcal{J} = \int_{t_0}^{t_f} dt \tag{4.8}$$

This is historically the first optimal control problem and a kind of trajectory optimization problem (brachistochrone problem proposed by Johan Bernoulli). Neutralizing a target with a missile and reaching a destination with an automobile are examples of the minimum time problem.

The problem is to find an appropriate control vector that pushes the system from a predetermined initial state x_{t_0} to a fixed (predetermined) final state x_{t_f} in the minimum possible time. Time optimal trajectory between x_{t_0} and x_{t_f} can be seen diagrammatically in Fig.4.7.

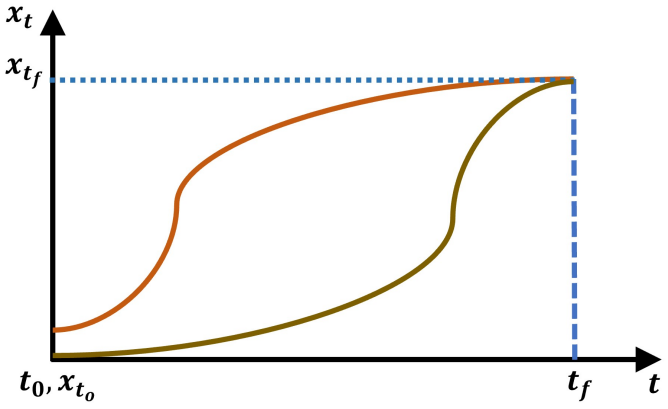

FIGURE 4.6: Fixed terminal state and time

- Terminal problem

$$\mathcal{J} = \|x_f - x_{t_f}\| \tag{4.9}$$

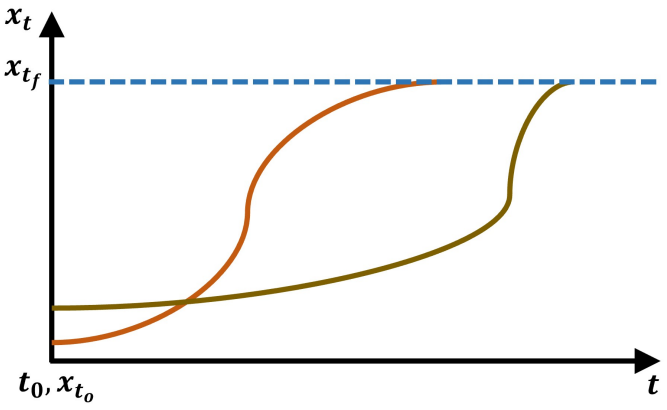

FIGURE 4.7: Fixed terminal state and free time

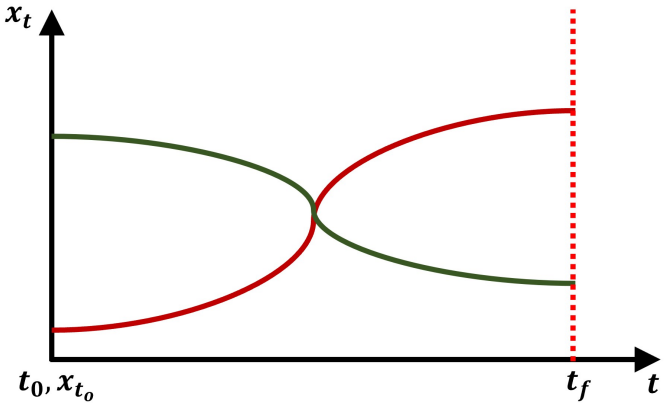

FIGURE 4.8: Free terminal state and fixed terminal time

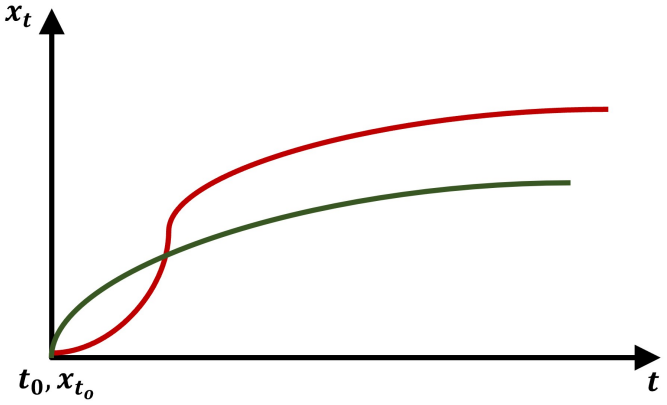

FIGURE 4.9: Free terminal state and time

This is an example of the homing problem for a stationary target, which represents minimizing the distance or range between desired and achieved.

The primary goal of this optimum problem is to directly describe the objective of the dynamic system to be maximized or decreased and graphically it

is represented by Figs.4.8 and 4.9.

- Linear quadratic problem

$$\mathcal{J} = 0.5 \int_{t_0}^{t_f} x^T \mathcal{Q} x + u^T \mathcal{R} u \, dt \tag{4.10}$$

Rudolf Kalman presented this problem for linear dynamic systems. $\mathcal{Q}$ and $\mathcal{R}$ are symmetric positive semi-definite and positive definite matrices, respectively. $\mathcal{Q}$ induces the state to move from x_{t_0} to the origin (zero) as quickly as possible and $\mathcal{R}$ ensures that this transition should be done with minimum control effort.

For this type of problem, the terminal time is usually defined, and then the objective is to choose an acceptable state presented in Fig.4.8 that minimizes the functional. This sort of functional is employed in the closed-loop optimality problem, which also ensures the closed-loop control's Lyapunov-based stability.

Constraints bind the system not to exceed its physical limits, provide safety or environmental protection, and define specific set points in the control loop. Constraints also help optimization methods to search the optimization search space and take various forms, such as equality and inequality constraints.

- Equality constraint

$$\mathfrak{h}(x, u, t) = 0 \qquad \forall\, t \in [t_{p0}, t_{pf}], [t_{p0}, t_{pf}] \subseteq [t_0, t_f] \tag{4.11}$$

This is referred to as a hard constraint and is usually an example of formation control that requires a constant distance at all times.

- Inequality constraint

$$\mathfrak{g}(x, u, t) \leq 0 \qquad \forall\, t \in [t_{p0}, t_{pf}], [t_{p0}, t_{pf}] \subseteq [t_0, t_f] \tag{4.12}$$

Inequality constraint is also of great practical interest because it can represent a limit on the system's state that should not be exceeded. Conventionally, such constraints are called soft constraints or box constraints of the form $x \in [x_{min},\, x_{max}]$, where x_{min} and x_{max} denote lower and upper bounds on x respectively.

In dynamic optimization, the dynamic system, a continuous time-dependent model, represents an additional set of equality constraints because it typically composes of a set of ordinary differential equations, and/or functional equations that, if satisfied during optimization, provide a mathematical representation of the phenomena occurring in the dynamic system.

$$\dot{x} = f(x, u, t) \qquad \forall\, t \in [t_{p0}, t_{pf}], [t_{p0}, t_{pf}] \subseteq [t_0, t_f] \tag{4.13}$$

Here the vector function f is defined as $f : \Re^{n^x} \times \Re^{n^u} \times [t_{p0}, t_{pf}] \subseteq [t_0, t_f] \rightarrow \Re^{n^x}$ If the trajectory x_t meets the initial condition $x_{t_0} = x_0$. After defining the cost functions, constraints, and dynamic system, a general form of the optimal control problem can be conceptualized as follows:

$$\begin{aligned}
&\mathcal{J} = min\{\mathcal{O}[x_{t_f}, t_f] + \int_{t_0}^{t_f} \mathfrak{O}(x(t), u(t), t)dt\} \\
&\dot{x} = f(x, u, t) \quad \forall\, t \in [t_{p0}, t_{pf}], [t_{p0}, t_{pf}] \subseteq [t_0, t_f] \\
&x_{t_0} = x_0 \\
&\mathfrak{h}(x, t) = 0 \qquad \forall\, t \in [t_{p0}, t_{pf}], [t_{p0}, t_{pf}] \subseteq [t_0, t_f] \\
&\mathfrak{g}(x, t) \leq 0 \qquad \forall\, t \in [t_{p0}, t_{pf}], [t_{p0}, t_{pf}] \subseteq [t_0, t_f] \\
&u_{min} \leq u(t) \leq u_{max}
\end{aligned} \tag{4.14}$$

To compute this problem, the necessary conditions are determined, and already existing techniques, such as indirect or direct methods, can be employed to discover the optimal control. To minimize the problem, the function can be combined with the system (4.13) introducing vectors of the adjoint variables $\lambda(t) \in R^{nx}$ (adjoint variables are sometimes called co-state variables). Similarly to the Lagrange

function in static optimization, a function called Hamiltonian $\mathcal{H}$ is introduced for dynamic optimization.

$$\mathcal{H} = \mathfrak{O}(x(t), u(t), t) + \lambda^T(t) f(x, u, t) \tag{4.15}$$

Using this notation, the necessary conditions can be deduced based on a few assumptions.

- The initial time is usually fixed ($t_0 = 0$).
- The initial conditions of dynamic system are mostly fixed ($x_{t_0} = x_0$).

The following are the necessary conditions for optimality:

- Optimal state equation

$$\dot{x}^* = \frac{\partial \mathcal{H}}{\partial \lambda} \qquad \forall t \in [t_0, t_f] \tag{4.16}$$

- Co-state equation

$$\dot{\lambda} = -\frac{\partial \mathcal{H}}{\partial x} \qquad \forall t \in [t_0, t_f] \tag{4.17}$$

- Optimal control equation

$$0 = \frac{\partial \mathcal{H}}{\partial u} \qquad \forall t \in [t_0, t_f] \tag{4.18}$$

The following are the boundary conditions for specified and unspecified terminal times:

- Co-state boundary condition

$$\begin{aligned} \lambda_{t_f} &= 0 \qquad if \qquad x(t_f) = free \\ \lambda_{t_f} &= free \qquad if \qquad x(t_f) = x_{t_f} \end{aligned} \tag{4.19}$$

- Transversality condition

$$\mathcal{H}(t_f) + \frac{\partial \mathcal{O}}{\partial t_f} = 0 \tag{4.20}$$

For inequality constraints, $\mathcal{H}$ can be expressed as

$$\mathcal{H} = \mathfrak{O}(x(t), u(t), t) + \lambda^T(t) f(x, u, t) + \mu^T \mathfrak{g} \begin{cases} \mu = 0 \;\; if \;\; \mathfrak{g} < 0 \\ \mu \geq 0 \;\; if \;\; \mathfrak{g} = 0 \end{cases} \tag{4.21}$$

The necessary conditions for inequality constraints are as follows:

- Optimal state equation

$$\begin{aligned} \dot{x}^* &= \frac{\partial \mathcal{H}}{\partial \lambda} \qquad if \;\; \mathfrak{g} < 0 \\ \dot{x}^* &= \frac{\partial \mathcal{H}}{\partial \lambda} \qquad if \;\; \mathfrak{g} = 0 \end{aligned} \tag{4.22}$$

- Co-state equation

$$\begin{aligned} \dot{\lambda} &= -\left(\frac{\partial \mathfrak{O}}{\partial x}\right)^T - \left(\frac{\partial f}{\partial x}\right)^T \lambda \qquad\qquad\qquad if \;\; \mathfrak{g} < 0 \\ \dot{\lambda} &= -\left(\frac{\partial \mathfrak{O}}{\partial x}\right)^T - \left(\frac{\partial f}{\partial x}\right)^T \lambda - \left(\frac{\partial \mathfrak{g}}{\partial x}\right)^T \mu \quad if \;\; \mathfrak{g} = 0 \end{aligned} \tag{4.23}$$

- Optimal control equation

$$\begin{aligned} 0 &= \left(\frac{\partial \mathfrak{O}}{\partial u}\right)^T + \left(\frac{\partial f}{\partial u}\right)^T \lambda \qquad\qquad\qquad if \;\; \mathfrak{g} < 0 \\ 0 &= \left(\frac{\partial \mathfrak{O}}{\partial u}\right)^T + \left(\frac{\partial f}{\partial u}\right)^T \lambda + \left(\frac{\partial \mathfrak{g}}{\partial u}\right)^T \mu \quad if \;\; \mathfrak{g} = 0 \end{aligned} \tag{4.24}$$

A sufficient condition that tells about maximization or minimization is as follows:

$$\begin{aligned} \frac{\partial^2 \mathcal{H}}{\partial u^2} &> 0 \qquad Minimum \;\; optimal \;\; control \\ \frac{\partial^2 \mathcal{H}}{\partial u^2} &< 0 \qquad Maximum \;\; optimal \;\; control \end{aligned} \tag{4.25}$$

Pontryagin's Minimum Principle (PMP) calculates the control by necessary conditions of optimality, and consequential control is the solution to the optimal control problem. PMP solves necessary conditions by considering the Two Point Boundary Value Problem (TPBVP) (the initial conditions and boundary conditions form the TPBVP) since system dynamics are solved in a forward fashion by considering

initial conditions, and co-state equations are computed in a backward fashion by employing boundary conditions of co-state. The PMP solution is mostly a combination of Control Vector Iteration (CVI) and Boundary Condition Iteration (BCI) [88].

The TPBVP solution is employed in the CVI approach by estimating the control vector using the maximum optimal control sensitivity (4.18) or (4.24), and the new estimate u^{k+1} is obtained by applying the adaptation formula using the old control vector u^k.

$$u^{k+1} = u^k - \mathfrak{W}\frac{\partial \mathcal{H}}{\partial u} \tag{4.26}$$

where $\mathfrak{W} \in [0, 1]$ is a adapting rate. CVI is initialized by the guess u_0, and then the dynamic system is solved by forward integration, followed by backward integration of the co-state equations. Finally, the whole procedure is repeated until the optimal condition (4.18) or (4.24) is satisfied. CBI solves the TPBVP by the successive update of the guesses for boundary conditions (4.19).

$\lambda^0(t_f)$ requires no initial guess (4.17) if the terminal state is free and the co-state equation is integrated in a backward manner. Initially, the guess $\lambda^0(t_0)$ is used to integrate the co-state equation in a forward manner with time if the terminal state of the dynamic system is fixed.

If co-state equations are in disagreement, a new guess of initial conditions for $\lambda^0(t_0)$ is made and the whole procedure is repeated until they are equal within the specified tolerance.

PMP has some disadvantages that limit the implementation options for dynamic optimization problems.

- The necessary conditions and transversality condition require detailed knowledge of the system and it may be difficult to construct H_x and H_u for the system if any variation occurs.
- Very sensitive for boundary conditions.
- The numerical solution of co-state equations can be very ill-conditioned.

- Because of the box constraints (path constraints), the complexity to solve $\mathcal{H}$ increases.

Example: The state equations for a continuous stirred-tank chemical reactor are given below [88].

$$\dot{x}_1 = -0.5 - 2x_1 + (0.5 + x_2)e^{\left(\frac{25x_1}{2+x_1}\right)} - (0.25 + x_1)u$$
$$\dot{x}_2 = 0.5 - x_2 - (0.5 + x_2)e^{\left(\frac{25x_1}{2+x_1}\right)}$$

Here the states of the plant are x_1 is the deviation from the steady-state temperature and x_2 is the deviation from the steady-state concentration.

u represents the effect of coolant flow on the chemical reaction with $0 \leq u \leq 1.2$ and initial conditions are $x_{t_0} = [0.05 \quad 0]^T$.

The performance measure to be minimized is

$$\mathcal{J} = \int_0^{0.8} (x_1^2 + x_2^2 + 0.1u^2)dt$$

Solution:

Hamiltonian $\mathcal{H}$ function for this problem is expressed as

$$\mathcal{H} = x_1^2 + x_2^2 + 0.1u^2 + \lambda_1(-0.5 - 2x_1 + (0.5 + x_2)e^{\left(\frac{25x_1}{2+x_1}\right)}$$
$$- 0.25u + ux_1) + \lambda_2(0.5 - x_2) - \lambda_2(0.5 + x_2)e^{\left(\frac{25x_1}{2+x_1}\right)}$$

The co-state equations are determined from the $\mathcal{H}$ as

$$\dot{\lambda}_1 = -\frac{\partial \mathcal{H}}{\partial x_1} = -2x_1 + 2\lambda_1 - \lambda_1(0.5 + x_2)\left(\frac{50}{(2+x_1)^2}\right)e^{\left(\frac{25x_1}{2+x_1}\right)}$$
$$+ \lambda_2 u + \lambda_2(0.5 + x_2)\left(\frac{50}{(2+x_1)^2}\right)e^{\left(\frac{25x_1}{2+x_1}\right)}$$

$$\dot{\lambda}_2 = -\frac{\partial \mathcal{H}}{\partial x_2} = -2x_2 - \lambda_1 e^{\left(\frac{25x_1}{2+x_1}\right)} + \lambda_2 + \lambda_2 e^{\left(\frac{25x_1}{2+x_1}\right)}$$

Optimal control relation is expressed as

$$\frac{\partial \mathcal{H}}{\partial u} = 0.2u - \lambda_1(x_1 + 0.25) = 0$$
$$u^* = 5\lambda_1(x_1 + 0.25)$$
$$\frac{\partial^2 \mathcal{H}}{\partial u^2} = 0.2 > 0$$

Since the final states are free and not explicitly present in the performance measure, the boundary conditions at $t = t_f$ are $\lambda(t_f) = 0$, and optimal states profiles in Fig. 4.10, co-states in Fig. 4.11, $\mathcal{H}$ function profile in Fig. 4.12, and optimal control profile in Fig. 4.13 can be visualized.

4.2 Problem Formulation

After discussing static and dynamic optimization in the preceding section, now the dynamic optimization problem for SUGV is formulated. When SUGV starts gliding from dispersion points (dropping parameters from the carrier platform) eventually it strikes the ground after covering some range. Gliding flight is directly related to endurance because it must stay in the air longer to achieve maximum range.

Consequently, achieving the maximum range becomes a combination of time optimization and a trajectory optimization problem. To deal with the time optimization problem especially where the terminal time is undetermined, time scaling approach is employed [89], and this approach is very acceptable for direct methods [90].

In this scheme, the time domain is transformed to a new fixed domain and this conversion is illustrated in Fig.4.14. The time scaling approach has the following relation.

$$\frac{dt}{d\tau} = \tan \mathfrak{T} = \mathfrak{P} \tag{4.27}$$

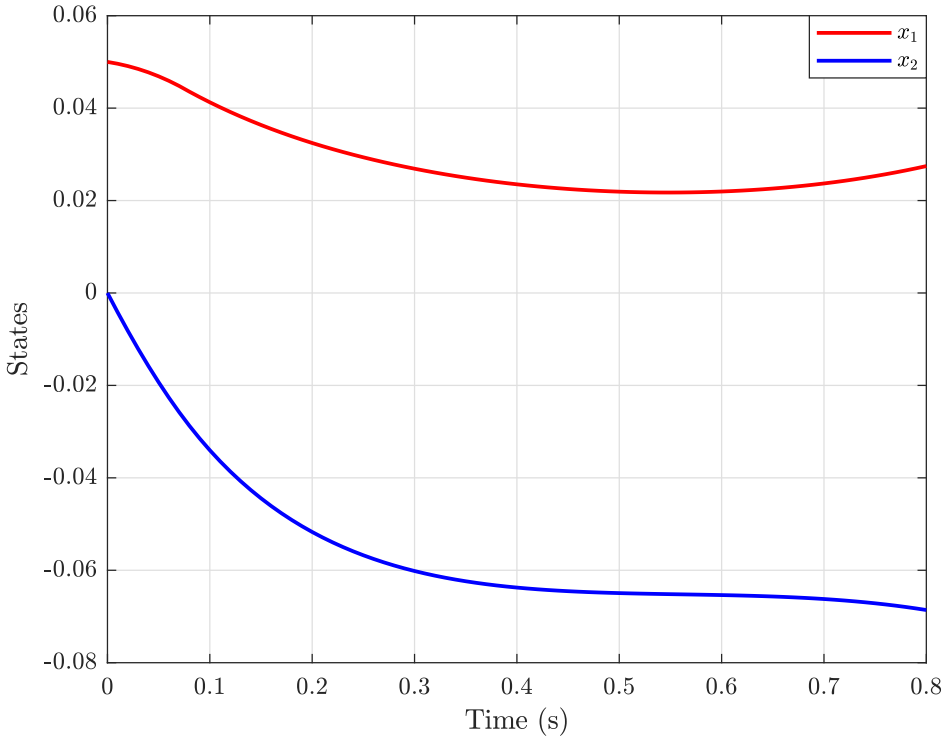

FIGURE 4.10: Optimal states.

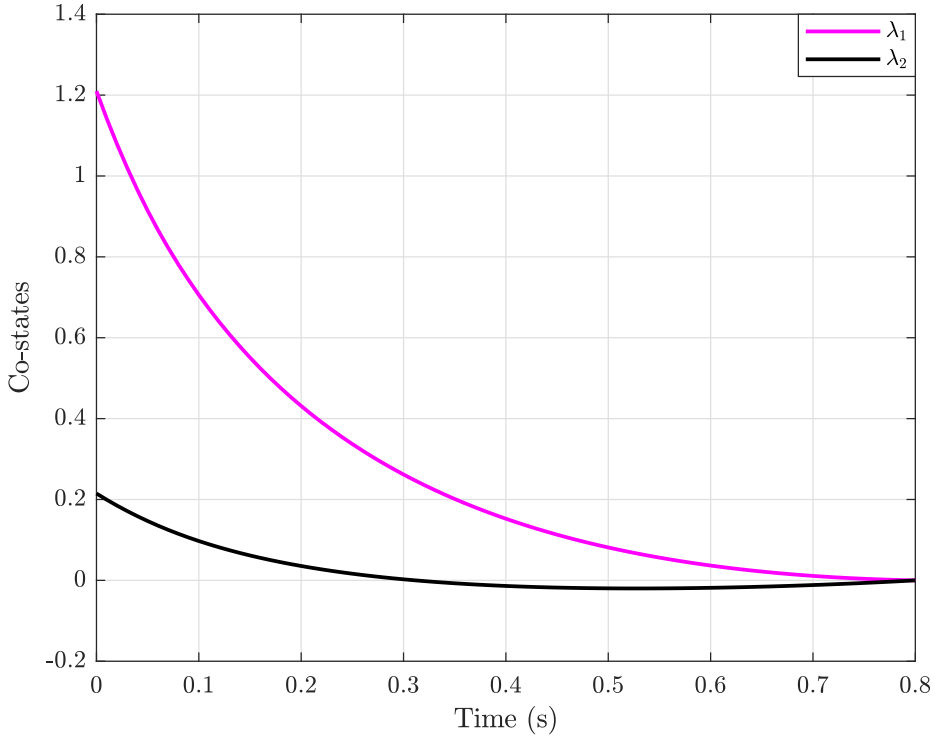

FIGURE 4.11: Co-states.

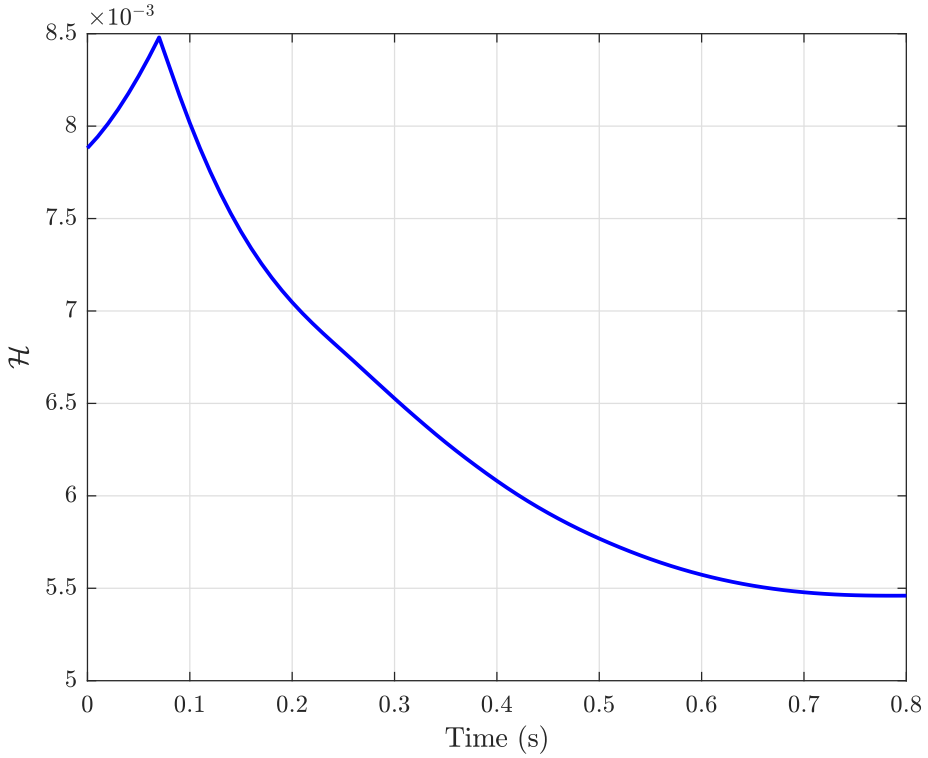

FIGURE 4.12: $\mathcal{H}$ function.

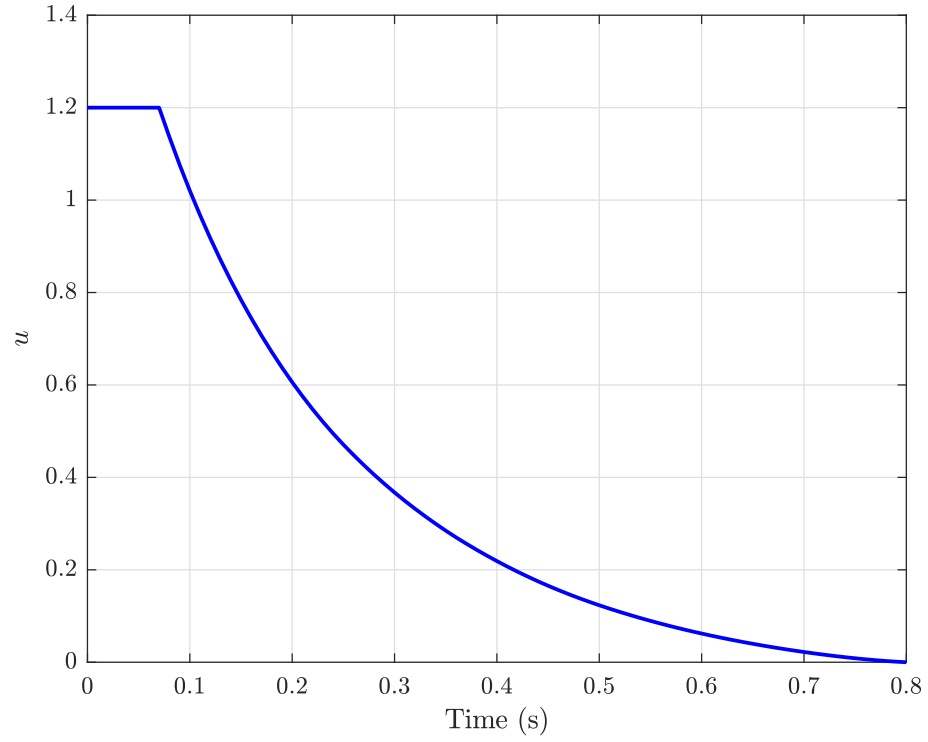

FIGURE 4.13: Optimal control.

where τ goes from *0* to *1* and $\mathfrak{P}$ is $(t_f - t_0)$, a positive constant to be determined, called the time scaling parameter. Thus, the modified optimization problem is

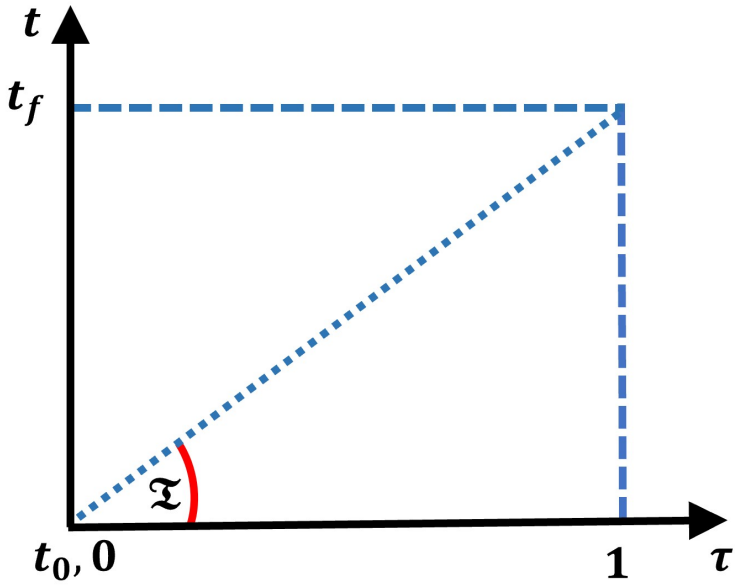

FIGURE 4.14: Time scaling approach [64].

formulated as follows:

$$\begin{aligned} \dot{x}^* &= \mathfrak{P} f(\tau, x, u,), \quad x_{\tau_0} = x_0 \\ \mathcal{J}^* &= \mathcal{O}[x_{\tau_f}, \tau_f] + \mathfrak{P} \int_0^{\tau_f} \mathfrak{O}(x(\tau), u(\tau), \tau) d\tau \end{aligned} \tag{4.28}$$

Here $\dot{x}^*$ is $\dfrac{dx}{d\tau}$. This transformation adds $\mathfrak{P}$ as an additional variable to the optimization problem and can be calculated by considering an additional control variable or optimal parameter [91]. Due to $\mathfrak{P}$, the computational burden and complexity of the optimization problem increase.

Hence to avoid the time scaling approach for achieving the maximum range of SUGV, an altitude dependent maximum stoppable time optimal problem is formulated in [92]. Consider the nonlinear SUGV system

$$\dot{X} = f(X, u) \quad t_0 \leq t_s \leq t_m \tag{4.29}$$

$$X^o = X(t_0) \tag{4.30}$$

where $X = (V, \alpha, Q, \theta, R, h)^T \in \Re^6$, X^o is the initial state, t_0 is the starting time, and t_m is the maximum stoppable time. For a nonlinear system, the stopping manifold is defined as follows [93]:

$$S_m = \{\Delta(X) = 0, X \in \Re^6\} \tag{4.31}$$

where Δ is a continuously differentiable function. When the system reaches the manifold S_m, it comes to a halt, and the time it took to get there is referred to as the stopping time t_s, which relies on the stopping constraint. A graphical representation of S_m and t_s is shown in Fig.4.15. Here, t_s is an implicit function

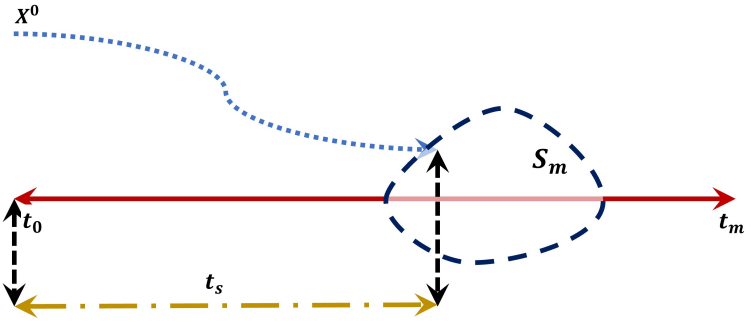

FIGURE 4.15: Stopping manifold.

of the control input u, since any change in u impacts the state response, resulting in a change in t_s. The stopping time is determined as follows:

$$\tau_u = \{t_0 < t \leq t_m,\ X(t|u) \in S_m\} \tag{4.32}$$

$$t_s = \inf_t \{\tau_u\} \tag{4.33}$$

Any $t_s \in \tau_u$ is expressed as an admissible stopping time, and if $t_s \leq t_m$, then the stopping constraint is computed as follows:

$$\Delta(X(t_s))|_{\tau_u} = 0 \tag{4.34}$$

A performance index for t_s is established as follows:

$$J = \int_{t_0}^{t_s} X(t)\ dt \tag{4.35}$$

Constraints on the states and control input are expressed as

$$x^L \leq X(t) \leq x^U \quad \forall\, t \in (0, t_s \leq t_m) \tag{4.36}$$

$$u^L \leq u(t) \leq u^U \quad \forall\, t \in (0, t_s \leq t_m) \tag{4.37}$$

where x^L, u^L and x^U, u^U are the lower and upper constraints on the states and control input, respectively.

4.2.1 Performance Index

The fundamental goal of unpowered gliding flight is to maximize the SUGV's gliding range, and for this purpose, a Lagrange performance index is illustrated:

$$J = max \int_{t_0}^{t_s} V \; dt \tag{4.38}$$

A subsidiary state is suggested to avoid integral complexity in the performance index:

$$\dot{\aleph} = V \quad \forall\, t \in (0, t_s \leq t_m) \tag{4.39}$$

After augmenting (4.39) with the longitudinal dynamics of a SUGV, the performance index can be expressed in Mayer form as follows:

$$J_{\aleph} = max \; \aleph(t_s) \tag{4.40}$$

4.2.2 Constraints

Let α be significant during gliding flight for an SUGV. If it is small, then it causes a free fall condition, and if it is large, then it creates a stall condition. Therefore, α needs to be limited. Furthermore, Q aids in the reduction in fluctuations produced by flight transition and offers stability during gliding flight. Therefore, a constraint on Q is required to decrease the influence of fluctuations. To achieve damped

gliding flight, both constraints are implemented, and these constraints are

$$\alpha^L \leq \alpha(t) \leq \alpha^U \quad \forall\, t \in (0, t_s \leq t_m) \tag{4.41}$$

$$Q^L \leq Q(t) \leq Q^U \quad \forall\, t \in (0, t_s \leq t_m) \tag{4.42}$$

where α^L, Q^L, α^U, and Q^U are the lower and upper constraints on α and Q, respectively. The Load Factor (LF) ensures the wing-level flight by imposing the constraint during gliding flight so that steady gliding flight can be obtained.

Therefore, a constraint on LF is employed to assure a steady gliding flight and is defined as

$$LF = \frac{\sqrt{(L(t))^2 + (D(t))^2}}{W} \leq LF_{max} \quad \forall\, t \in (0, t_s \leq t_m) \tag{4.43}$$

where L, D, and W are lift force, drag force and weight, and LF_{max} is the maximum value of LF. A constraint on elevator deflection is applied to elude the stall condition during gliding flight as follows:

$$\delta_e^L \leq \delta_e(t) \leq \delta_e^U \quad \forall\, t \in (0, t_s \leq t_m) \tag{4.44}$$

where δ_e^L and δ_e^U are the lower and upper bounds on the elevator deflection, respectively. The height from the dispersion point steadily decreases to zero until the SUGV strikes the earth.

As a result, in this study, the height is regarded a stopping constraint.

$$h(t_s) = 0 \tag{4.45}$$

4.3 Control Vector Parameterization

In this section, the concept of control vector parameterization (CVP) with uniform and non-uniform subintervals is discussed. Sargent [94] introduced the CVP approach and he also employed it to solve dynamic optimization problems. CVP is

a very straightforward notion because the time vector of an optimization problem is broken into a predetermined number of subintervals, the beginning and end of which are referred to as nodes in the CVP process. Then, the control variables are selected at certain nodes, known as nodal control variables. The control profile is then built using a spline or interpolation approach, such as piecewise linear polynomials or piecewise constant functions.

After this, the dynamic model is integrated, referred to as the Initial Value Problem (IVP). After computing the IVP, the nodal control variables are subjected to a nonlinear programming approach in order to optimize the problem. The transformation of the infinite-dimension optimization problem into a finite-dimension optimization problem by taking into account a predefined number of nodal control variables is a key feature of CVP.

A generic description of the CVP procedure is given below:

(i) Specify the desired $N > 1$ number of nodes and split the supplied time vector t_m into $N - 1$ subintervals:

$$t_i = t_0 < t_1 < t_2 < \cdots < t_{N-1} = t_m$$

The nodal time $t_i, i = 0, 1, 2, \ldots N - 1$ may be uniform or non-uniform.

(ii) At each node, make an initial guess for the control variable. The following control vector (CV) $u(t)$ is expressed as

$$u(t) = [\overline{u}_0, \overline{u}_1, \overline{u}_2, \ldots \overline{u}_{N-1}]$$

where $\overline{u}_i, i = 0, 1, 2, \ldots N - 1$ is a nodal control variable.

(iii) Use an interpolation polynomial to approximate the CV profile.

(iv) Solve the IVP by considering the approximated CV profile.

(v) Compute the performance index as well as the constraints. If the performance index and constraints are satisfied, then the output will be the optimal solution; otherwise, proceed to step (iii) after optimizing the nodal control variables with any suitable optimizer.

Fig.4.16 depicts a flowchart describing the CVP implementation process.

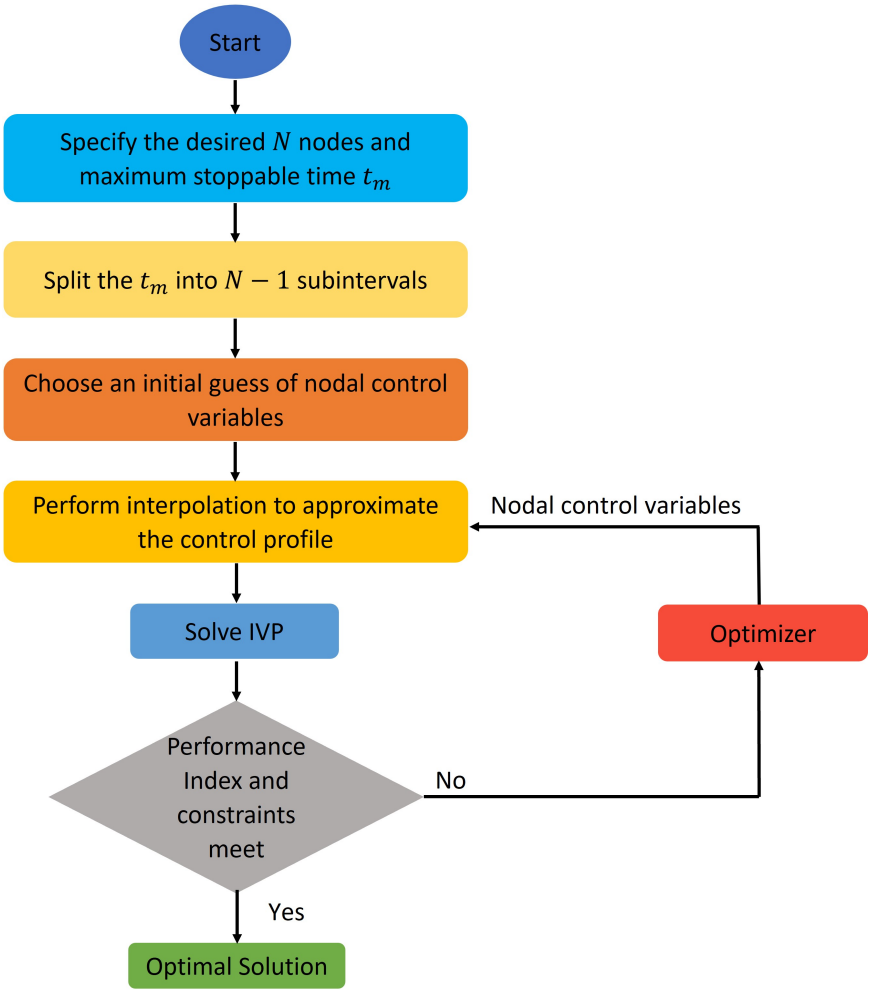

FIGURE 4.16: CVP flowchart.

4.3.1 Uniform CVP

We will provide a brief overview of the uniform subinterval method for CVP in this subsection. This method divides the time vector $t \in (t_o, t_m)$ into $N-1$ subintervals

for the maximum stoppable time t_m. For a uniform subinterval, the subinterval size d_e is assessed as follows:

$$d_e = \frac{t_m - t_0}{N-1} \tag{4.46}$$

Consequently, the nodal times t_i for a uniform time vector are determined as follows:

$$t_i = t_o + id_e \quad i = 0, 1, 2, \ldots, N-1 \tag{4.47}$$

In Fig.4.17, the uniform CV approach with nodal times $(t_o, t_1, \ldots, t_m)$ and nodal control variables $(\overline{u}_0, \overline{u}_1, \overline{u}_2, \ldots \overline{u}_{N-1})$ at uniform subintervals are graphically depicted.

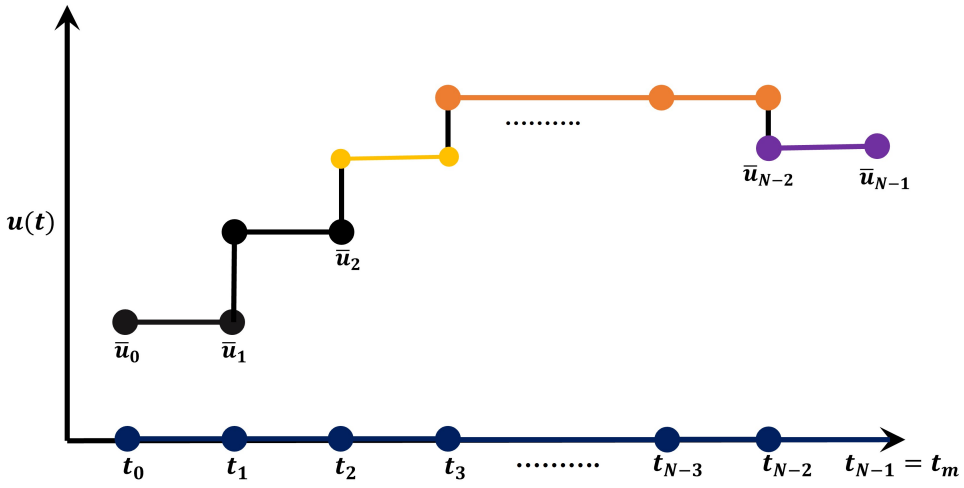

FIGURE 4.17: Uniform CVP.

4.3.2 Non-Uniform CVP

After the acquisition of the dispersion points, the SUGV enters the disequilibrium phase, and fluctuations occur during gliding as a result of this phase change. Fast damping may be performed quickly to lessen fluctuations by establishing constraints on α and Q.

To achieve a steady glide path, the load factor is also crucial. Consequently, a non-uniform CVP strategy is required to more effectively address these problems. On

the foundation of the idea of exponential spacing as pictorially shown in Fig.4.18 , a new formulation for non uniform subintervals is presented.

According to this formulation, the time vector $t \in (t_o, t_m)$ is broken into $N-1$ subintervals, and low spacing happens at the beginning of the time vector, whereas large spacing occurs toward the end.

Assume that μ_o and $log_{10}(\chi)$ represent the lower and upper bounds of an exponential curve 10^a in a logarithmic scale. For computing the logarithmic vector,

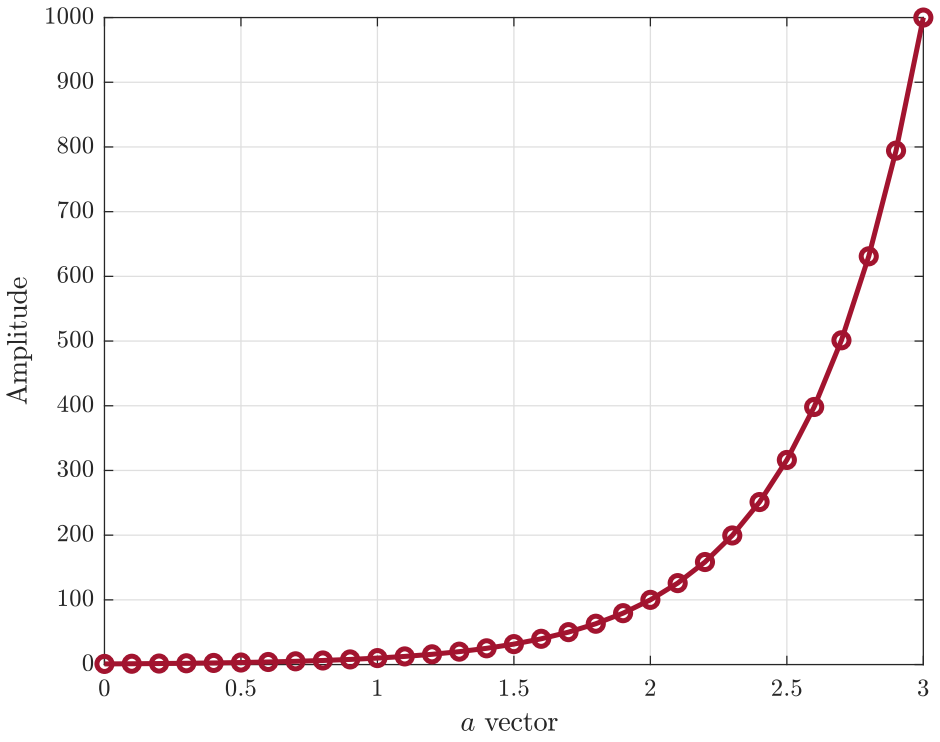

FIGURE 4.18: 10^a exponential curve.

the interval size Υ is calculated using these bounds as follows:

$$\Upsilon = \frac{log_{10}(\chi) - \mu_o}{N-1} \tag{4.48}$$

Notably, μ_o will always be set to zero, and the logarithmic vector ℓ is computed as follows:

$$\ell = \mu_o + i\Upsilon \quad i = 0, 1, 2, ..., N-1 \tag{4.49}$$

Using ℓ, the following relation is given to obtain an exponential vector T_{exp}:

$$T_{exp} = 10^{\ell} - 1 \tag{4.50}$$

Hence, the relation shown below is used to map the maximum stoppable time onto an exponential vector:

$$T = \frac{t_m - t_0}{T_{exp}^{max}} T_{exp} \tag{4.51}$$

where χ is exponential spacing factor with an inverse relation with the exponential spacing of the time vector T and is the upper bound of the exponential curve 10^a.

Fig.4.19 depicts a graphical representation of the non-uniform CVP approach based on exponential spacing of the nodal times $[T_o, T_1, \ldots, T_{N-1}] = t_m$ and nodal control variables $[\overline{u}_0, \overline{u}_1, \overline{u}_2, \ldots \overline{u}_{N-1}]$. A derivation procedure of exponential spacing based non-uniform CVP is shown in the Fig.4.20.

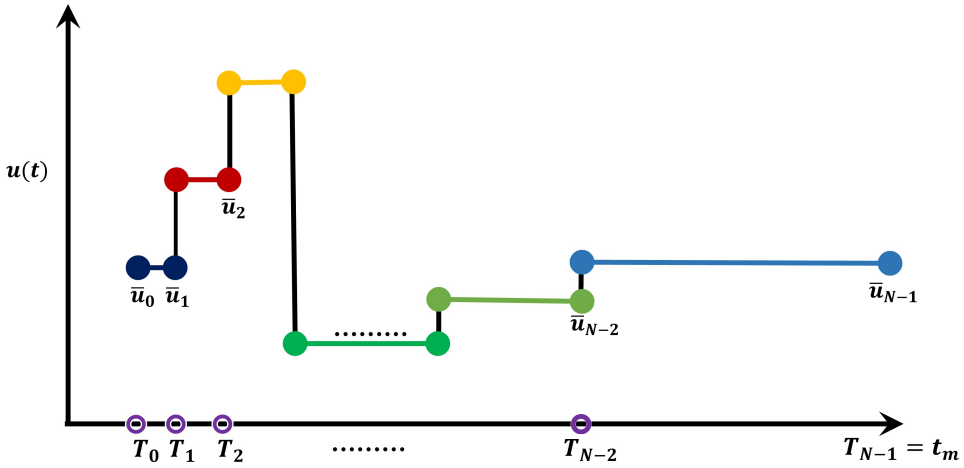

FIGURE 4.19: Non-uniform CVP.

4.3.2.1 Non-uniform CVP analysis

The spacing between intervals in non-uniform CVP can be arbitrarily tuned by a controlling knob χ which is the exponential spacing factor. It can be reviewed in Fig.4.21 that for the finite time vector and constant number of nodes N, χ is inversely related to the intervals space.

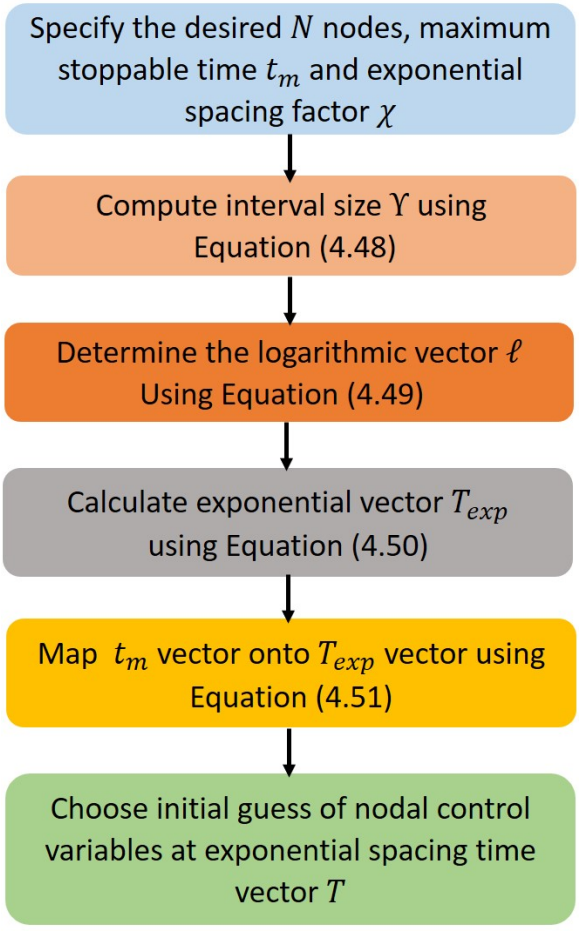

FIGURE 4.20: Non-uniform CVP Derivation.

As we increase χ, the initial spacing decreases and consequently the saturation effect begins to emerge. So the design engineer only has the freedom to adjust χ according to the design problem.

The impact of altering the number of nodes with a constant χ and a finite time vector is exhibited in Fig.4.22, and it can be observed that increasing the number of nodes also induces a saturation effect in the beginning intervals of the time vector.

As we expand the time vector with constant χ and N, the interval spacing at the beginning of the time vector increases due to which the reduction of the saturation effect occurs and can be judged in Fig.4.23.

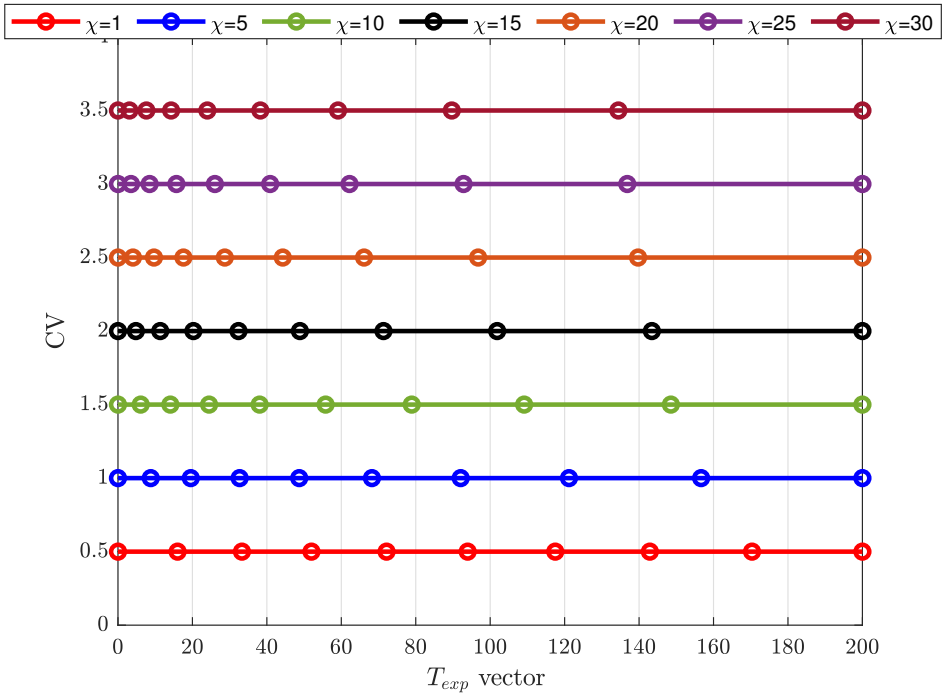

FIGURE 4.21: Effect of χ with constant number of nodes and finite time vector.

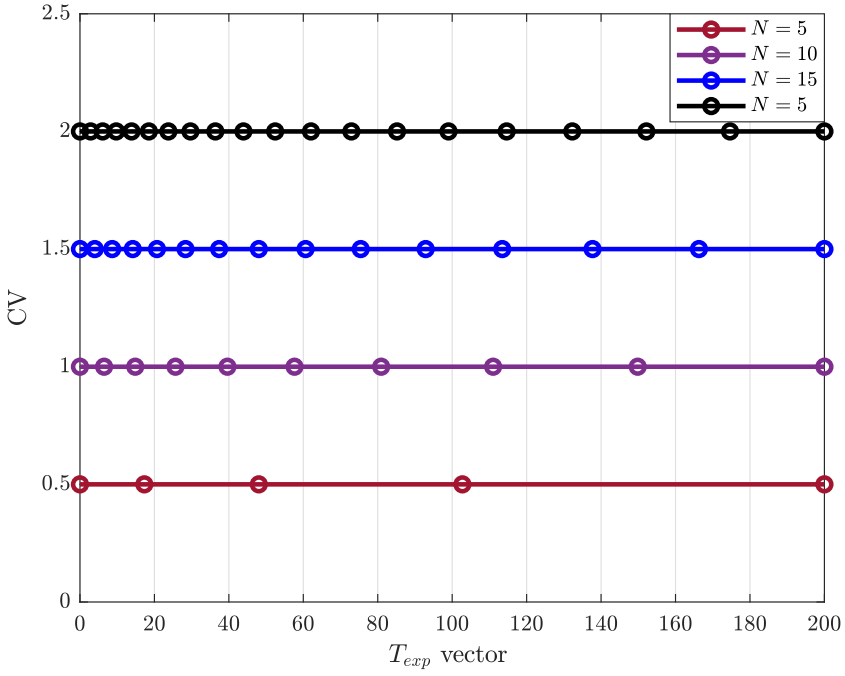

FIGURE 4.22: Effect of varying the number of nodes with constant χ and finite time vector.

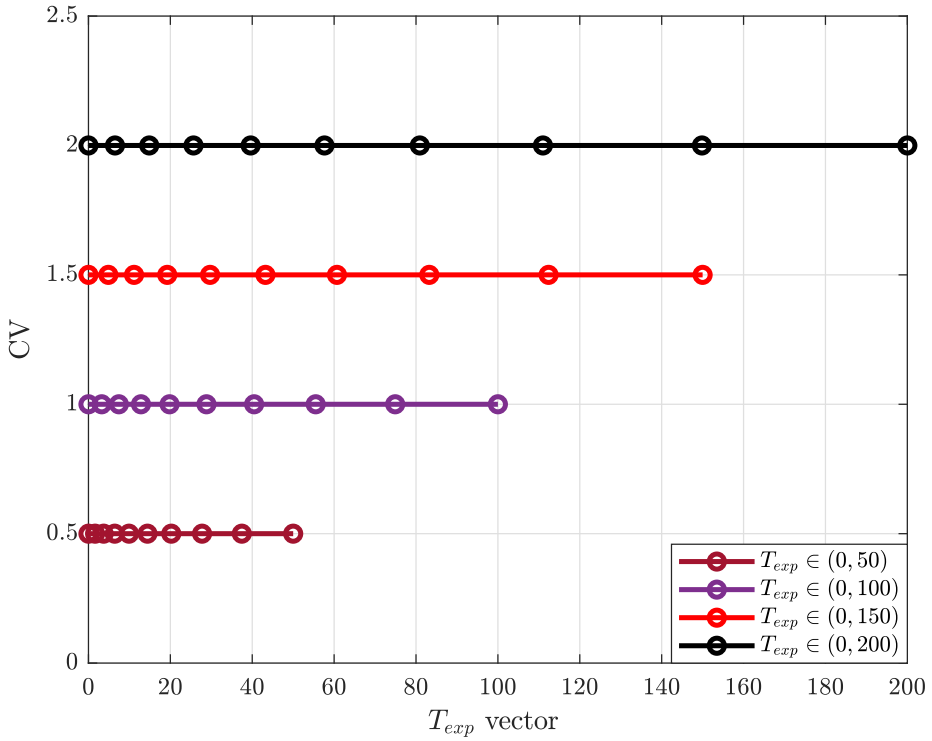

FIGURE 4.23: Effect of time vector with constant χ and number of nodes.

Non-uniform CVP analysis can be summarized as

- χ has inverse relation with exponential spacing in the presence of constant N and finite time vector.
- N has direct relation with exponential spacing in the presence of constant χ and finite time vector.
- Expansion of time vector decreases the exponential spacing if χ and N are considered fixed.
- χ and N are tuning factors which can be adjust according to optimal problem for fixed time vector.

4.3.3 Interpolation

When collecting data from experimentation, such as for such a data set, good geometric reconstruction is essential, such as to prevent excessive behavior around sudden changes in the data. Geometric reconstruction is expected to represent the internal shape inferred from the original data set in many technical and scientific applications.

Under specific conditions, interpolation specifies a polynomial function that traverses the data points in the data set and links them, and interpolation techniques include Lagrange, Hermite, spline, and Newton interpolation.

For example, given points $\{(x_1, y_1), (x_2, y_2), ..., (x_n, y_n)\}$ lie on the graph of a known function $\mathcal{F}$ and our goal is to find $\hat{\mathcal{F}}$ globally at some interval $\mathcal{F}$ $[\mathcal{U}\ \ \mathcal{V}]$, where $\mathcal{U} = x_1$ and $\mathcal{V} = x_n$. Hence an interpolation polynomial is a straightforward solution to this problem.

When the number of interpolation points (data points in the data set) rises, a higher order of the polynomial is necessary to conduct interpolation. Furthermore, the higher-order polynomial has a tendency to fluctuate, which becomes particularly undesirable when the intended function includes additional properties such as monotonicity and convexity. To avoid the challenges associated with interpolation polynomials, a piecewise polynomial approach is adopted in which the interval is further broken into smaller subintervals, and then a low-order polynomial is applied to the subintervals [95].

The places at which the polynomial changes are referred to as knots and the data on the knots is referred to as nodes [96]. When the number of nodes rises in piecewise polynomial interpolation, the overall interpolation function remains relatively simple and therefore the basic elegance of polynomial interpolation is maintained.

The choice of interpolation method in a dynamic optimization problem can influence the performance of a nonlinear programming approach through the integration of a set of differential equations. In the nonlinear programming approach, the

interpolation nodes are the same design variable $[\overline{u}_0, \overline{u}_1, \overline{u}_2, \ldots \overline{u}_{N-1}]$, and a slight modification of the nodes results in a different interpolation response, which affects the performance index. In the high-order interpolation approach, piecewise cubic spline scheme, a small change in one node modifies the entire interpolation at all intervals. while even this minor change might result in significantly non-linear behavior, which causes a slew of problems for the optimization problem and the dynamic system. The piecewise cubic spline method, a third-order polynomial, has a smooth formation and nonlinear behavior, yet even a slight change in one node alters the interpolation's overall formation at all intervals. By applying a cubic spline to the control function, the control box constraints around the nodes are also violated [97].

Because of this, cubic spline is ineffective in highly nonlinear optimization problems. Consequently, to overcome the concerns of sensitivity to node variations and violation of control box constraints, a smooth and well-behaved interpolation approach, Piecewise Cubic Hermite Interpolation Polynomial (PCHIP), a 3rd order approach, is recommended because changes in a node only affect its neighbors [97].

The PCHIP function is capable of preserving the composition of the original vector due to its smooth first derivative [98]. In addition, it can be inferred from Fig. 4.24 that PCHIP has no overshooting problem and less oscillation than spline. The following are the attributes of PCHIP:

- It has the ability to preserve shape.
- It has the capability of monotonicity in intervals with monotonic data.
- This is the best option to deal with control box constraint and is less sensitive to node variation.
- It has less overshoot and undershoot than the spline.
- It evaluates the first derivative along the first and last intervals at the nodes.

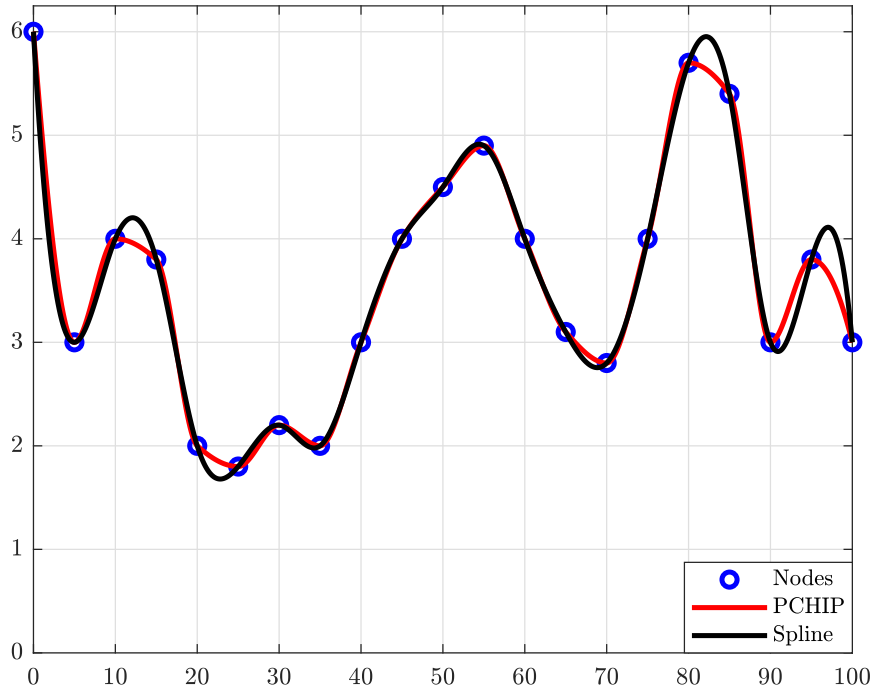

FIGURE 4.24: PCHIP vs. Spline.

In our case, to deal with discontinuity in nodes, the PCHIP function is employed to approximate the smooth CV using nodal control variables $\overline{u}_i$ for each time interval $t \in (t_i, t_{i+1})$. It is easy to put into action, and the PCHIP function in mathematical form is demonstrated as

$$u(\tau) = \hat{\beta}_0 \overline{u}_j + \hat{\beta}_1 \overline{u}_{j+1} + \bigtriangledown(\tilde{\beta}_0 \mathcal{D}_j + \tilde{\beta}_1 \mathcal{D}_{j+1}) \tag{4.52}$$

where $\bigtriangledown, \hat{\beta}_0, \hat{\beta}_1, \tilde{\beta}_0$ and $\tilde{\beta}_1$ are defined as follows

$$\bigtriangledown = t_{j+1} - t_j \tag{4.53}$$

$$\hat{\beta}_0 = (1 + 2\wedge)(1 - \wedge)^2 \tag{4.54}$$

$$\hat{\beta}_1 = (3 - 2\wedge)\wedge^2 \tag{4.55}$$

$$\tilde{\beta}_0 = \wedge(1 - \wedge)^2 \tag{4.56}$$

$$\tilde{\beta}_1 = \wedge^2(\wedge - 1) \tag{4.57}$$

where $\wedge = \frac{t-t_j}{\nabla} \quad t_j \leq t \leq t_{j+1}, j = 0, 1, 2, ..., N-1$, t_j is nodal time. While $\mathcal{D}_j$ shows the derivative of the nodal control variable and a detailed discussion about derivatives is given in [99].

4.3.4 Control Vector Parameterization Framework

This section will describe how the optimization framework is customized to execute optimal gliding trajectories. The major purpose of this research is on establishing the strategy for identifying the search space for the optimal dynamic trajectory. Many optimization problems do not have benchmark cases and therefore require an existing technique that can generate unique solutions in a real-time environment.

The optimization software capable of creating the optimal gliding trajectory in real time was chosen carefully while carrying out this study, which incorporates the two ideas of maximum stoppable time and stopping constraint. The majority of technical studies employed iterative numerical optimization software such as General Purpose Optimal Control Software (GPOPS) [100], Nonlinear Programming Solver (NPSOL) [101], Graphical Environment for Simulation and Optimization (GESOP) [102], Advanced Launcher Trajectory Optimization Software (ALTOS) [103] and Imperial College London Optimal Control Software (ICLOCS) [104].

A graphical user interface type software DS Simulia Isight has been used in this study to obtain the maximum range of SUGV. It is embedded with MATLAB where MATLAB works as SUGV. In this optimization software, according to the suggested CVP technique, the nodal control variables are regarded as output variables and the cost function and constraints are considered input variables.

A graphical illustration of the implementation framework is expressed in Fig. 4.25. DS Simulia Isight in conjunction with MATLAB performs Sequential Quadratic Programming (SQP) with multiple shooting method as a solver to compute uniform CVP and non-uniform CVP. In the SQP method, an iterative programming method, a quadratic programming (QP) problem is solved at each iteration.

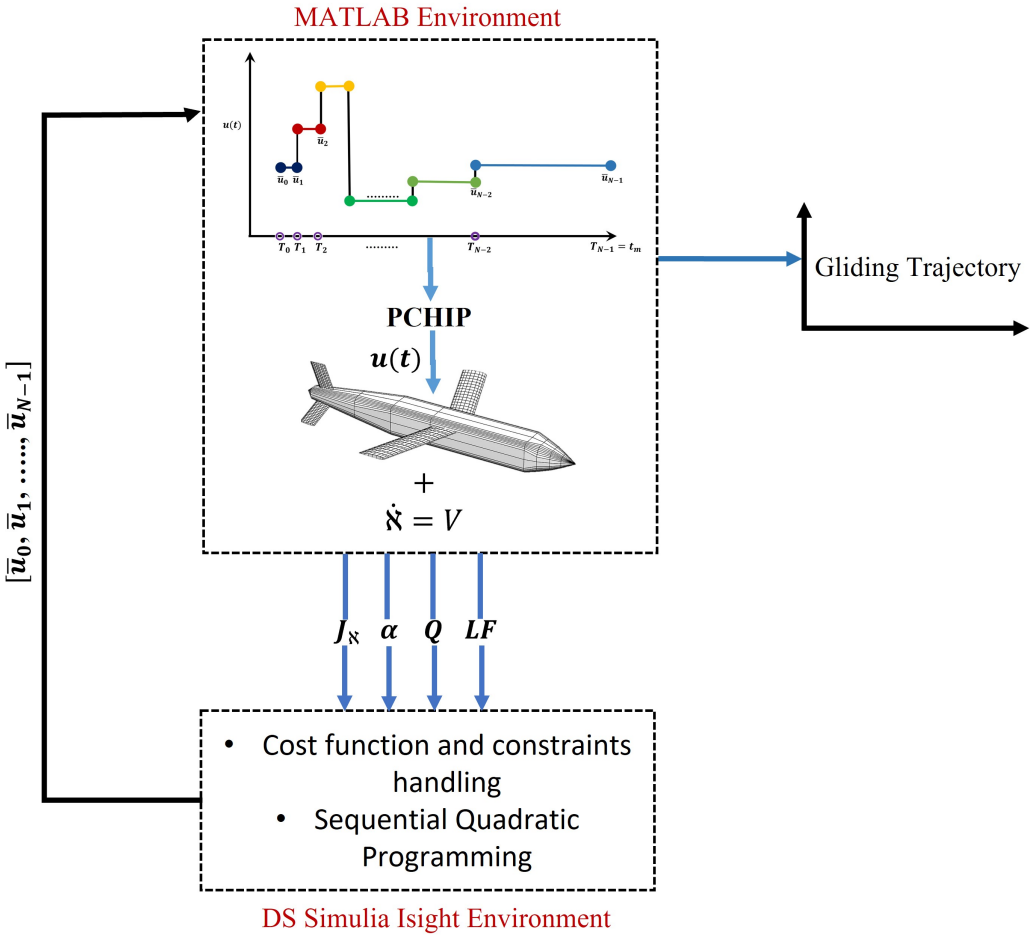

FIGURE 4.25: CVP implementation framework.

QP approximates the gradient and Hessian at each iteration. SQP has an important advantage in this software that it does not depend on convergence because the QP subproblem if it is solvable at all, is solved in a finite number of iterations. The QP subproblem is solved by finding a search direction 'd' that is feasible with respect to all the constraints (feasibility step) and the optimal solution of the quadratic problem (optimal step).

4.4 Results and Discussion

The feasibility and effectiveness of the exponential based non-uniform CVP approach for an SUGV's gliding range is compared with the maximum elevator step

δ_e and classical uniform CVP approach in this section. For performance progression, we set t_m to 850 s and N to 10, 15, and 20. A time vector with a specified N had its χ able to be adjusted as desired and for this study, the χ corresponding to the given nodes are tabulated in Tab.4.1. Simulations of the SUGV range maxi-

TABLE 4.1: χ Values.

N=10	N=15	N=20
108	56	53.1

mization were performed using the dispersion points [92] given in Table 4.2. To

TABLE 4.2: SUGV Dispersion Points.

States	Dispersion Points	Units
V	216	ms^{-1}
α	0	deg
Q	0	deg s^{-1}
θ	0	deg
R	0	Km
h	10	Km

achieve the maximum glide range using the CVP approach, the bounds on α, δ_e and LF are given in [92]. We arrived at a constraint that fit our problem solving criterion by examining the impact of several restrictions on Q, and all constraints are listed in Table 4.3.

TABLE 4.3: SUGV constraints.

Angle of Attack (deg)	Pitch Rate (deg s^{-1})	Load Factor	Elevator Deflection (deg)
$0 \leq \alpha \leq 2.65$	$-1 \leq Q \leq 1$	$LF \leq 1.007$	$0 \leq \delta_e \leq 6$

4.4.1 Case 1: N = 10

The simulation results for 10 nodes, comparing the proposed CVP approach with the maximum step input (Max δ_e) of 6 deg and the conventional CVP approach

are elaborated. In the uniform CVP approach, the optimizer tried to obtain faster damping to generate steady gliding flight compared with the maximum step input. Fig.4.26 shows that when the SUGV dropped from the carrier platform, the optimizer produced a low angle of attack, which induced free fall, and then the optimizer tried to stabilize the gliding flight. As demonstrated in Fig.4.26, the non-uniform CVP approach provided excellent results for fast damping and steady gliding flight, reducing the impacts of fluctuations and increasing the gliding range by 121.25 km in Fig.4.27.

The variation in constraint profiles is shown in Figs.4.28, 4.29 and 4.30. Uniform CVP met the α requirement, with variations that stabilized after 280 s, but non-uniform CVP had a smooth α profile. The findings for the Q constraint demonstrate that the non-uniform CVP approach beat the other reference approaches when it came to performance. The uniform CVP approach sought to keep the Q profile between the limits but was unsuccessful. Fig.4.30 for the uniform CVP approach and maximum step input illustrates a violation and considerable variability in the load factor constraint profile.

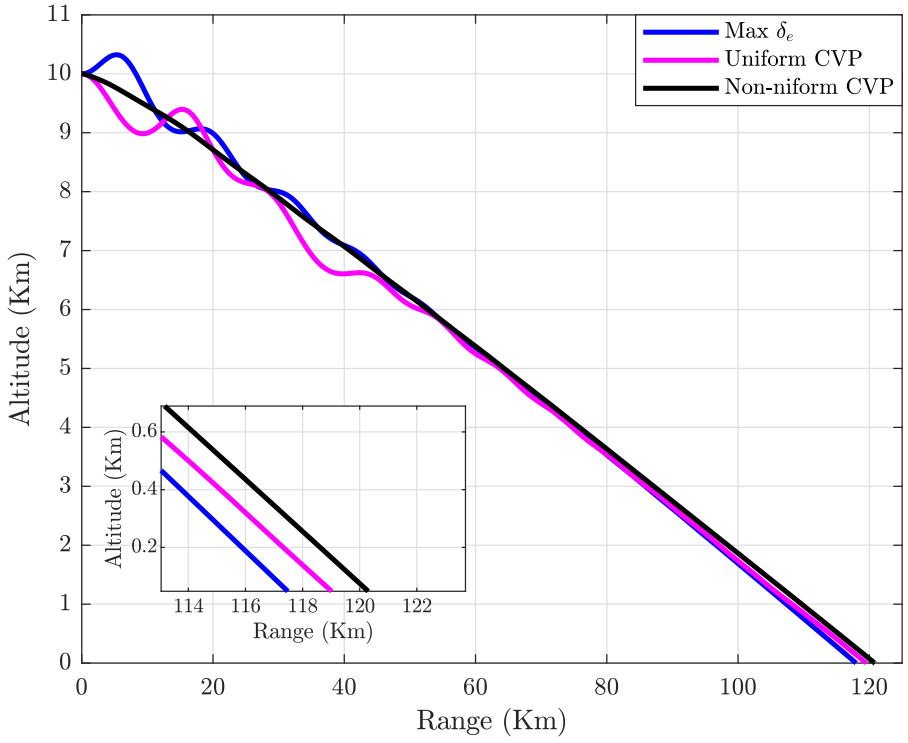

FIGURE 4.26: $N = 10$: Gliding trajectory.

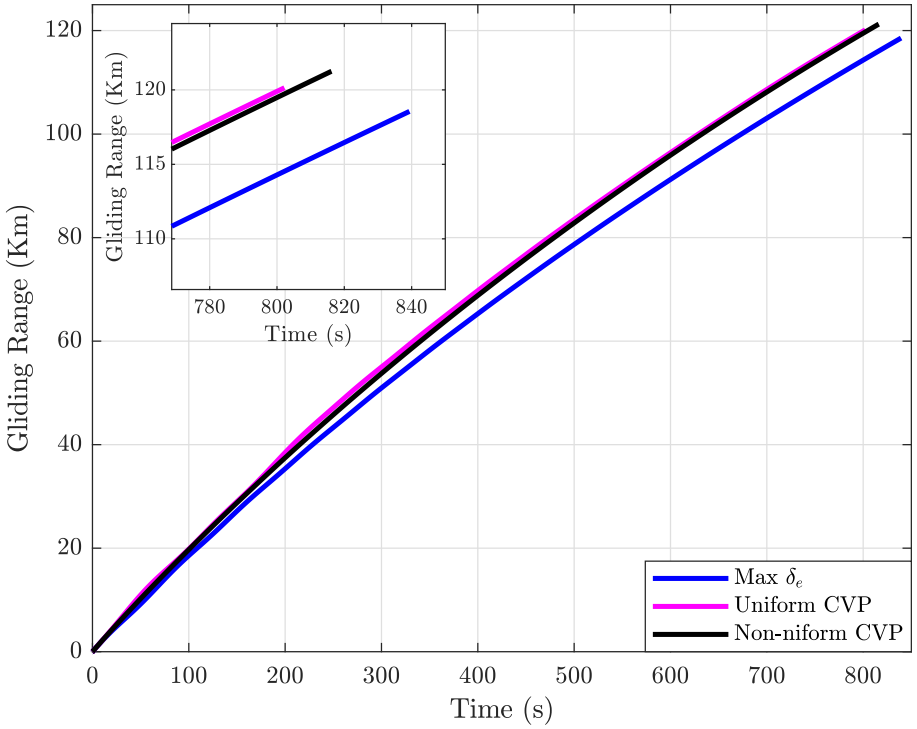

FIGURE 4.27: $N = 10$: Gliding range.

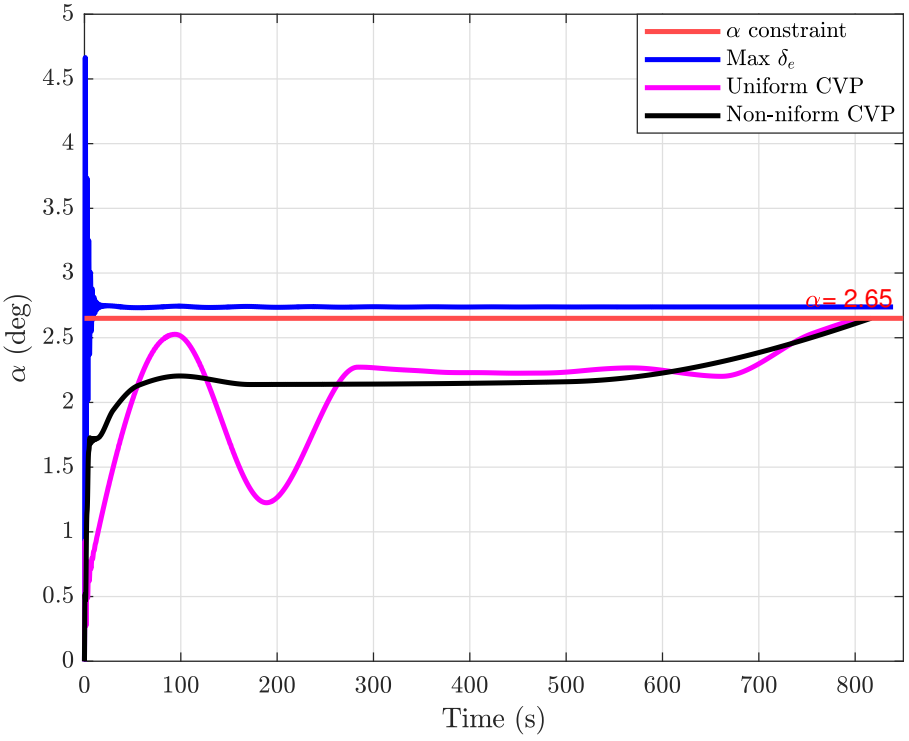

FIGURE 4.28: $N = 10$: α constraint.

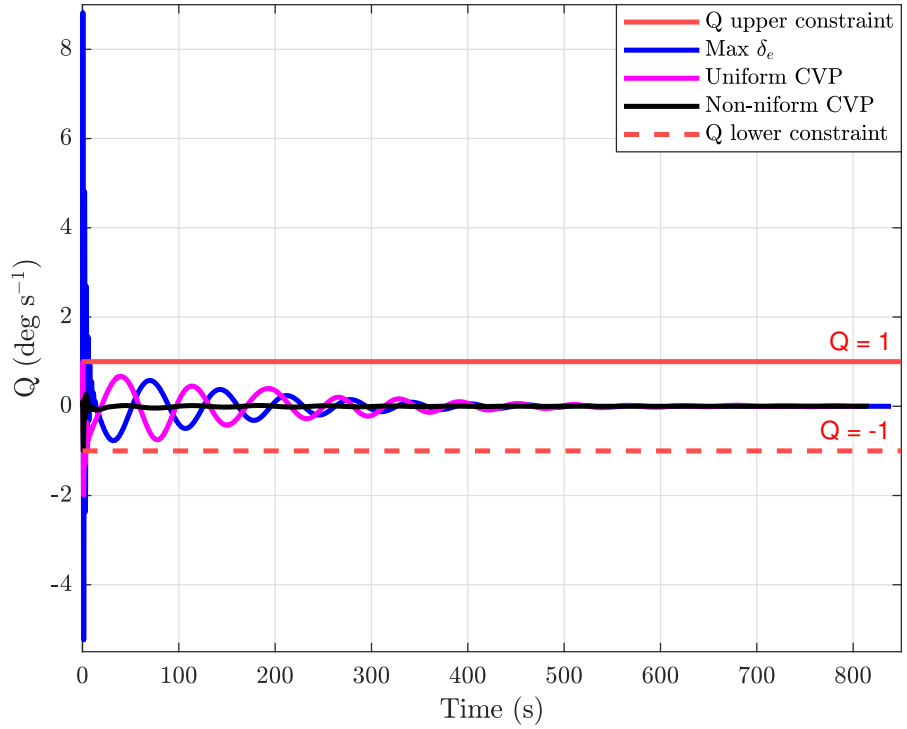

FIGURE 4.29: $N = 10$: Q constraint.

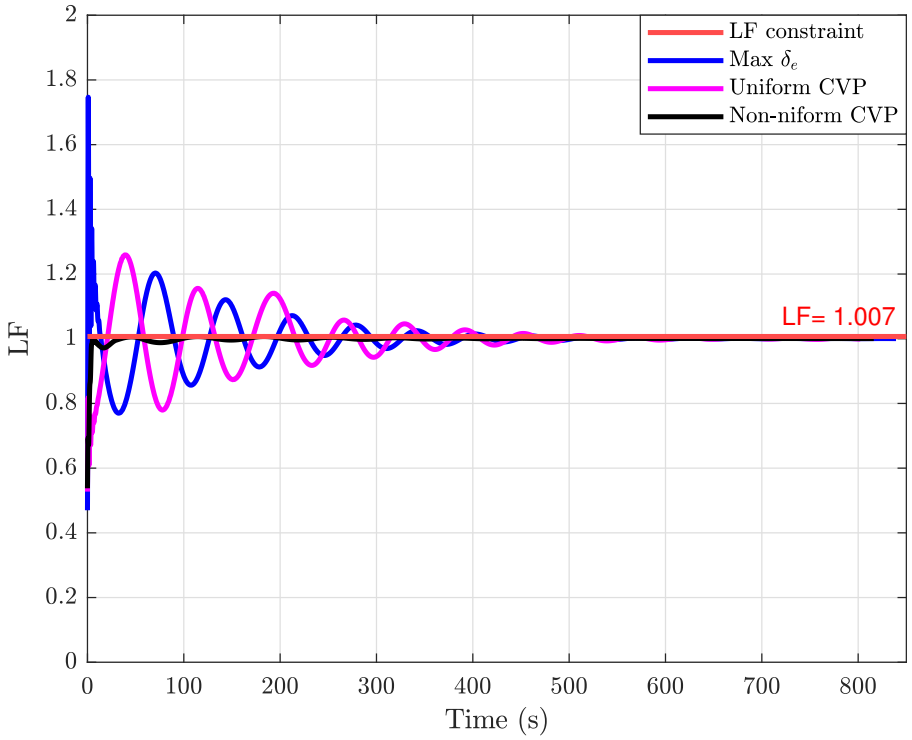

FIGURE 4.30: $N = 10$: LF constraint.

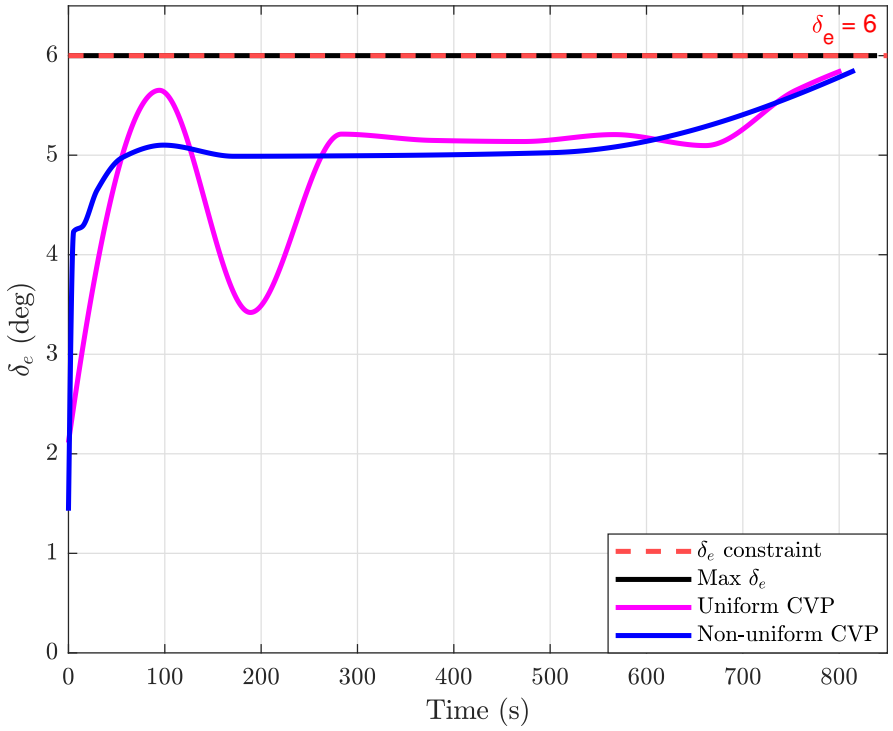

FIGURE 4.31: $N = 10$: δ_e Constraint.

The non-uniform CVP approach,on the other hand, provided a less varying load factor constraint profile that assured steady gliding flight. Comparatively, the constraint profiles illustrate the maximum range progression and efficacy for the SUGV in addition to the suggested CVP approach for steady gliding flight.

The non-uniform CVP approach generated a control profile with less variability and less amplitude than the uniform CVP approach, as shown in Fig.4.31, ensuring the optimal gliding range and achieving steady gliding flight with less pressure on the elevator actuators.

4.4.2 Case 2: N = 15

This case illustrates the simulation outcomes with 15 nodes for the maximum step input of 6 deg, the conventional uniform CVP approach, and the proposed non-uniform CVP approach. By increasing the number of nodes, the control profile for the uniform CVP method became more variable, hence affecting the glide path.

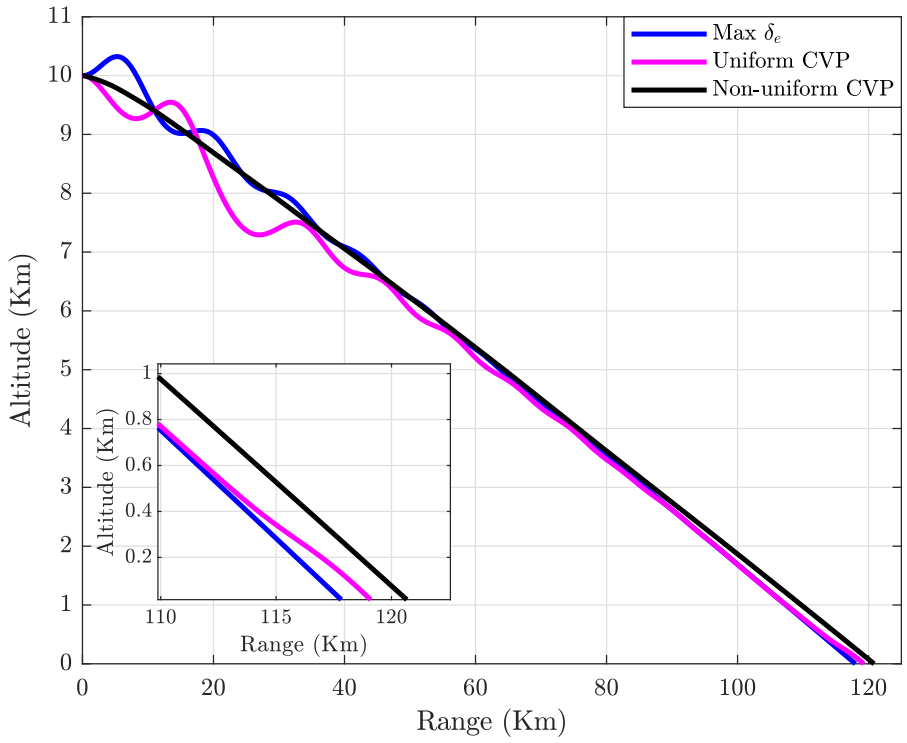

FIGURE 4.32: $N = 15$: Gliding trajectory.

Uniform CVP for 15 nodes resulted in less free falling behavior than the uniform CVP for 10 nodes. In the uniform CVP strategy, the optimizer attempted to raise the alpha value closer to the ground to maximize the gliding range relative to the maximum elevator input. The uniform CVP technique did not provide promising results in terms of damped and steady gliding flight, but Figs.4.32, 4.33 illustrates that the suggested non-uniform CVP approach produced fast damping and steady gliding flight.

The suggested non-uniform CVP approach obtained a gliding range of 121.26 km and a horizontal range of 120.84 km, which are both encouraging results in damped and steady gliding flight when compared with the approaches discussed.

Figs.4.34, 4.35, and 4.36 demonstrate the constraint profile. Due to the increase in the number of nodes for the uniform CVP approach, the α constraint exhibited significant variance, while the suggested non-uniform CVP approach resulted in a negligible variance in the α constraint after commencement of gliding flight.

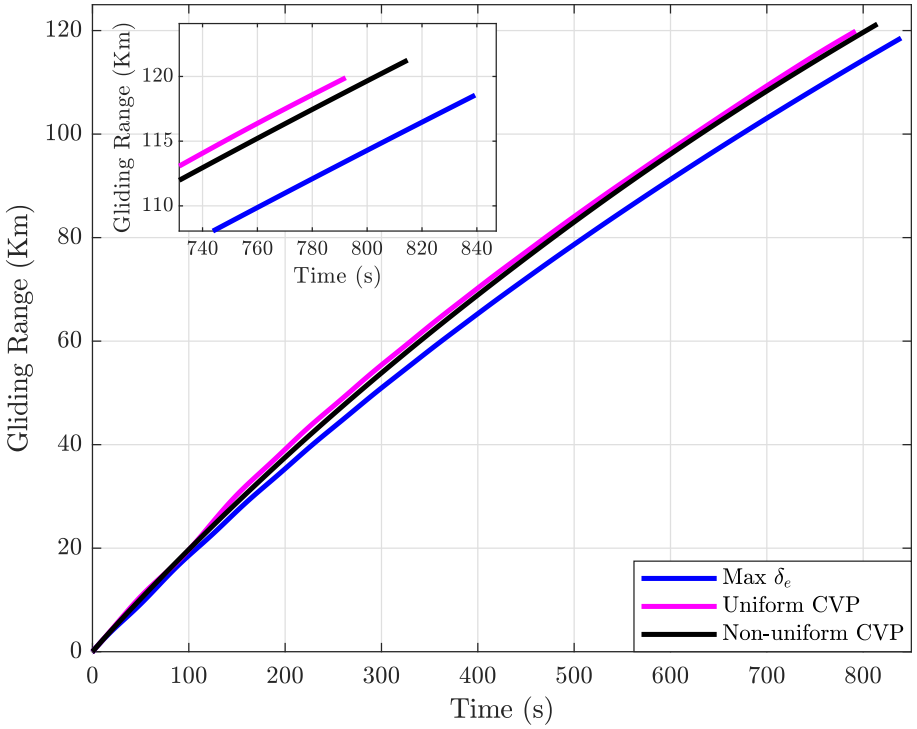

FIGURE 4.33: $N = 15$: Gliding range.

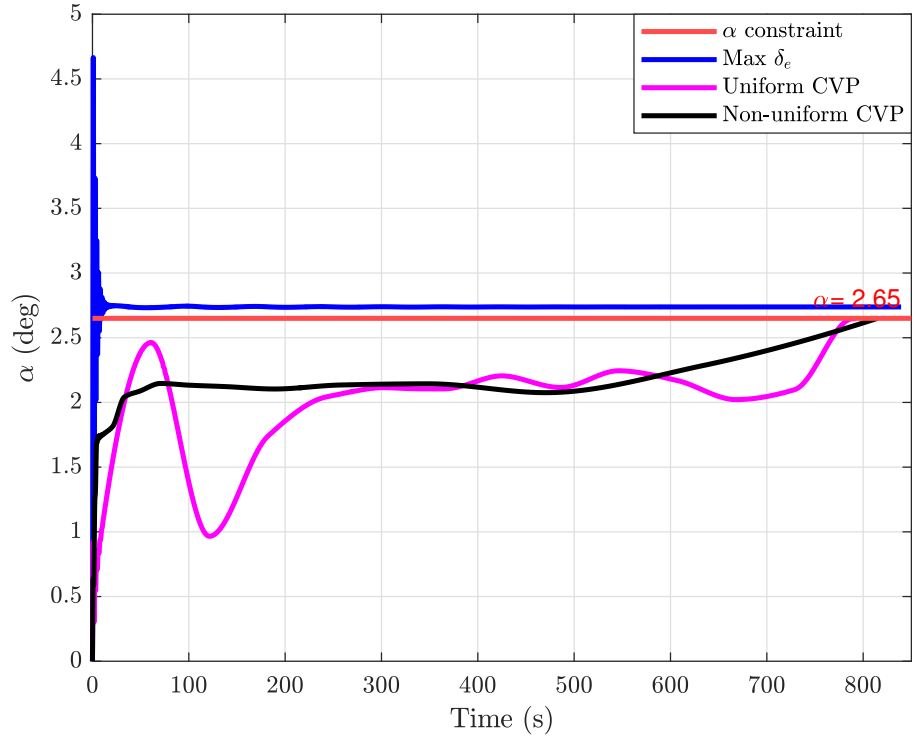

FIGURE 4.34: $N = 15$: α constraint.

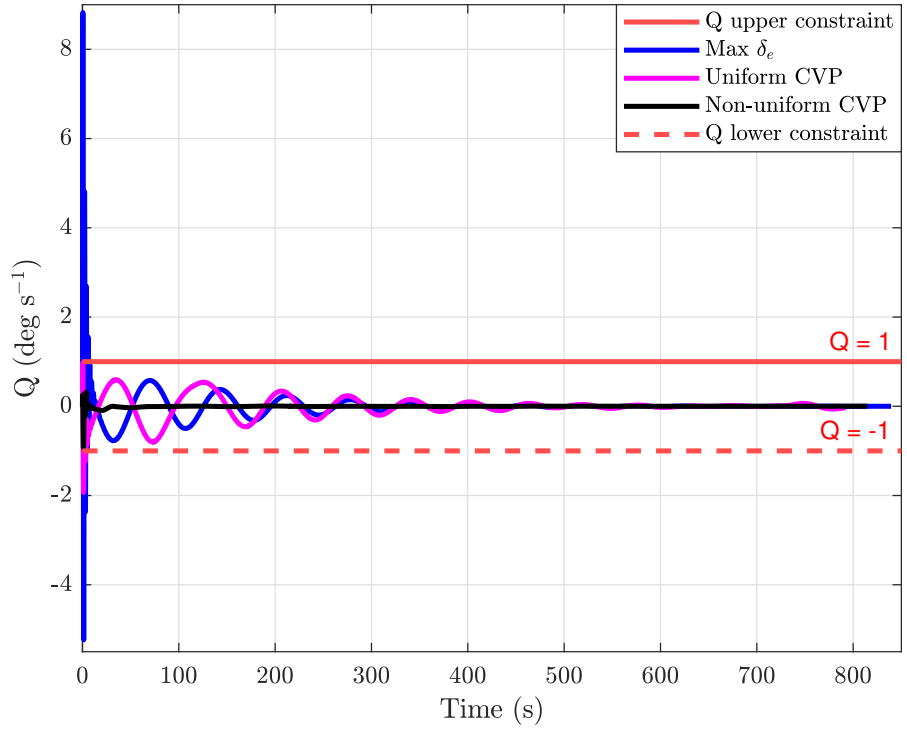

FIGURE 4.35: $N = 15$: Q constraint.

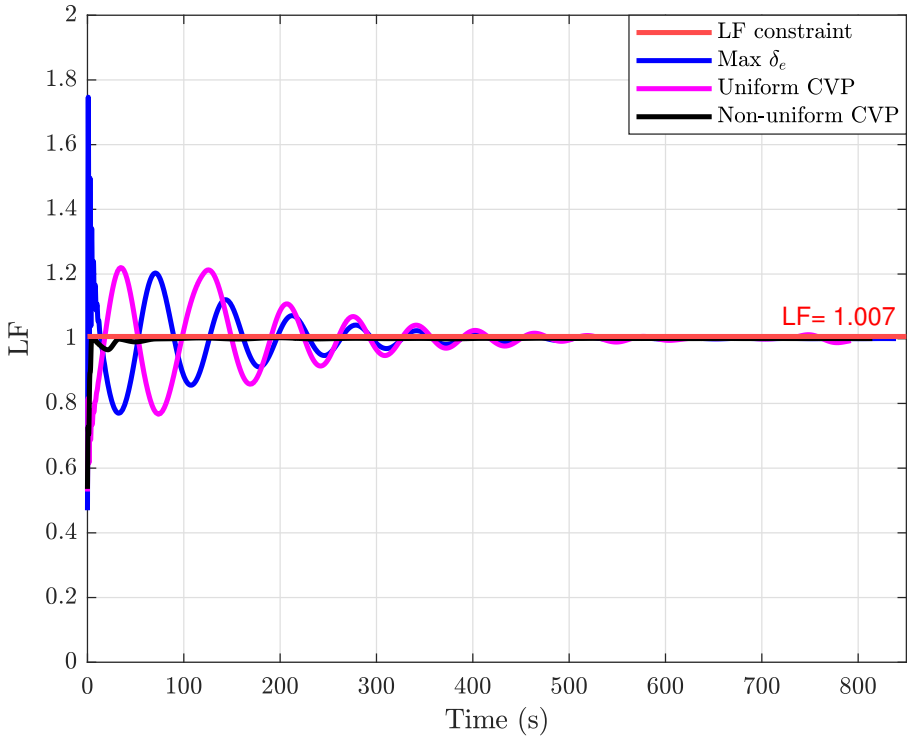

FIGURE 4.36: $N = 15$: LF constraint.

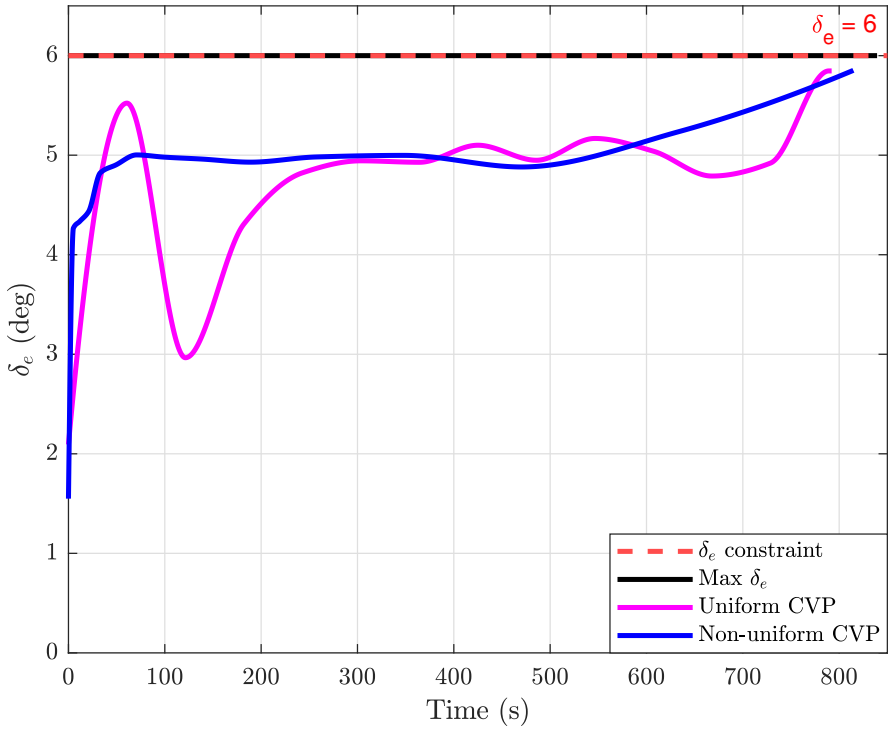

FIGURE 4.37: $N = 15$: δ_e Constraint.

Despite the uniform CVP approach's attempts to limit oscillations in the Q constraint profile, the lower bound was exceeded. The suggested non-uniform CVP method met the Q restrictions, and node increases caused saturation in the lower spacing of the CV, with this impact seen in the Q profile.

The LF profile demonstrates that the non-uniform CVP approach yielded a profile with little variation while meeting the requirement that ensured steady gliding flight. The constraint on the control input is expressed in Fig. 4.37. Despite the increase in the number of nodes, the control profile demonstrates that the suggested non-uniform CVP provided less stress on the elevator actuators and a smooth profile with little variance.

4.4.3 Case 3: N = 20

The optimal outcomes based on 20 nodes for the proposed non-uniform CVP, maximum step input. Fig.4.38 demonstrates that the optimizer tried to calculate

damped and steady gliding flight using a uniform CVP approach in contrast to the maximum step input results, while the uniform CVP technique resulted in fewer free fall situations than the prior cases.

The proposed non-uniform CVP method effectively generated an optimal gliding trajectory to address sluggish damping and unsteady gliding flight issues, and it optimized the gliding range to 121.28 km and the horizontal distance to 120.856 km. The uniform CVP approach, unlike the maximum step input, decreased the magnitude of the changes in Q and α but did not result in damped and steady gliding flight. Figs.4.40, 4.41 and 4.42 illustrate the significance of the suggested non-uniform CVP method via the modification of restrictions.

The non-uniform CVP method provided the constraint results with a damped profile and satisfied the constraint values, but the suggested CVP revealed the increase in the number of nodes as saturation in the load factor. Fig.4.43 portrays the optimal control input profile. It can be observed that the uniform CVP method caused a minimal change in the input profile with low actuator pressure.

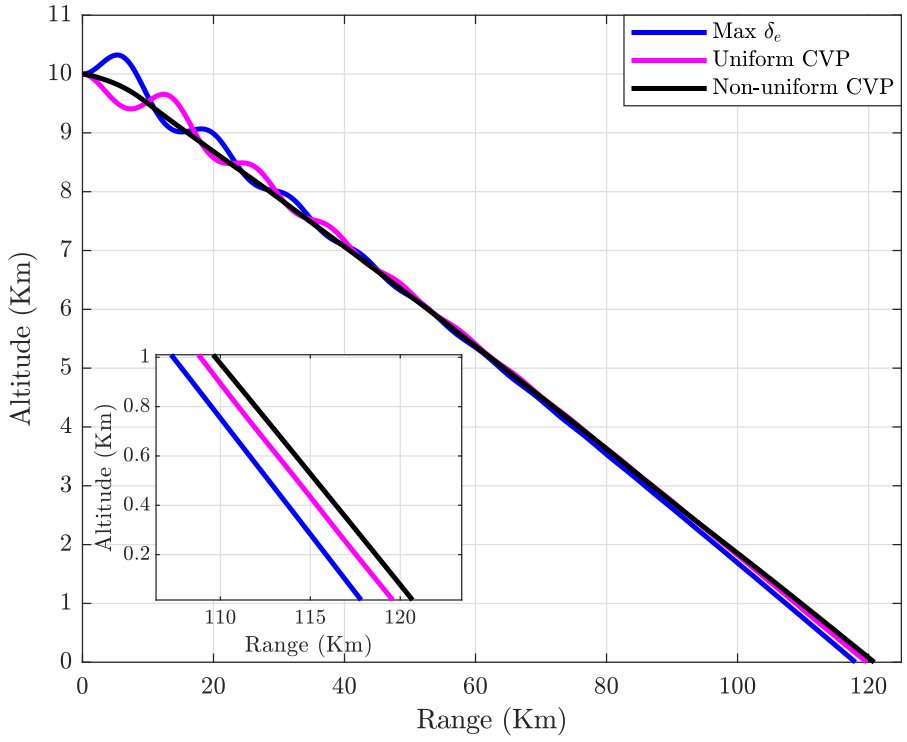

FIGURE 4.38: $N = 20$: Gliding trajectory.

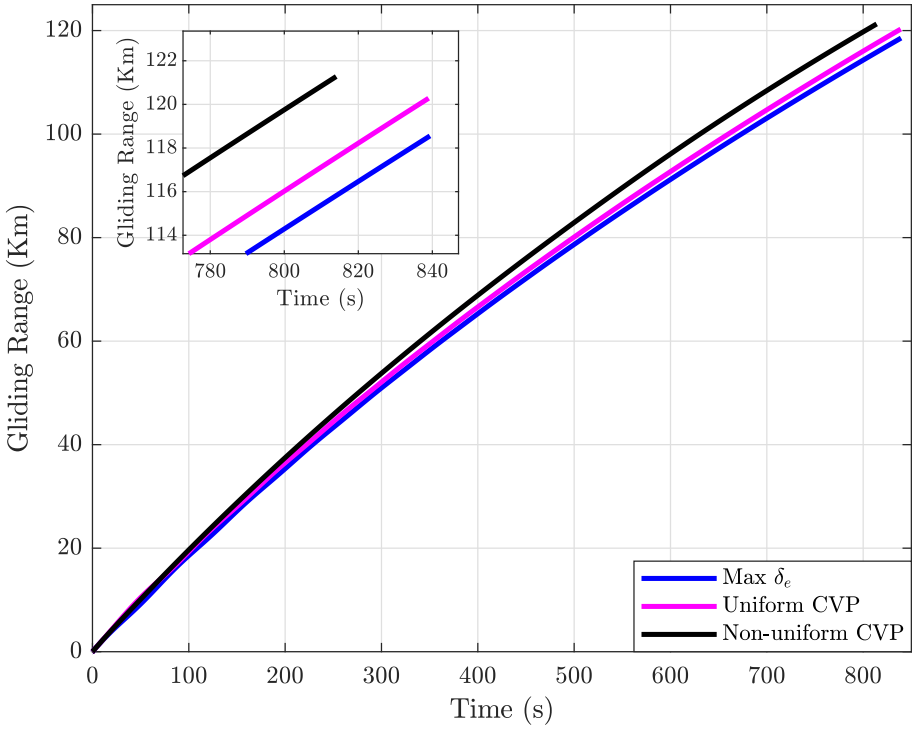

FIGURE 4.39: $N = 20$: Gliding range.

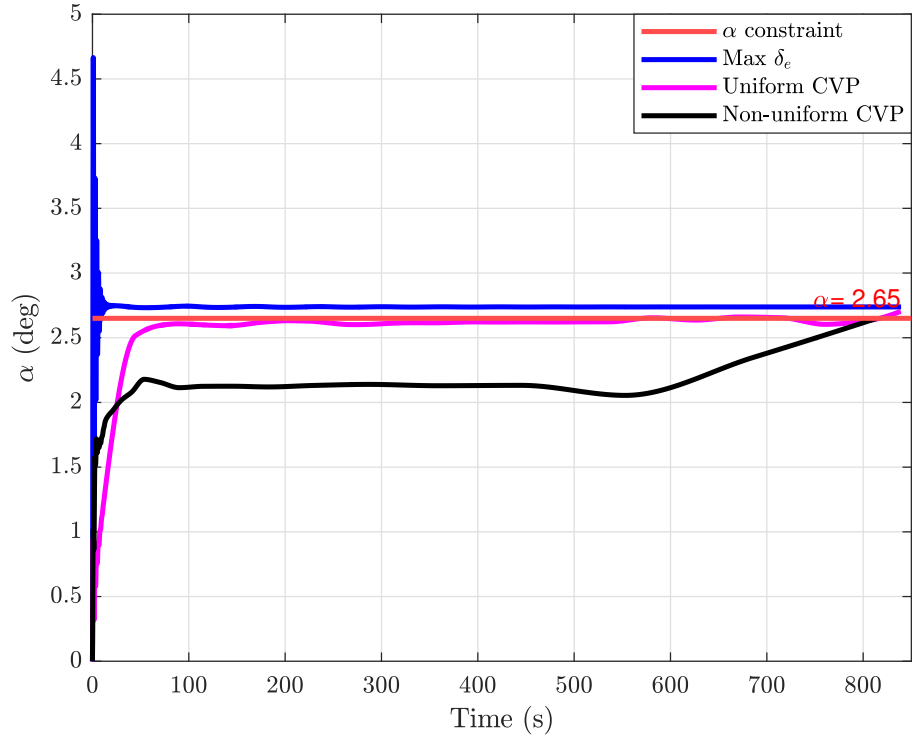

FIGURE 4.40: $N = 20$: α constraint.

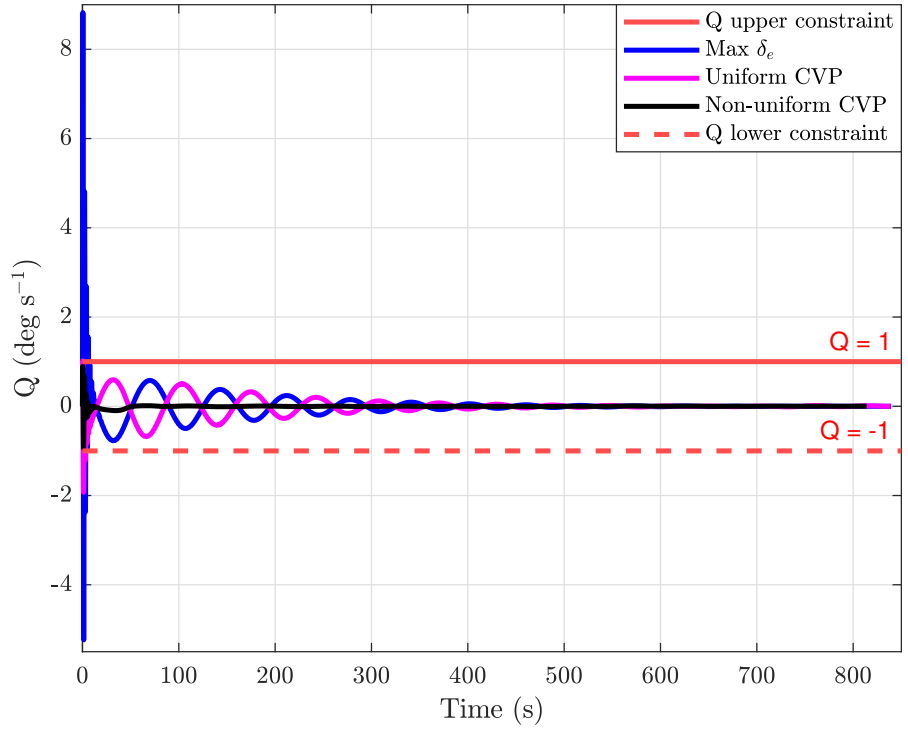

FIGURE 4.41: $N = 20$: Q constraint.

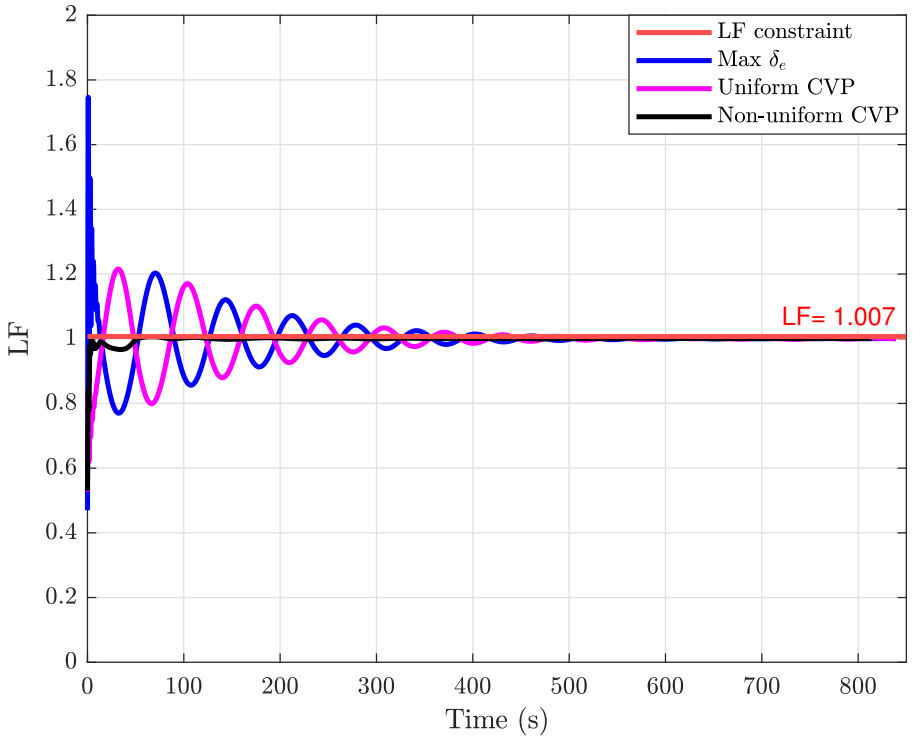

FIGURE 4.42: $N = 20$: LF constraint.

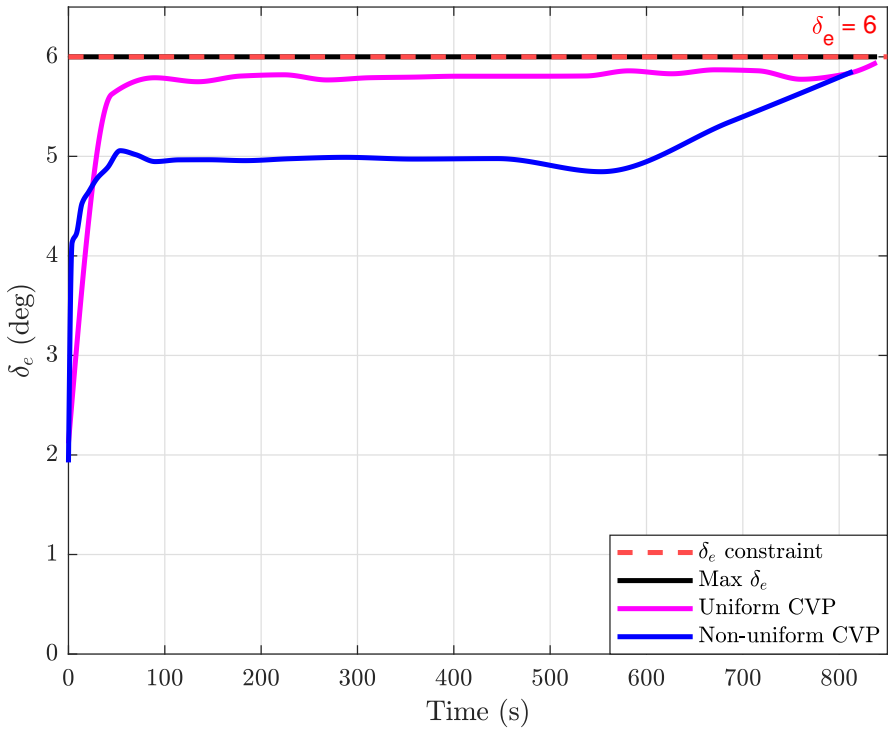

FIGURE 4.43: $N = 20$: δ_e Constraint.

To optimize the gliding range, it was found that the optimizer for the proposed CVP method mimicked the best control profile, with a tiny variance owing to the node increase at the outset. The maximum values of the constraint profiles for the chosen techniques are shown in Table 4.4 for numerical observation.

It can be seen that the constraint profiles of the non-uniform CVP approach based on exponential spacing met all of the constraints throughout the SUGV's gliding flight in the provided cases, while the maximum values of the LF and Q for the non-uniform CVP technique in Table 4.4 could also be used to assess the impact of the increment on the number of nodes.

To observe the superiority of the proposed non-uniform CVP, stopping values such as the stopping time t_s, gliding range R_g, and horizontal range R_h of the SUGV after hitting the ground could be compared with other referenced methods, which are listed in Table 4.5.

It can be noted that the stopping time for the maximum step input was longer than the uniform and non-uniform CVP approaches because the pull-up condition avoided the free fall condition when releasing the SUGV from the carrier platform. Damping was slow due to unstable gliding flight, and because of this, the SUGV took longer to hit the ground.

On the other hand, the uniform CVP approach suffered from the free-fall problem for nodes 10 and 15 after leaving the dispersion points, which caused unsteady gliding flight, whereas the uniform CVP for node 20 experienced a lower free fall condition, which caused an increase in the gliding range compared with nodes 10 and 15.

It was also noticed that the suggested non-uniform CVP method required an average stopping time for the maximum gliding flight when compared with the maximum input and uniform CVP approach because the non-uniform CVP approach successfully produced damped and steady gliding flight.

Table 4.5 indicates that the non-uniform CVP approach outperformed the maximum step input and uniform CVP approach for R_g (maximum value of glide range) and R_h (maximum value of horizontal range) values higher than 121 km and 120 km, respectively.

4.4.4 GPOPS vs Non-Uniform CVP

In this subsection, a comparison of the proposed CVP approach with the hp-adaptive Gaussian quadrature collocation technique [105, 106] to maximize the range of SUGV is presented. The Lagrange polynomial is employed in the Gaussian quadrature collocation technique to estimate the state, and the points corresponding to the Gaussian quadrature are treated as the support points of the Lagrange polynomial.

On the other hand, the Gaussian quadrature collocation method is accomplished as a p-method, wherein increasing the degree of polynomial approximation leads to convergence inside the single interval.

Table 4.4: SUGV constraint values.

Constraints	Max δ_e	Uniform CVP			Non-Uniform CVP		
		$N = 10$	$N = 15$	$N = 20$	$N = 10$	$N = 15$	$N = 20$
α (deg)	4.6652	2.6480	2.6467	2.7040	2.6499	2.6500	2.6498
Q^L (deg s^{-1})	-5.2350	-1.9868	-1.9298	-1.9269	-1.0000	-0.9302	-0.9387
Q^U (deg s^{-1})	8.8224	1.0000	0.9761	1.0191	0.2654	0.3114	0.8970
LF	1.7466	1.2591	1.2199	1.2155	1.0069	1.0064	1.0063
δ_e (deg)	6.0000	5.8487	5.8464	5.9430	5.8522	5.8524	5.8521

Table 4.5: SUGV stopping values.

Constraints	Max δ_e	Uniform CVP			Non-Uniform CVP		
		$N = 10$	$N = 15$	$N = 20$	$N = 10$	$N = 15$	$N = 20$
t_s (s)	839.351	802.215	792.177	838.989	816.190	814.735	814.023
R_g (km)	118.556	120.141	119.901	120.282	121.250	121.259	121.278
R_h (km)	117.993	119.553	119.260	119.758	120.831	120.840	120.856

A hp-adaptive approach combines the p-method with the h-method, modifying the number of mesh intervals and the degree of polynomial closeness within each mesh interval. To achieve a certain accuracy in the numerical solution of the dynamic optimal control problem, the hp-adaptive method takes advantage of the exponential convergence of the global Gaussian quadrature method by ensuring a smooth solution.

Additionally, it introduces more mesh points around discontinuities or rapidly changing solutions. The number of segments and the degree of the polynomial on each segment are modified until the user-specified tolerance is reached by taking into account the global approximation for the state variables.

GPOPS is a well-known tool for solving trajectory optimization and optimal control problems using the hp-adaptive Gaussian quadrature collocation technique. The gliding trajectory outcomes are presented in Fig. 4.44, and the suggested strategy outperformed the GPOPS response in obtaining the maximum range.

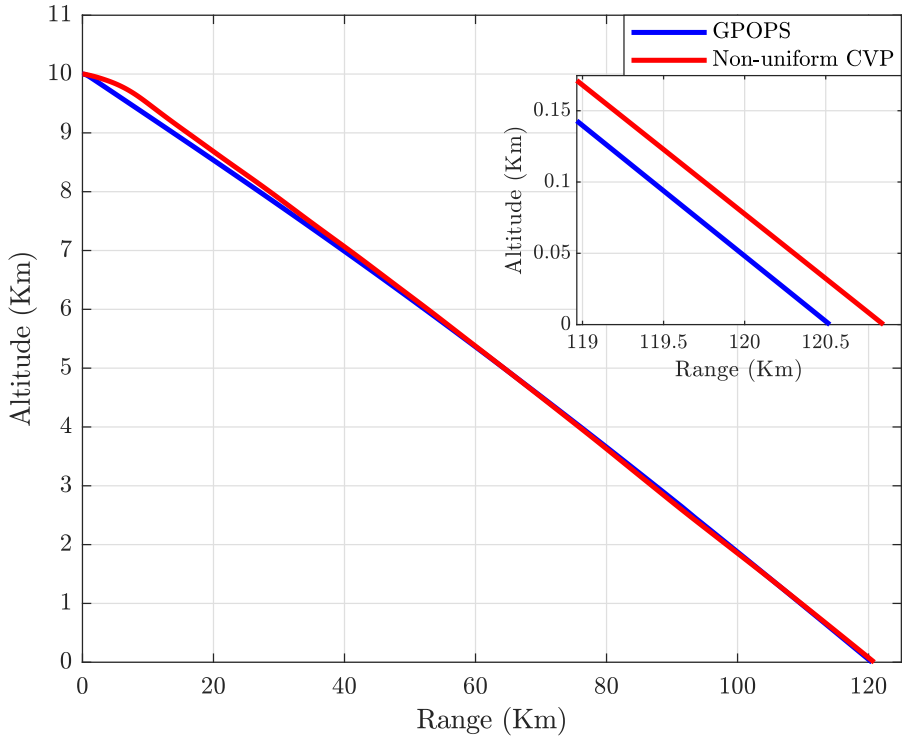

FIGURE 4.44: Gliding Trajectory.

The proposed CVP method defeated the GPOPS across a 300 m horizontal range difference. Fig. 4.45 illustrates a comparison of the gliding range (performance index profiles), revealing that the non-uniform CVP approach enhances the gliding range compared to GPOPS.

In Fig. 4.46, the smooth alpha constraint profile was generated using GPOPS, after a 722-sec glide flight, the α profile encountered the constraint boundary and stayed there until it made contact with the ground. Conversely, the CVP technique yielded a nonsmooth profile, but it touched the constraint at the point of impact.

The GPOPS optimizer attempts to maintain the SUGV's nose up, whereas the CVP scheme optimizer maintains an almost constant α between 90 and 480 seconds, and after this, the optimizer increases airspeed by pointing the nose down, then increases lift force by pointing the nose up to improve the gliding range.

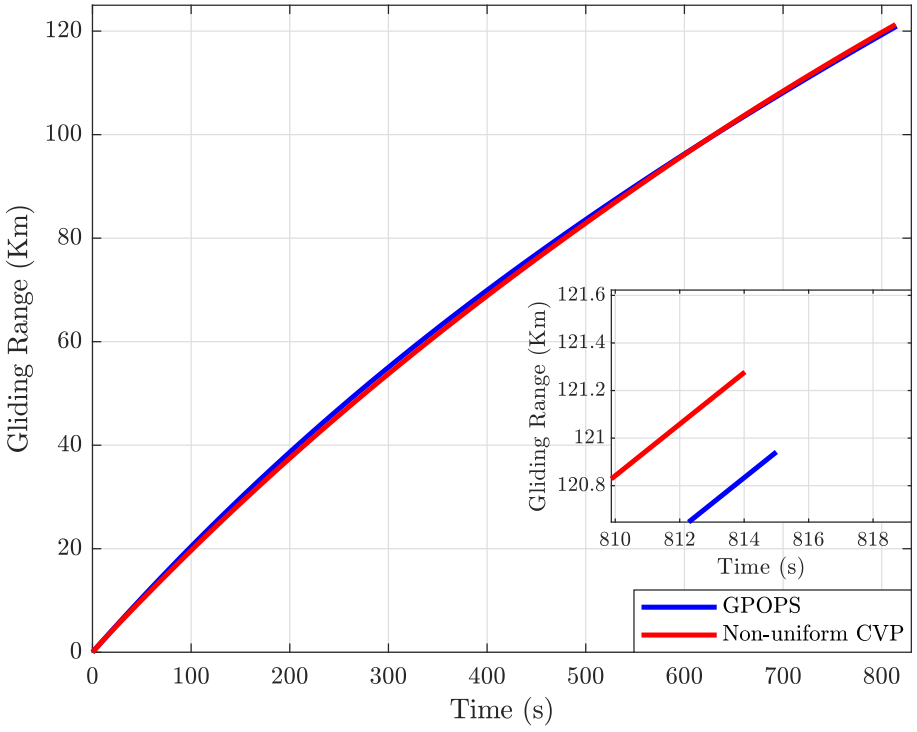

FIGURE 4.45: Gliding Range.

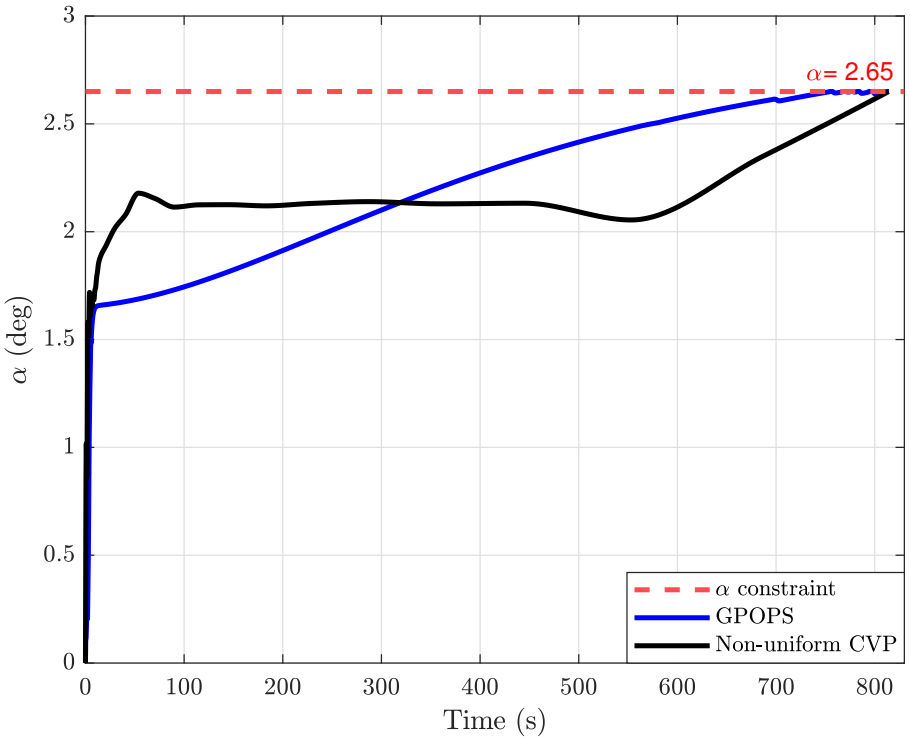

FIGURE 4.46: α Constraint.

The pitch rate Q constraint ensures stability during gliding flight, and GPOPS achieved faster stability than the prescribed CVP due to its adaptive technique. In Fig. 4.47, the Q constraint profile is shown, and the GPOPS-based response reaches a lower limit and shows minimal variation in contrast to the CVP response.

The load factor constraint profile that allows for wing-level steady gliding flight is depicted in Fig. 4.48. Fig. 4.49 reveals the elevator deflection constraint profile for maximizing glide range. Compared to the optimizer of the GPOPS, the optimizer of the CVP method produced the optimal elevator deflection profile with less stress on the SUGV elevators. While, the GPOPS remains on the edge of the elevator deflection constraint to prevent violating the angle of attack limitation.

Furthermore, to evaluate the effectiveness of the proposed CVP approach, the optimal values of the constraints and stopping values are expressed in Tables 4.6 and 4.7.

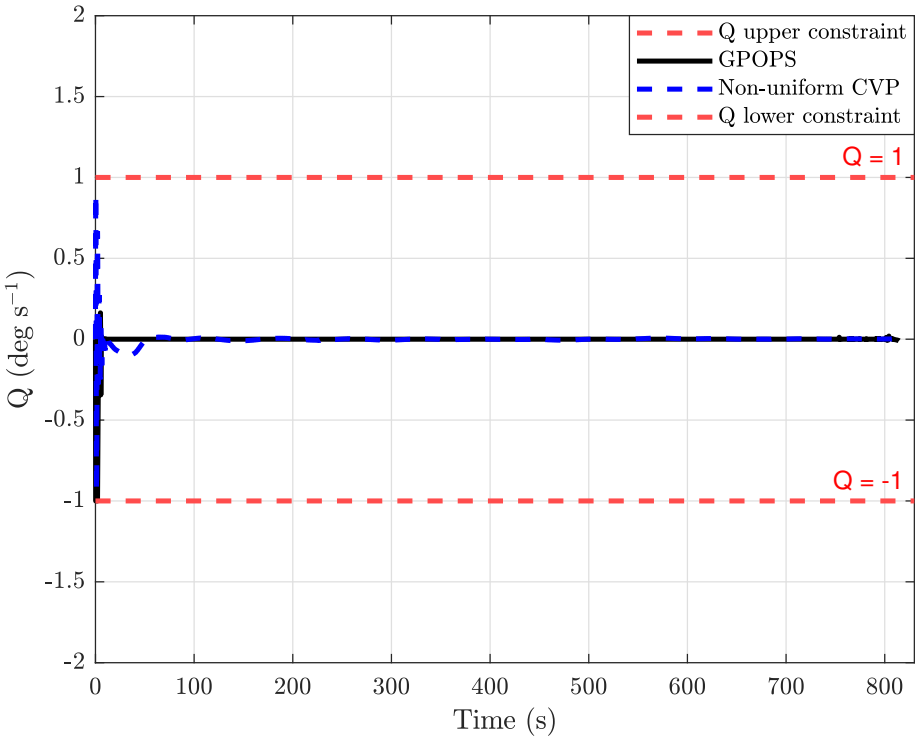

FIGURE 4.47: Q Constraint.

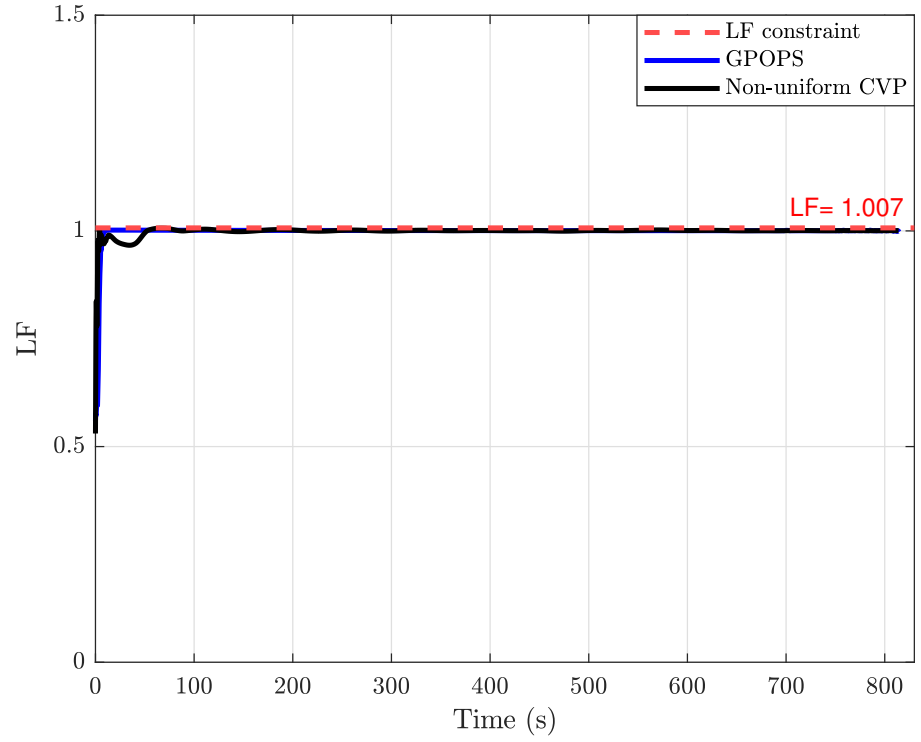

FIGURE 4.48: LF Constraint.

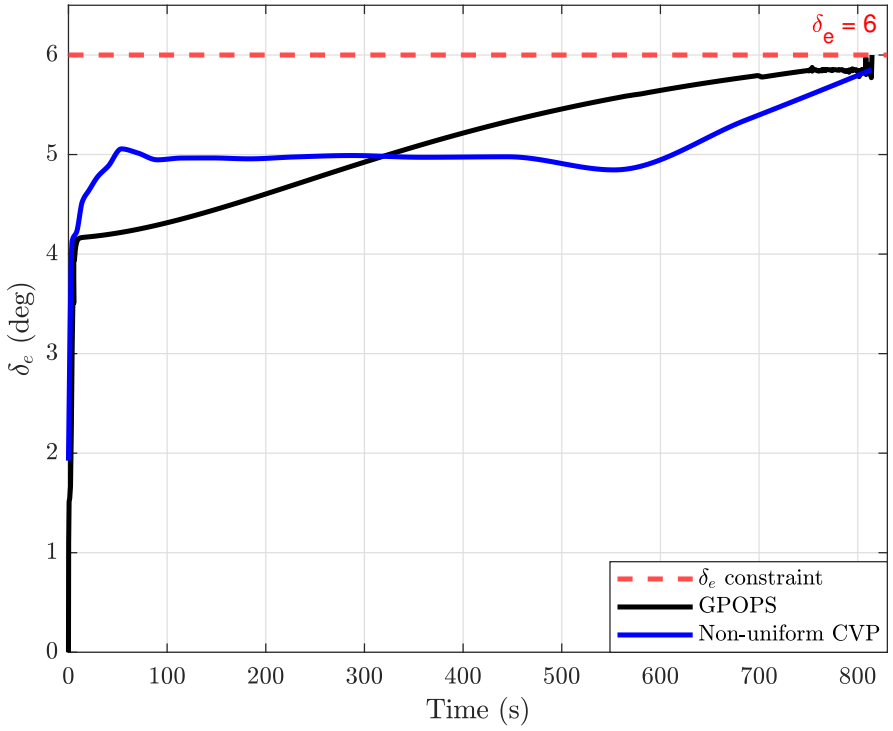

FIGURE 4.49: δ_e Constraint.

TABLE 4.6: GPOPS vs CVP constraint values.

Constraints	GPOPS	CVP
α (deg)	2.6500	2.6498
Q^L (deg s^{-1})	-1.0000	-0.9387
Q^U (deg s^{-1})	0.1629	0.8970
LF	1.0068	1.0063
δ_e (deg)	6.0000	5.8521

TABLE 4.7: GPOPS vs CVP stopping values.

Values	GPOPS	CVP
t_s (s)	815.001	814.023
R_g (km)	120.942	121.278
R_h (km)	120.525	120.856

4.5 Summary

In this chapter, Instead of employing a time-scaling approach, the concept of considering the height as a stopping constraint was modified for the maximum stoppable time to achieve the maximum gliding range. To enhance the gliding range of an SUGV, a non-uniform CVP approach based on the notion of exponential spacing was presented to provide damped and steady gliding flight. The beauty of the proposed non-uniform CVP approach is that the exponential spacing via χ can be changed to suit the needs of the problem and χ has an inverse relationship with exponential spacings between the intervals.

The proposed CVP approach does not have a complex derivation procedure and is easy to implement because the exponential spacing factor χ and the number of nodes N are design parameters to achieve the desired optimal response within a specified t_m. According to the simulation results in all three cases, the proposed non-uniform CVP approach outperformed the uniform CVP approach in terms of optimal control throughout the gliding flight, ensuring damped and steady gliding flight and maximizing the gliding range. Increasing the node count (Cases 1 to 3) in the proposed CVP approach decreased the convergence rate, increased the complexity of the optimizer, and increased the saturation at the start of the time vector.

Compared with the maximum step input simulations, the proposed non-uniform CVP presented gliding flight with an increase of 2.722 km in the gliding range and 2.863 km in the horizontal range. The non-uniform CVP approach increased the gliding range by 1.377 km and the horizontal range by 1.098 km relative to the uniform CVP approach. Furthermore, the non-uniform CVP approach achieved a horizontal range 856 m higher than the horizontal range of 120 km given in the literature. The efficacy of the proposed non-uniform CVP approach were validated by simulations executed in the MATLAB and DS Simulia Isight environments. To perform the dynamic optimization based on the proposed CVP approach, the SQP method is adopted as an optimizer in DS Simulia Isight and during this study, MATLAB plays its role as a dynamic system of SUGV.

To further evaluate the performance of the proposed non-uniform CVP approach, a comparison is made with the hp-adaptive Gaussian quadrature collocation technique. GPOPS, a very well-known tool based on the hp-adaptive Gaussian quadrature collocation technique, has been successfully used to compare the profiles of SUGV constraints and glide trajectories. GPOPS met all the constraints, but the proposed CVP outperformed the horizontal range with 330 m.

Chapter 5

Range Guidance and Control for SUGV

The application of UGV range extension is the major theme of this dissertation. This chapter describes the development of Sliding Mode Control (SMC) techniques based on the highly nonlinear model presented in Chapter 3. In this chapter, a range guidance scheme dependent on dispersion points is formulated to ensure attaining the desired range. The saturation effect in the control input and fluctuations in the range guidance command cause a terminal error in the desired range.

To overcome these problems, Integral Action (IA) based SMC (IA SMC) has been designed. Additionally, simulations based on PID SMC and IA SMC are carried out for two different ranges of 120 km and 125 km to asses the terminal error. Additionally, a quantitative analysis is conducted between PID SMC and IA SMC to observe the effectiveness.

The basic theory of SMC is described in Section 5.1. Range guidance formulation and problem formulation are described in Sections 5.2 and 5.3, respectively. The implementation of the designed controllers is explained in section 5.4. In section 5.5, simulation results are discussed, and a quantitative analysis is described in section 5.5.3. Finally, Section 5.6 concludes the chapter.

5.1 Sliding Mode Control

Sliding mode control (SMC) originated in the former USSR in the 1950s but became popular in the wider control engineering community in the 1960s after Utkin's [107] landmark research. SMC has gained considerable recognition in the field of linear [108], nonlinear [109], and robust control [110] communities and has made significant contributions to both theoretical and practical control engineering [111–115].

SMC has mainly attracted the interest of control engineers or theorists due to its inherent robustness property and it offers desirable performance even in the presence of disturbances, unmodeled dynamics, and parametric uncertainties. The main advantage of SMC is its low sensitivity to system parameter variations, which avoids the need for exact modeling. During controller design, there is always a dissimilarity between the actual model and its mathematical model.

Unstructured or unmodeled uncertainty can result from a glitch in a mathematical model, whereas structural or parametric uncertainty might result from an inaccuracy in the actual system. Designing a controller for the intended performance in the midst of disturbance and uncertainty is a difficult challenge. If disturbances and uncertainties are not managed properly, they have a negative impact on the system and can lead to dynamic instability.

A robust control strategy is needed to avoid instability and disruption. A robust controller is primarily composed of feedback control laws that maintain stability with additional laws that ensure robustness against disturbances. Hence SMC is a suitable control approach that has stability and robustness capability and can be designed for both linear and nonlinear systems. SMC law is not time-dependent and it has the characteristic of variable structure control as it continually modifies its control structure in accordance with the location of the system trajectories.

Creating the sliding surface in error space or state space before designing the SMC law is the most crucial stage. The sliding surface, which may be linear [116] or nonlinear [117], is a user-defined criterion that determines how well the sliding mode

controller performs [118]. The SMC comprises a high-speed switching control that directs the trajectory of the system to a designated sliding surface and compels it to stay there at all times.

The states of the system must continually pass and repass the sliding surface until the divergence from the surface is zero, and the system eventually glides down the surface. The SMC generates a discontinuous control signal for this purpose.

The corresponding state of the system is known as sliding mode, and the accompanying motion is known as sliding motion. To restrict the discontinuous control signal generated in response to the sliding motion, a switching function with a predetermined amplitude is required.

While from any initial conditions in the state space, the system's trajectory is compelled to contact the sliding surface. This phase is known as the reaching phase.

Consequently, there are two key phases to executing the overall sliding mode control approach.

- Reaching phase: The phase in which the system trajectory is steered in a finite time from any initial condition to the sliding surface.
- Sliding motion: During this phase, the trajectory of the system is propelled to slide along the sliding surface and approach the origin.

A graphical demonstration of these two phases is also shown in Figure 5.1, in turn give rise to a two-step design strategy.

Furthermore, the design of the SMC law consists of two design phases.

- Sliding surface design: A sliding surface is chosen with the desired dynamic properties and can be linear or nonlinear.
- Control law design: A control law is usually a combination of equivalent control and discontinuous control. This law has to meet the criteria of stability, sliding on the surface, and reaching in finite time.

5.1.1 Sliding Surface Design

The selection of a stable surface in the state space or error space on which the sliding motion is always confined is referred to as the sliding surface. In the literature, sliding surfaces are referred to by various names such as sliding manifolds, switching surfaces, and discontinuous surfaces.

The sliding surface depends on the dynamics of the system, so it must be designed in such a way that it meets all the requirements. In principle, SMC design entails determining a sliding surface that reflects desirable stable dynamics for the closed-loop system, and the trajectories of the controlled system are pushed onto the sliding surface, ensuring that the design parameters are met.

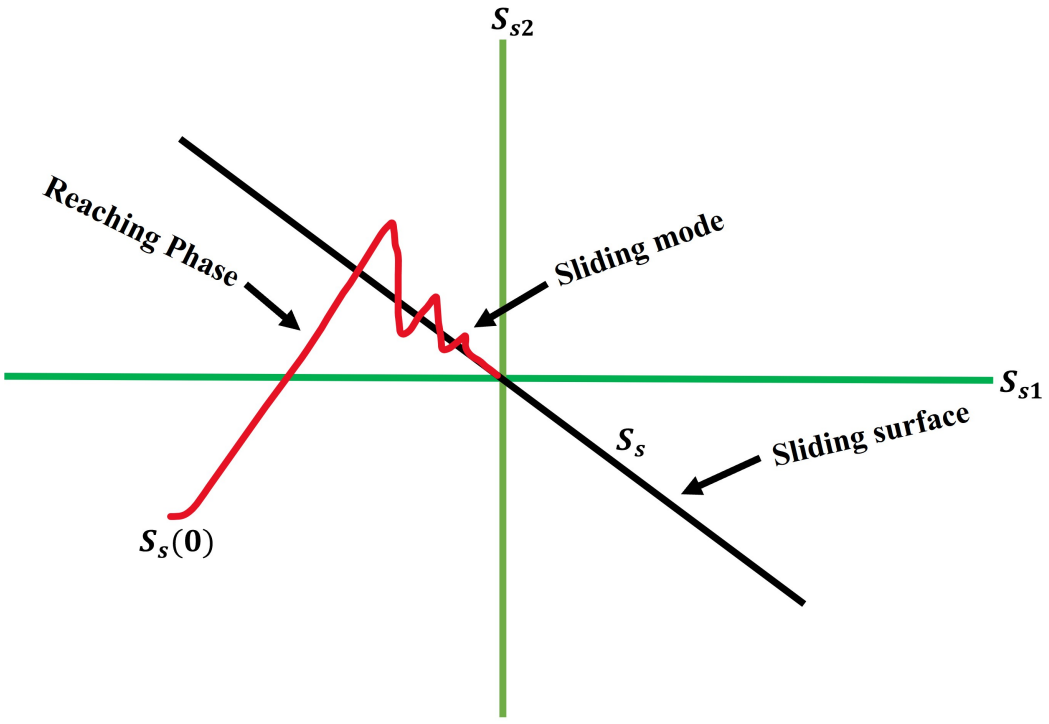

FIGURE 5.1: Demonstration of phases.

Starting from a given initial condition, the trajectories of the system are brought along the sliding surface, and at this stage, the system is sensitive to parametric uncertainties and perturbations. The trajectories of the system are insensitive to parametric uncertainties and disturbances once SMC initiates the sliding motion on the sliding surface [119].

To avoid or reduce the sensitivity problem, several methods have been published [120]. After accomplishing the design of sliding surface, The desired closed loop performance can be possible If the velocity vectors of the system trajectories are always pointing towards the sliding surface.

In light of this discussion, the design summary of the sliding surface can be itemized as

- The sliding motion is entirely related to the design of the sliding surface.
- A sliding surface can be designed as linear or nonlinear regardless of whether the actual system is linear or nonlinear.
- The sliding surface dynamics reveal the system's performance during the sliding motion.

5.1.2 Control Law Design

The SMC law guarantees that system trajectories will attain reaching phase and slide motion in the finite time given any initial conditions in state space or error space. A sliding mode controller, on the other hand, is a hybrid of equivalent control and discontinue control.

Hence, SMC law u is

$$u = u_{eq} + u_{dis} \tag{5.1}$$

The equivalent part of control law ensures that the system dynamics converge to the equilibrium point and stay on the sliding surface and discontinue part ensures that system dynamics remain in sliding motion in sliding mode.

5.1.2.1 Equivalent Control

Equivalent control acts as a continuous control during contact with the sliding surface and ensures that the change in trajectory of the system is perpendicular

to the sliding surface [121]. If switching control is considered and can be observed in the Figure 5.2, the trajectory of the system is not perpendicular to the sliding surface.

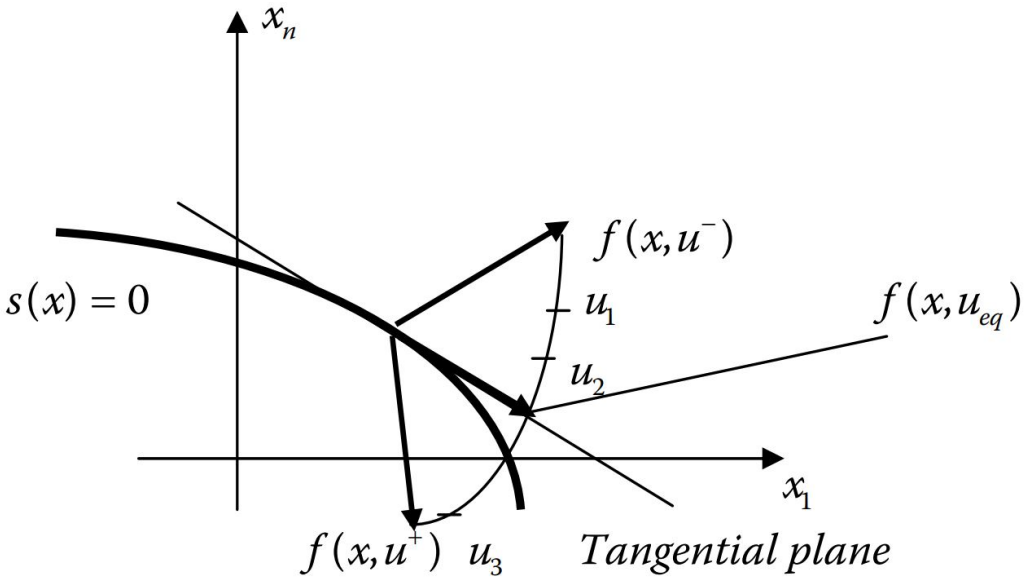

FIGURE 5.2: Concept of equivalent control [121].

In essence, the trajectory's dynamic motion on the sliding surface is averaged over the trajectory dynamics on both sides of the sliding surface. Thus dynamics during sliding can be calculated from $\dot{S}_s = 0$ and by solving $\dot{S}_s = 0$, equivalent control u_{eq} is obtained.

5.1.2.2 Discontinue Control

The discounting control u_{dis} is a high-frequency switching control that ensures the finite time convergence and the sliding motion of the system trajectory on the sliding surface. Moreover, SMC becomes insensitive to the disturbance because of u_{dis}. Various u_{dis} rules have been proposed in the existing literature as follows

- Constant reaching law:

$$U_{dis} = -ksign(S_s) \quad k > 0 \tag{5.2}$$

where k is rate of decay to converge the sliding surface.

- Exponential reaching law:

$$U_{dis} = -k_1 sign(S_s) - k_2 S_s \quad k_1, k_2 > 0 \tag{5.3}$$

where $k_2 S_s$ increases the speed of trajectories to approach the sliding motion.

5.1.3 Chattering

To maintain the sliding motion, the trajectories of the system crosses and recrosses the sliding surface, and this phenomenon produces high-frequency fluctuations. Unfortunately, this fluctuation is the main drawback of SMC and is known as chattering, as shown in the Fig. 5.3. Chattering is caused by the switching function within the S-plane of the sliding surface $S_s = 0$.

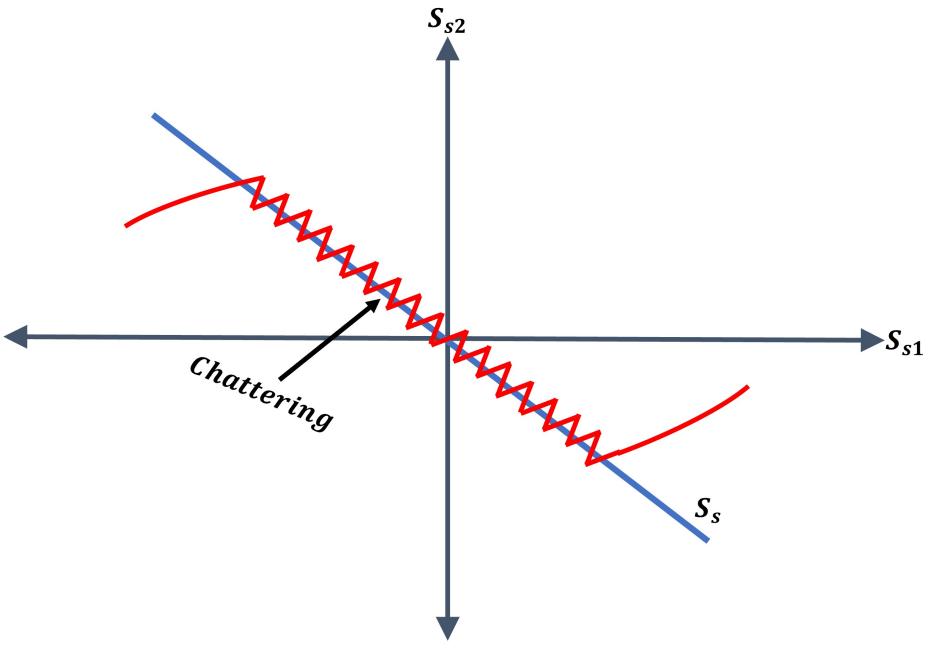

FIGURE 5.3: Chattering Problem.

$$U_{dis}(t) = \begin{cases} U_{dis}^{+}(x,t) & S_s(x) > 0 \\ 0 & S_s(x) = 0 \\ U_{dis}^{-}(x,t) & S_s(x) < 0 \end{cases} \tag{5.4}$$

Furthermore, chattering accelerates the wear and tear of actuators, reduces the accuracy of the controller and increases the probability of dynamics not predicted by the models.

To deal with the chattering problem, high-order sliding mode like super twisting algorithm [122], Real twisting algorithm [123], dynamic sliding mode [124], boundary layer approximation [125], decaying boundary layer of sliding surface [126], and various functions such as sigmoid, saturation and hyperbolic [127–129] have been proposed to smooth the discontinues control law.

5.1.4 Relative Degree and Stability Analysis

Relative Degree

The relative degree can be understand as control input u first appears explicitly only in the *rth* total time derivative of output y [130]. The relative degree is of great importance for designing the sliding surface.

A Horowitz polynomial is a very common way to design a sliding surface that depends on relative degree.

To understand the concept of relative degree, consider a triple integral problem, where $y = x_2$ is the output.

$$\dot{x}_1 = x_2$$

$$\dot{x}_2 = x_3$$

$$\dot{x}_3 = u$$

Let the above problem be solved to find the relative degree.

$$\dot{y} = \dot{x}_2 = x_3 \Rightarrow \ddot{y} = \dot{x}_3 = u$$

Thus in the above example finding u requires differentiating the output twice, and the relative degree r of the problem is two.

Stability Analysis

The SMC law is formulated in such a way that it moves the state of the system to the sliding surface ensuring the existence of the sliding mode. The reachability condition, which is placed on the control law, is used to verify the sliding mode.

Generally, Lyapunov stability analysis is used to identify the condition of the reachability condition. The stability analysis of the sliding surfaces can be determined by representing a quadratic Lyapunov functional and its time derivative as follows

$$V = 0.5S_s^2 \tag{5.5}$$

$$V = S_s\dot{S}_s \tag{5.6}$$

SMC law is designed to assure the reachability condition that guarantees the finite time convergence.

$$S_s\dot{S}_s < 0 \tag{5.7}$$

The following conditions must be satisfied to check asymptotic stability for closed-loop SMC.

- $\dot{V} < 0 \quad \text{for} \quad S_s \neq 0$
- $\lim_{|S_s|\to\infty} \quad V = \infty$

5.2 Range Guidance Formulation

A graphical formulation of range guidance for a SUGV during gliding flight is shown in figure 5.4. where u and w are the velocity components of the wind speed V. DP_R and DP_h are the dispersion points (dropping parameters from carrier platforms such as aircraft, fixed-wing drones) of the SUGV.

The relationship between dispersion points and horizontal range is as follows

$$\eth = \frac{h_o - DP_h}{R_g - R_o} \tag{5.8}$$

where R_o can be replaced by DP_R since both variables are showing the initial value of the horizontal range which is zero in this scenario. R_g in (5.8) represents the intended horizontal range and ð represents the glide ratio.

The following relation, based on the assumption that the glide angle and the flight path angle are the same, is used to determine the flight path angle γ based on R_g.

$$\gamma = tan^{-1}(ð) \tag{5.9}$$

To achieve unpowered range guidance, a range guidance command pitch angle θ_c is produced in (5.10), depending on α and γ in (5.9).

$$\theta_c = \alpha + \gamma \tag{5.10}$$

where α is the current state of the SUGV. One thing worth noting here about the range guidance command θ_c is that it directly depends on the intended range R_g and α. While γ will remain constant for this guidance command θ_c but α merely has the flexibility to alter.

5.3 Problem Formulation

Consider the general form of the SUGV nonlinear system shown below.

$$\dot{x} = f(x) + g(u) \tag{5.11}$$

$$y = hx \tag{5.12}$$

$$x_{DP} = x_{t_0} \tag{5.13}$$

where f and g are vector fields. This is considered to be the relation of x to $\Re^n$ for $t \geq$ but is usually interpreted as $x \in \Re^n$. x represents the state vector of the SUGV system (5.11). $h \in \Re^{m \times n}$ denotes the output vector, $y \in \Re^m$ is the desired scalar output that needs to be controlled, and $x_{DP} \in \Re^n$ is the dispersion point

vector. Before moving on to the design challenge, we must first understand the basic concepts of controllability, output controllability, and observability. Because these factors decide whether or not a system is appropriate for controller design.

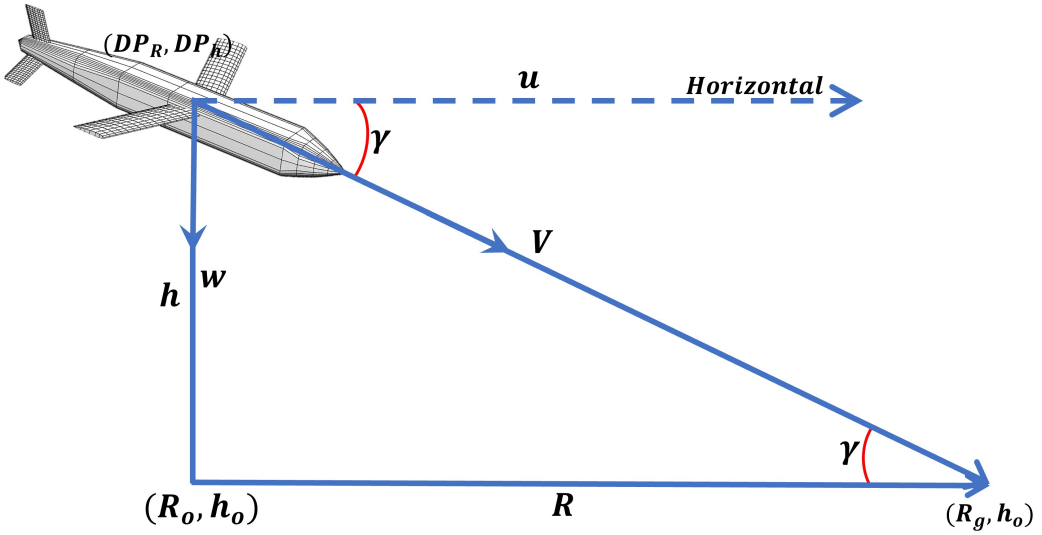

FIGURE 5.4: Range Guidance.

Controllability: If the control inputs cannot control any of the states of the depicted system, then the intended controller cannot control the states. We are implying that the control input must influence the behavior of each state.

This idea is crucial for state feedback control, stabilization control, and optimal control. Controllability may be described as the input to a system that moves each state from an initial state to a desired final state, and a system that meets the criteria is controllable, otherwise, the system is uncontrolled.

Controllability can therefore be defined in mathematical language as a nonlinear system (5.11), with vector fields f and g, is controllable, if and only if there exists a region D such that the vector fields $\{g, ad_f g, ..., ad_f^{n-1} g\}$ are linearly independent in D.

To verify controllability, the following steps are required.

- Compute the vector field $\{g, ad_f g, ..., ad_f^{n-1} g\}$ by the Lie derivatives.
- Check whether the vector field is full rank or not.

Output controllability: Output controllability is slightly different from controllability as it relates to the input and output of the system. This concept is very helpful for controllers that rely on output tracking. The ability of a system input to move a desired system output from any initial condition to the final condition in a finite time is referred to as output controllability.

The output controllability can be considered as a nonlinear system (5.11), with f, g and h vector fields, is output controllable, if and only if there exists a region $\tilde{D}$ such that the vector fields $\{hg, had_f g, ..., had_f^{n-1} g\}$ are linearly independent in $\tilde{D}$.

The output controllability can be calculated mathematically by the following step.

- Compute the vector field $R = \{g, ad_f g, ..., ad_f^{n-1} g\}$.
- Check the vector field *rank(R)=n* to verify output controllability.

Observability: So far, for the conditions of controllability and output controllability, it has been assumed that all states of a nonlinear system exist. Sometimes the availability of states is important for fault detection, fault-tolerant control, and system monitoring.

Unfortunately, no single state of the system is rarely available because a sensor on each state is expensive and then requires the available measured output to reconstruct the state. This reconstruction of the state depends on observability. If this condition is fulfilled, it means that the state can be built. Observability can be stated as if at any initial condition a state vector can be extracted from the output of the system in a finite time, then the system is observable, otherwise, it is unobservable.

In mathematical form, observability can be described as the f and h vector fields are observable, if and only if there exists a region $\hat{D}$ in which the vector fields $\{h, had_f, ..., had_f^{n-1}\}^T$ are linearly independent in $\hat{D}$.

The observability of any nonlinear system can be calculated as

- Compute the vector field $\varnothing = \{h, had_f, ..., had_f^{n-1}\}^T$.

- If $rank(\varnothing) = n$ then observability exits.

The following is the controller design statement for unpowered range guidance:

Problem: Given a desired command signal $\theta_c \in \Re$, design a feedback control approach in terms of the control u such that the desired command θ_c is an attractive set for θ, so that there exists an $\epsilon > 0$, such that $\theta(t : t_o, x_{DP}) \to \theta_c$, as $t \to \infty$ for any initial condition $(t_o, x_{DP}) \in \Re^+ \times B(\theta_c : \epsilon)$. While designing the controller, a few assumptions are also taken into consideration.

- **Assumption 1:** SUGV nonlinear dynamics are controllable and output controllable.
- **Assumption 2:** All states are measurable.
- **Assumption 3:** Nonlinear disturbances such as atmospheric conditions, unmodel dynamics, and parameter uncertainties are neglected.

5.4 Controller Design

In this section, the SMC-based nonlinear controller design is presented and the sliding surface is constructed in such a way that it acts like a PID sliding surface.

5.4.1 Integral Action

To mitigate the saturation effect in range guidance law and to facilitate the smooth guidance command θ_c generated from (5.10), an integral action denoted by $\Omega \in \Re^1$, is established as follows

$$\dot{\partial}_{\theta_c} = \Xi(\theta_c - \partial_{\theta_c}) \tag{5.14}$$

$$\Omega = \int e \, dt \tag{5.15}$$

where $\Xi \in \Re$ is strictly positive, constant design gain, and $\partial_{\theta_c} \in \Re^1$ is filtered command.

To quantify the desired task, an output tracking error, illustrated by $e \in \Re^1$, is defined as

$$e = \partial_{\theta_c} - \theta \tag{5.16}$$

5.4.2 Sliding Surface Design

The initial stage in constructing the sliding mode controller is to design the sliding surface. To design the sliding surface, the Hurwitz polynomial for Ω is selected as

$$S_{S_{IA}} = \Omega \left(\tilde{C}_1 \frac{d}{dt} + \tilde{C}_2 \right)^{r_d - 1} \tag{5.17}$$

where $r_d \in \Re$ identifies a relative degree which is 3 in the case of (5.11). Hence the desired sliding surface $S_{S_{IA}}$ is computed as follows

$$S_{S_{IA}} = \tilde{C}_1^2 \ddot{\Omega} + 2\tilde{C}_1 \tilde{C}_2 \dot{\Omega} + \tilde{C}_2^2 \Omega \tag{5.18}$$

where $\tilde{C}_1$, $\tilde{C}_2 \in \Re$ are designing parameters. In (5.18), substitute Ω from (5.15) for simplicity.

$$S_{S_{IA}} = K_p e + K_i \int e + K_d \dot{e} \tag{5.19}$$

where k_P, k_i and k_d are $2\tilde{C}_1\tilde{C}_2$, $\tilde{C}_2^2$ and $\tilde{C}_1^2$, respectively and a graphical structure of (5.19) can also be expressed in Fig. 5.5.

5.4.3 Range Guidance Law

SMC law is a sum of $\tilde{U}_{eq}$ and $\tilde{U}_{dis}$ to ensure reaching phase, and it has to ensure that the trajectory stays on the sliding surface after it has reached the sliding surface.

Equivalent control $\tilde{U}_{eq}$ is calculated by taking time derivative of $S_{S_{IA}}$ (5.19) and put equal to zero.

$$\dot{S}_{S_{IA}} = K_p \dot{e} + K_i e + K_d \ddot{e} \tag{5.20}$$

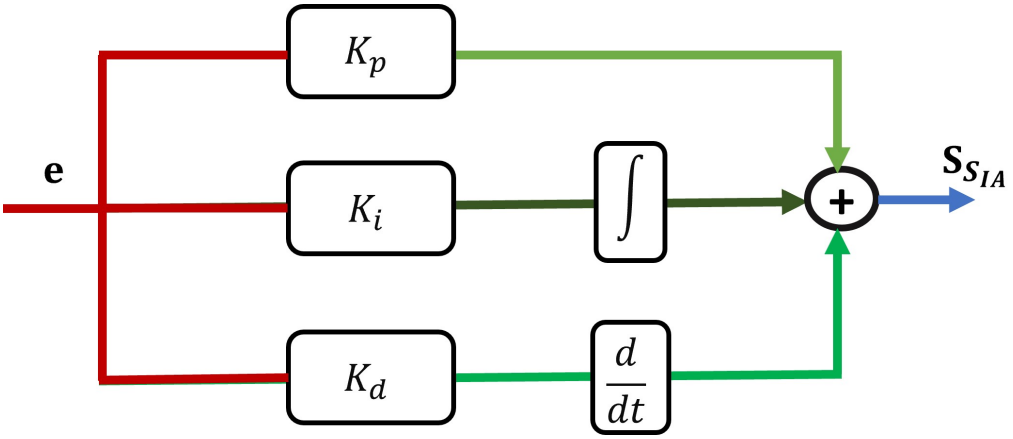

FIGURE 5.5: Graphical structure of $S_{S_{IA}}$.

Plugging (3.28, M from (3.32), C_M from 3.34) and (5.16), $\dot{S}_{S_{IA}} = 0$ is written as

$$0 = K_p\dot{e} + K_i e + K_d(\ddot{\partial}_{\theta_c} - a_{11} - a_{00}\tilde{U}_{eq}) \tag{5.21}$$

After simplification, expression of $\tilde{U}_{eq}$ is

$$\tilde{U}_{eq} = \frac{1}{a_{00}K_d}(K_p\dot{e} + K_i e + K_d(\ddot{\partial}_{\theta_c} - a_{11})) \tag{5.22}$$

where a_{00} and a_{11} are $\frac{\rho V^2 S\bar{C}C_{M_{\delta_e}}}{2I_y}$, $\frac{\rho V^2 S\bar{C}}{2I_y}\left(C_{M_\alpha}\alpha + \frac{C_{M_Q}Q\bar{C}}{2V}\right)$, respectively.

A fundamental disadvantage of SMC known as "chattering" has already been highlighted, and a modified strong exponential reaching law based on atan function is used to eradicate the chattering. atan, $\forall\ S_S \in \Re$ is a smooth continuous, differentiable, nonlinear, odd, and real-valued S-shaped function which can operate as a smooth switching function. Additionally, atan has the following properties:

$$\begin{aligned} \max_{S_S\in\Re} \wp(S_S) &= \lim_{S_S\to\infty} \wp(S_S) = \jmath \\ \min_{S_S\in\Re} \wp(S_S) &= \lim_{S_S\to-\infty} \wp(S_S) = -\jmath \end{aligned} \tag{5.23}$$

where $\jmath$ presents the bounds on the function atan, and it is $\frac{2}{\pi}$, and can be seen in Fig. 5.6. From the Fig. 5.6, it can be checked that the atan function is an antisymmetric, monotonic, and uniformly bounded function.

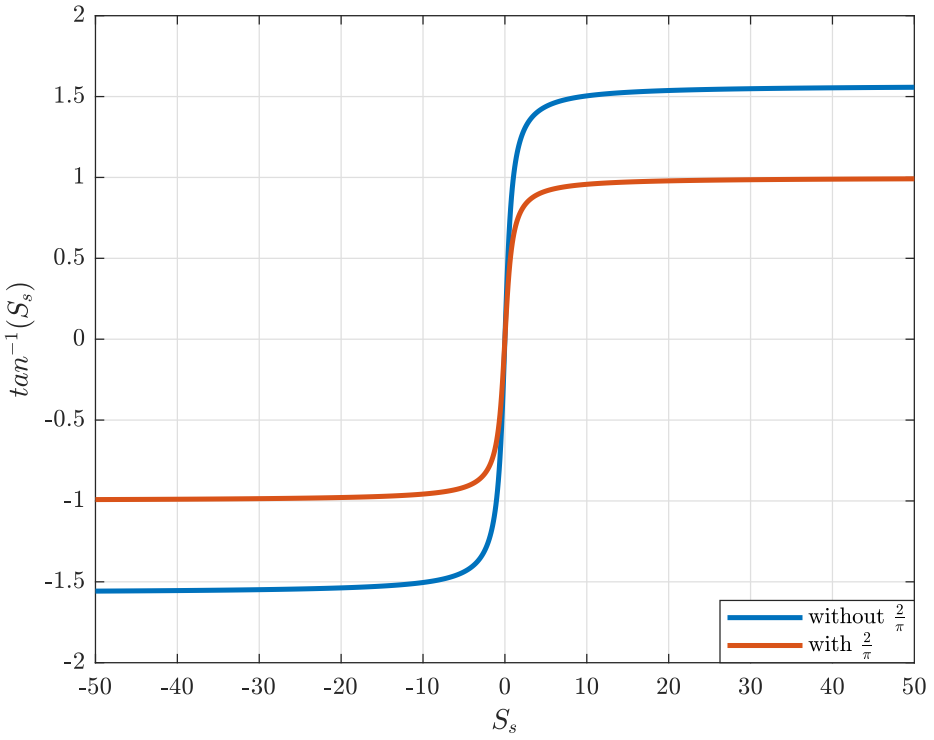

FIGURE 5.6: atan switching function with bound.

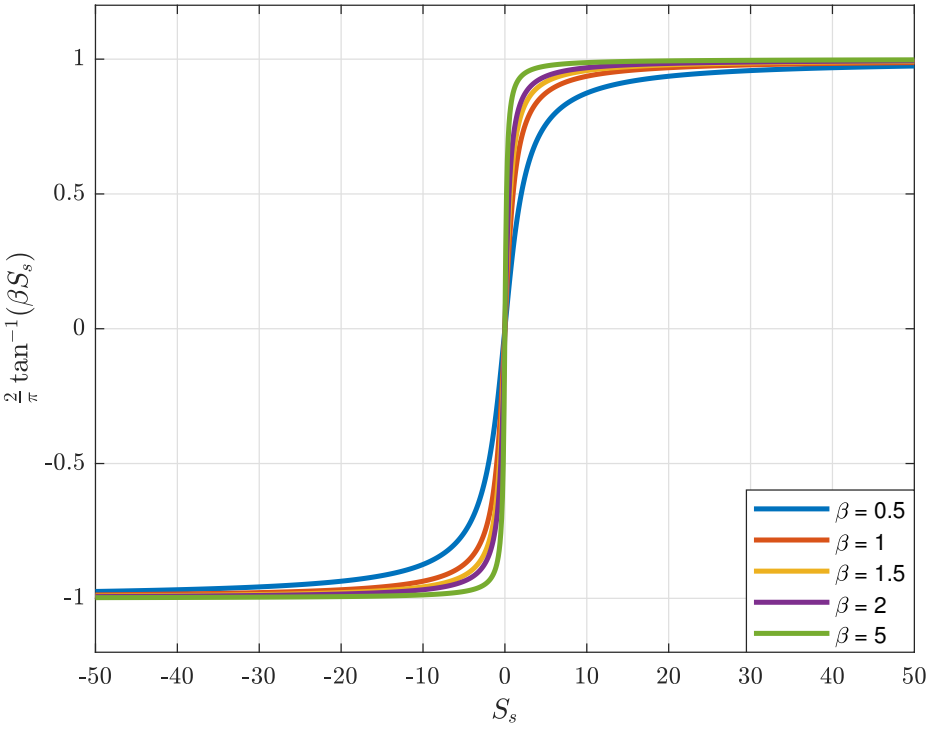

FIGURE 5.7: atan switching function with different slopes.

atan function with various β slopes is also displayed in Fig. 5.7. It is also noted that when β is adjusted, it originates the changeable boundary layer width around the sliding surface. An additional term $S_{S_{IA}}^3$ is introduced in the exponential reaching law based on atan to increase the response to reach the equilibrium point of the sliding surface whether the system is moving away from or near the sliding surface. In strong exponential reaching law, to ensure the fast approach, the designing gains of $S_{S_{IA}}$, $S_{S_{IA}}^3$ should be increased while the gain of $\tan^{-1}(S_{S_{IA}})$ should be decreased. So the following discontinuous control law $\tilde{U}_{dis}$ is employed as

$$\tilde{U}_{dis} = b_{00}\frac{2}{\pi}\tan^{-1}(\beta S_{S_{IA}}) + b_{11}S_{S_{IA}} + b_{22}S_{S_{IA}}^3 \tag{5.24}$$

where b_{00}, b_{11}, $b_{22} \in \Re$ are designing gains for $\tilde{U}_{dis}$ and the entire range guidance law is given as follows

$$\begin{aligned}\tilde{U} = &\frac{1}{a_{00}K_d}(K_p\dot{e} + K_i e + K_d(\ddot{\partial}_{\theta_c} - a_{11})) \\ &+ b_{00}\frac{2}{\pi}\tan^{-1}(\beta S_{S_{IA}}) + b_{11}S_{S_{IA}} + b_{22}S_{S_{IA}}^3\end{aligned} \tag{5.25}$$

5.4.4 Stability Analysis

To ensure the stability of the controller for SUGV range guidance, the AI SMC must satisfy the following theorem.

Theorem 5.1. *Considered the SUGV nonlinear system in (5.11) and the range guidance law in (5.25) then the AI SMC is asymptotically stable as*

$$\dot{\varrho} \leq -\Lambda_1|S_{S_{IA}}| - \Lambda_2 S_{S_{IA}}^2 - \Lambda_2 S_{S_{IA}}^4 \tag{5.26}$$

where Λ_1, Λ_2 and Λ_3 are the positive design constants.

Proof. To prove this theorem, consider the time derivative of sliding surface $S_{S_{IA}}$ represented in (5.20), one obtains

$$\dot{S}_{S_{IA}} = K_p\dot{e} + K_i e + K_d\ddot{e} \tag{5.27}$$

After substituting the error from (5.16) and range guidance law (5.24) in (5.27) then resultant time derivative of $S_{S_{IA}}$ becomes

$$\begin{aligned}\dot{S}_{S_{IA}} = & -a_{00}K_d(b_{00}\frac{2}{\pi}\tan^{-1}(\beta S_{S_{IA}}) \\ & - b_{11}S_{S_{IA}} - b_{22}S^3_{S_{IA}})\end{aligned} \tag{5.28}$$

To check the stability condition, a quadratic Lyapunov candidate function is chosen as

$$\varrho = 0.5S^2_{S_{IA}} \tag{5.29}$$

Time derivative of (5.29) yields

$$\dot{\varrho} = S_{S_{IA}}(-a_{00}K_d(b_{00}\frac{2}{\pi}\tan^{-1}(\beta S_{S_{IA}}) - b_{11}S_{S_{IA}} - b_{22}S^3_{S_{IA}})) \tag{5.30}$$

$$\dot{\varrho} \leq -\Lambda_1 S_{S_{IA}}\frac{2}{\pi}\tan^{-1}(\beta S_{S_{IA}}) - \Lambda_2 S^2_{S_{IA}} - \Lambda_2 S^4_{S_{IA}} \tag{5.31}$$

where Λ_1, Λ_2 and Λ_3 are $a_{00}K_d b_{00}$, $a_{00}K_d b_{11}$ and $a_{00}K_d b_{22}$, respectively. It is evident from Fig. 5.6 that $S_{S_{IA}}\frac{2}{\pi}\tan^{-1}(\beta S_{S_{IA}})$ can be transformed into $|S_{S_{IA}}|$ then (5.31) is negative definite if $\Lambda_1, \Lambda_2, \Lambda_3 > 0$.

Consequently, the following result confirms the negative definiteness of the AI SMC scheme.

$$\dot{\varrho} \leq -\Lambda_1|S_{S_{IA}}| - \Lambda_2 S^2_{S_{IA}} - \Lambda_2 S^4_{S_{IA}} \tag{5.32}$$

Now, stepping back to understand, the AI SMC based $\tilde{U}$ ensures the enforcement of θ to ∂_{θ_c} . Therefore, this results in asymptotic convergence of the measured state of the SUGV to the range guidance command. □

5.5 Results and Discussion

In this section, for range guidance, performance studies of the proposed Integral Action (IA) SMC and PID SMC are presented. The obtained outcomes are succinctly demonstrated to authenticate the improvements in gliding flight for a range of 120 km and 125 km. A closed loop range guidance approach has been expressed

in the Fig.5.8. For PID SMC, sliding surface is written as

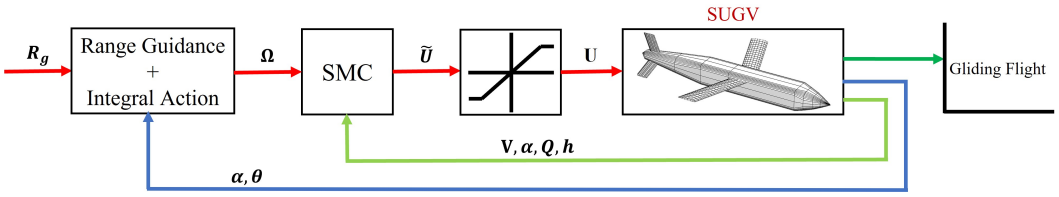

FIGURE 5.8: AI SMC scheme for range guidance.

$$S_{S_{PID}} = K_p e + K_i \int e + K_d \dot{e} \tag{5.33}$$

where e is $\theta_c - \theta$. The design gains for $S_{S_{IA}}$, $S_{S_{PID}}$ and $\tilde{U}_{dis}$ are kept identically to make a comparison between PID SMC and IA SMC and all design gains are tabulated in Table 5.1. For range guidance, simulations are performed using the Dispersion Points (PDs) [92] listed in Table 5.2.

TABLE 5.1: Design gains for AI SMC and PID SMC.

K_p	0.0621	b_{00}	0.9
K_i	0.0100	b_{11}	0.7
K_d	0.0964	b_{22}	0.6

TABLE 5.2: Dispersion Points for range guidance.

States	DPs
V	216 ms^{-1}
α	0 deg
Q	0 deg s^{-1}
θ	0 deg
R	0 km
h	10 km

5.5.1 Case A: 120 km

An unpowered gliding flight response for the PID SMC and IA SMC controllers is shown in Fig. 5.9. After launching the SUGV, the PID SMC controller employs a slow reaction to stabilize the vehicle, and this reaction encounters the free fall effect between the 0.8 km range and to 2.2 km range.

In the presence of the PID SMC controller, however, a terminal error of 281.3 m is recorded, which the controller cannot regulate because of the non-smooth response of α in the range guiding command (5.10).

In the context of PID SMC, this is also one of the main reasons that cause a terminal error. On the other hand, the IA SMC follows a filtered range guidance command that is free of fluctuations and thus a terminal error of 0.35 m is observed.

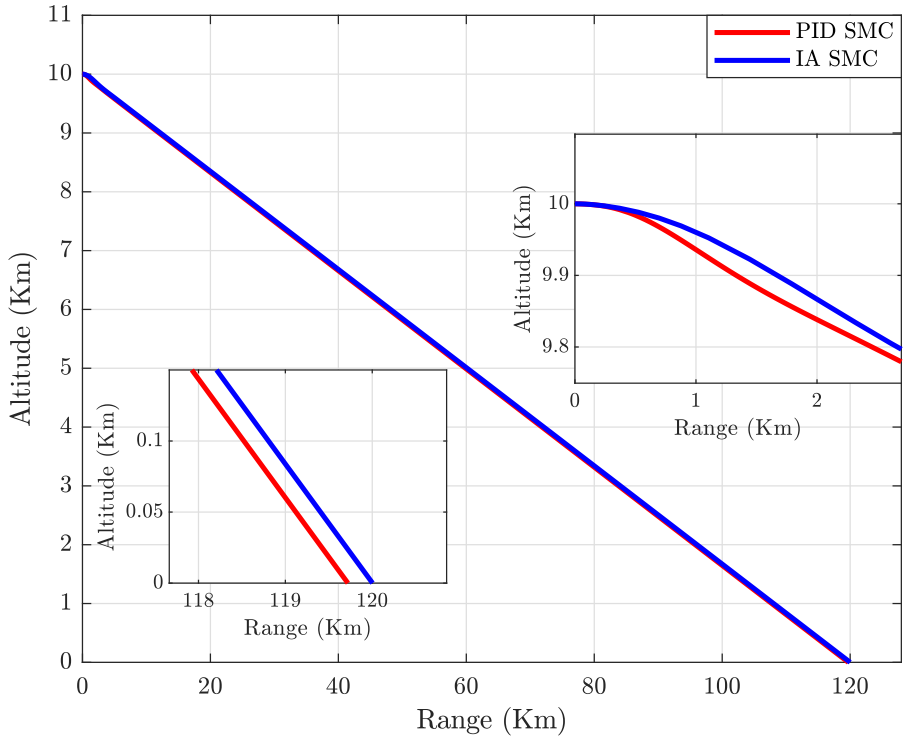

FIGURE 5.9: Gliding flight for 120 km range.

The combination of α and Q provides damped and stable gliding flight which is additionally treated to decrease Phugoid oscillations. In the case of PID SMC, the α profile begins with a negative angle, indicating that the SUGV's nose is down and the weight is greater than the lift force.

At the same time, pitch rate Q, which is also responsible for dynamic stability, has a value of -2.5 deg s^{-1}, indicating that the SUGV experienced jerky angular momentum, leading to free fall behaviour.

The IA SMC controller, on the other hand, provides faster damping and stabilization to the SUGV. This can be noted in Figs. 5.10 and 5.11. The output tracking response of commanded profile for the PID SMC and IA SMC is displayed in Figs. 5.12 and 5.13.

The range guiding command (5.10) swings in the PID SMC tracking situation due to the rapid shift in α. On the other hand, in the case of IA SMC tracking, range guiding command is smooth due to integral action (5.14, 5.15).

The flight path angle γ in Fig. 5.14 can also be considered as the tracking criterion between PID SMC and IA SMC because the range guidance command is a combination of α and γ. In other words, if we indirectly monitor γ, we control θ because θ is also a sum of γ and α, which is the inherent state of SUGV.

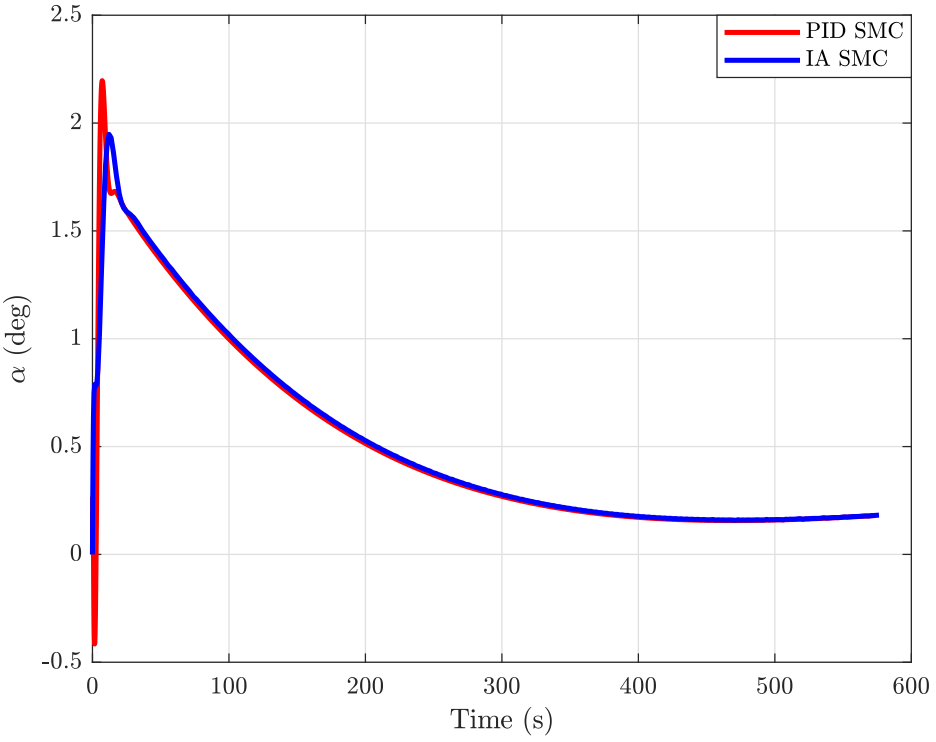

FIGURE 5.10: α profile for 120 km range.

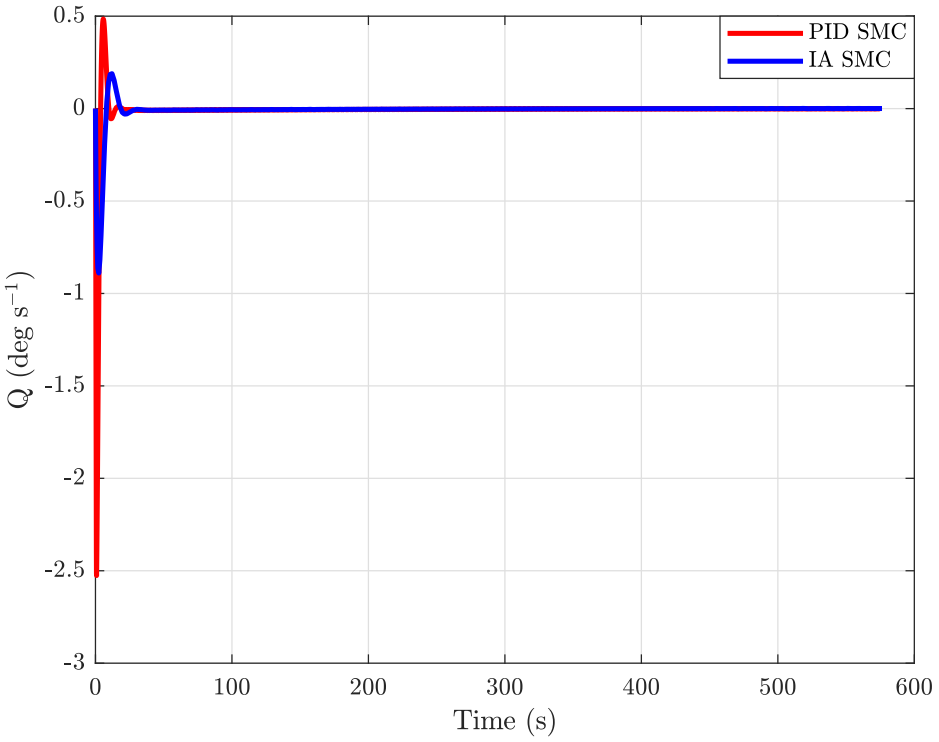

FIGURE 5.11: Q profile for 120 km range.

Every physical system has some limit on the control input, if the control input exceeds the limit it can become uncontrollable or degrade the performance but in our study, the elevator deflection ranges from 0^o to 6^o.

To achieve the actuation limit, a saturation block is introduced, which can be noticed in Fig. 5.8. When the PID SMC scheme is employed to attain the attended range, the actuation effect from Fig. 5.15 can be assessed and this is also a source of the terminal error in the gliding range.

Consequently, the proposed control scheme is completely independent of the actuator limiting effect and produces a smooth profile with less burden on elevators. The sliding surfaces of both controllers can also be visualized in Fig.5.16.

The sliding surface of the proposed controller exhibits a fast reaching phase than the PID SMC controller which is also a significant factor of the IA SMC controller in achieving the expected glide range.

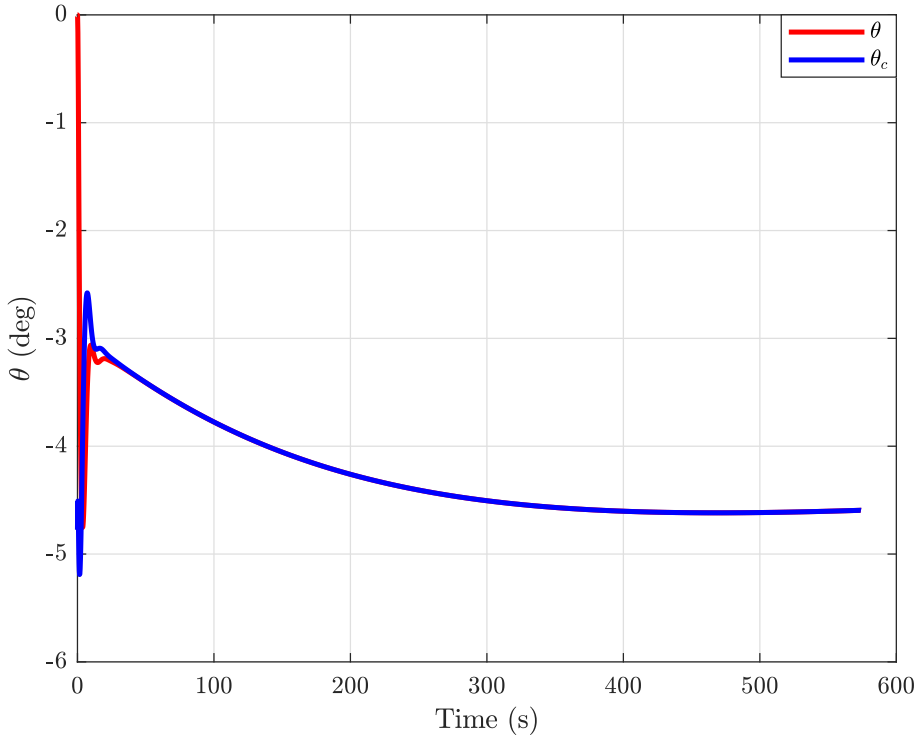

FIGURE 5.12: PID SMC tracking profile for 120 km range.

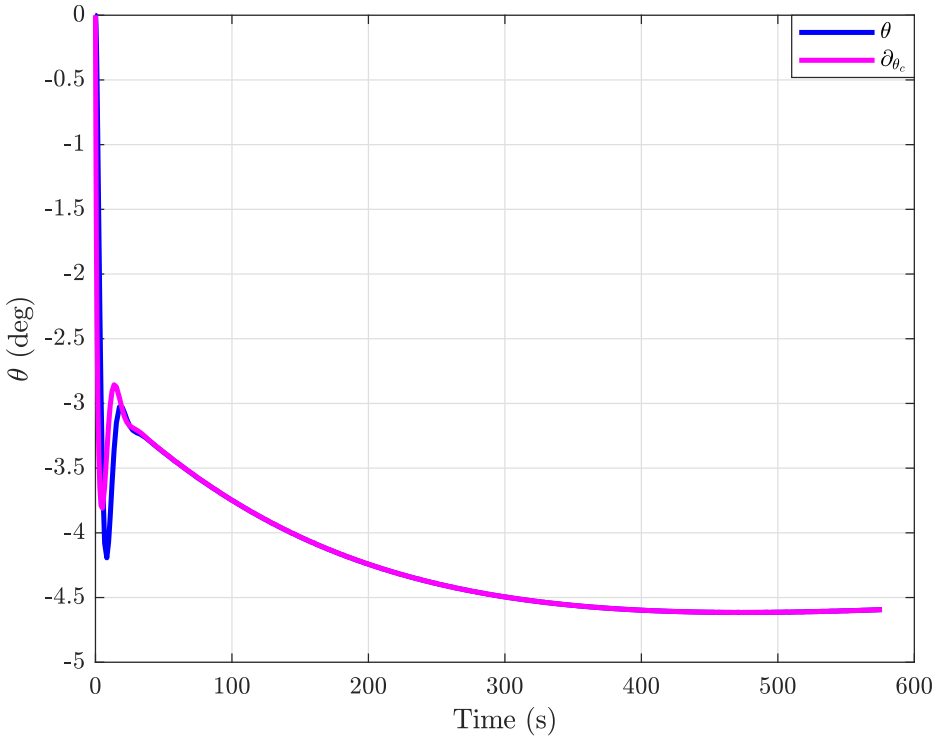

FIGURE 5.13: AI SMC tracking profile for 120 km range.

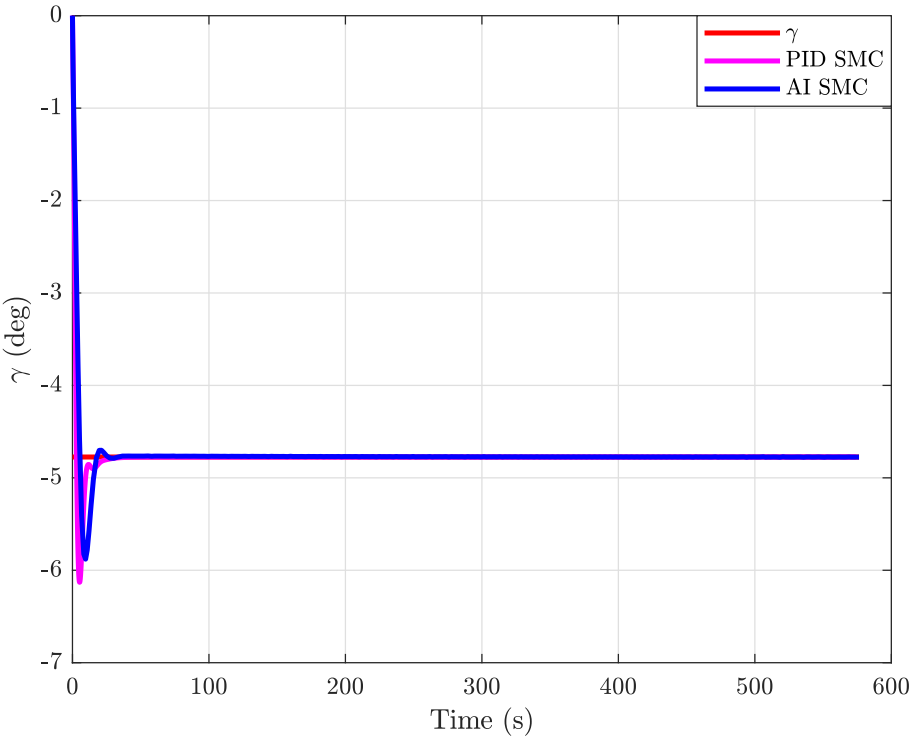

FIGURE 5.14: γ tracking profile for 120 km range.

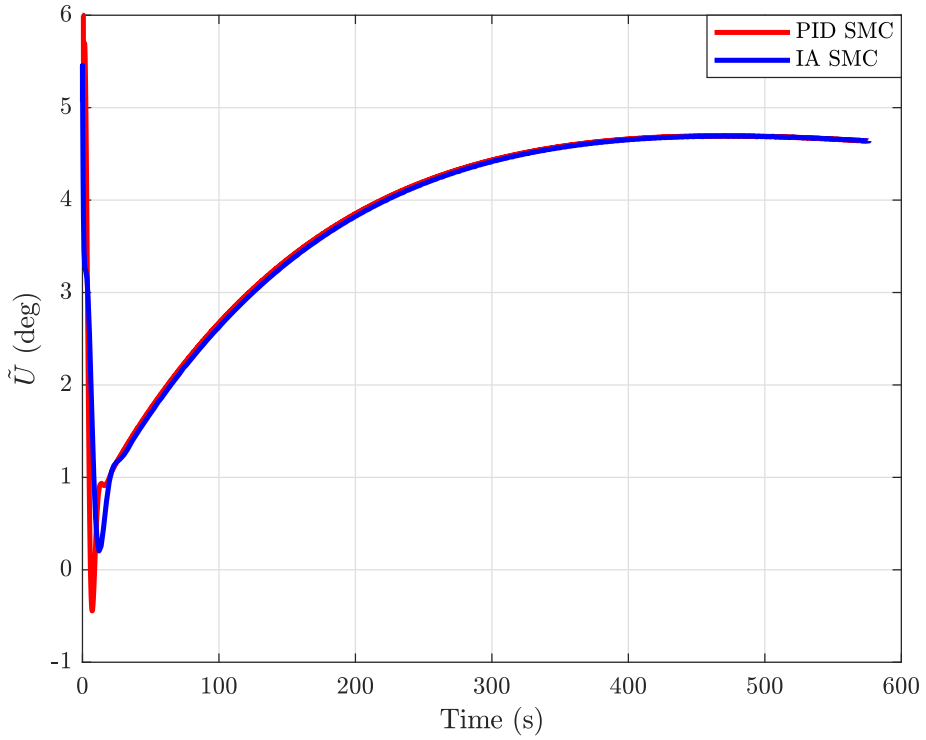

FIGURE 5.15: Control input profile for 120 km range.

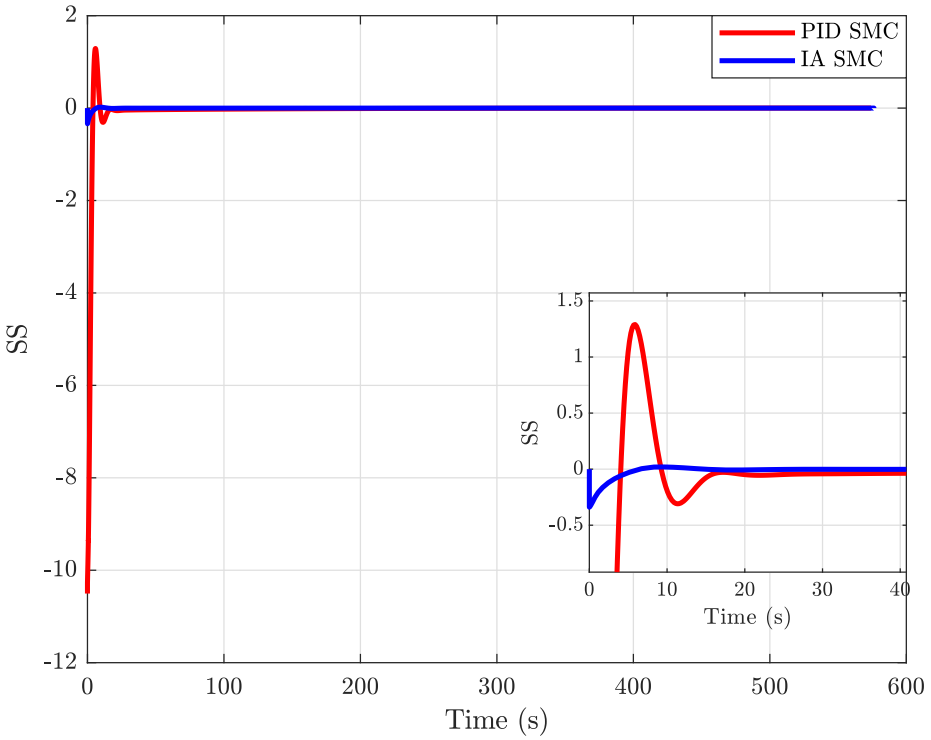

FIGURE 5.16: Sliding surface profile for 120 km range.

5.5.2 Case B: 125 km

Gliding flight for 125 km range is expressed in Fig. 5.17 with PID terminal error of 273.8 m in case of PID SMC. AI SMC generates a stable flight after launching from carrier platform and in this case, terminal error is 0.29 m.

Proposed Control scheme generates the control input such that the α become small so that in range guidance, guidance command θ_c and flight path angle almost remain same. Pitch rate Q ensures the dynamic stability of gliding vehicle and relates with angular momentum. So small amplitude of Q and become zero as soon as possible provides fast stability.

During gliding flight phugoid oscillation can be handle by controlling the α and Q. Proposed controller provides fast damping and small α, can be seen in Figs. 5.18, 5.19, after launching the SUGV that provides the help to attain stable flight and tracking the guidance command.

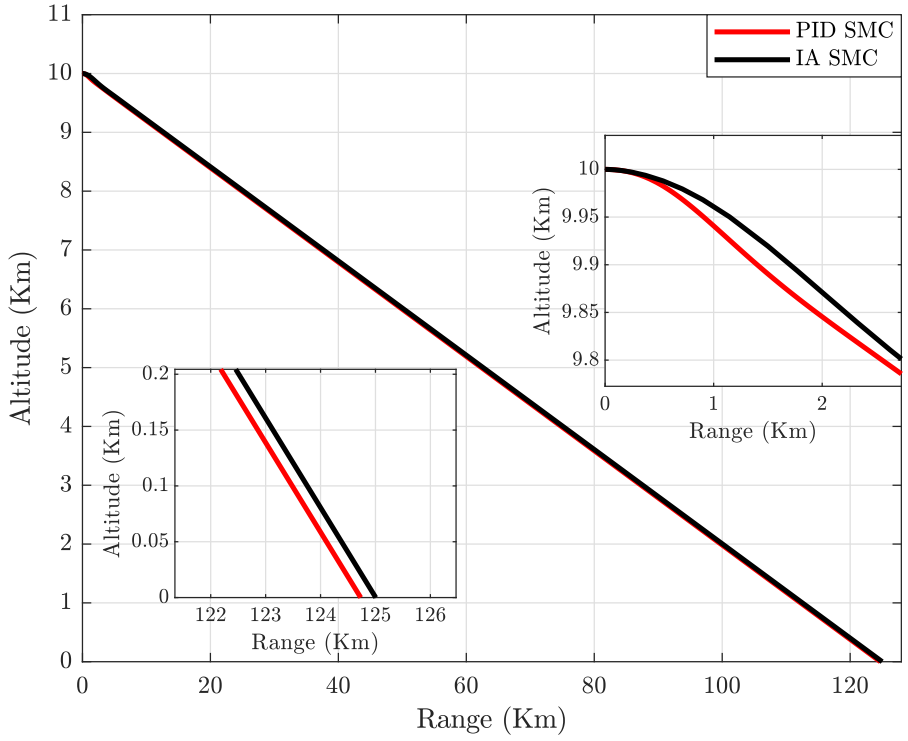

FIGURE 5.17: Gliding flight for 125 km range.

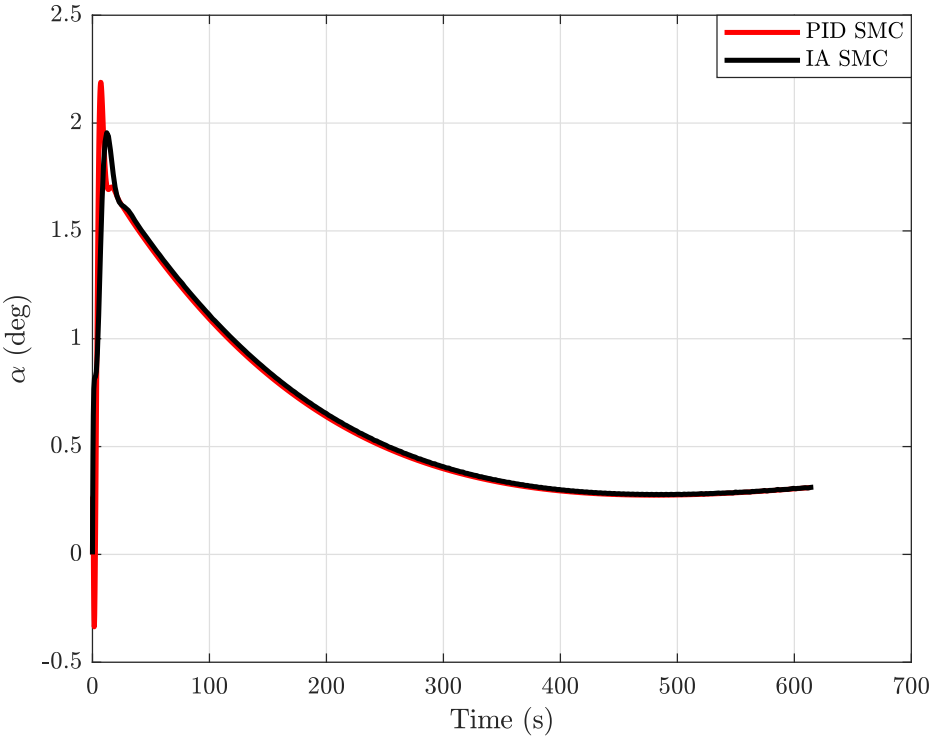

FIGURE 5.18: α profile for 125 km range.

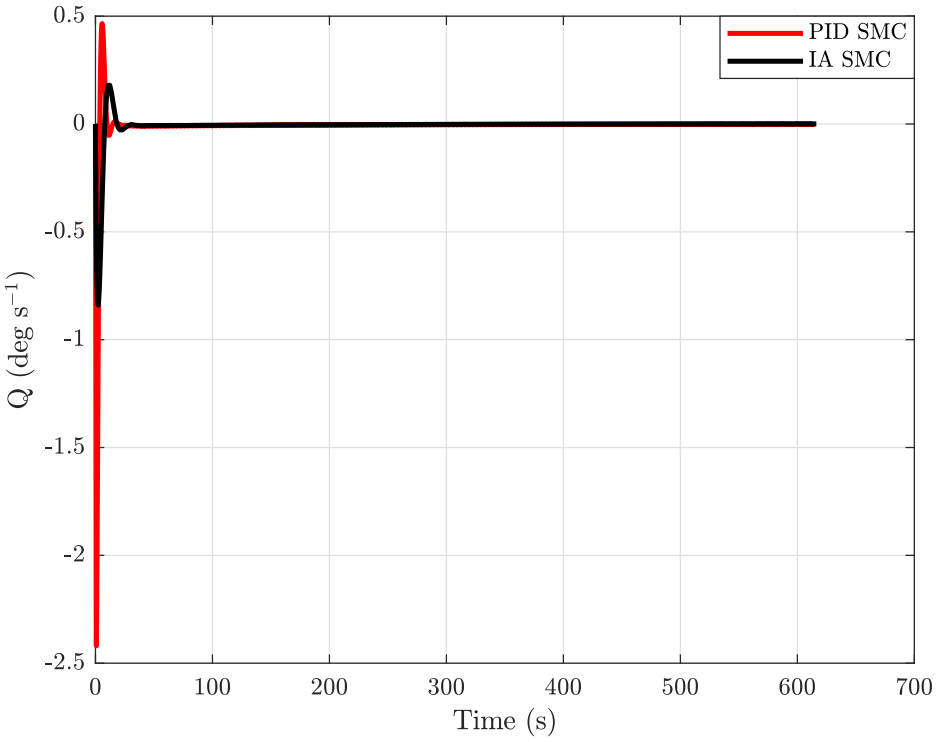

FIGURE 5.19: Q profile for 125 km range.

Flight path angle tracking response for both controller is shown in Figure. 5.22 and proposed controller provides the fast tracking in comparison to the PID SMC response.

Elevator deflection has inverse relation with pitch angle response. When elevator deflection is positive then nose of SUGV is down and it is negative then nose is up. Proposed controller generates a smooth control input profile as compared to PID SMC control scheme.

It can be examined that IA SMC controller start with 5.56^o deflection and after sometime decrees the deflection which means it tries to nose up and to attain lift so that it can achieve more gliding flight.

Comparison of sliding surfaces in Fig. 5.24 demonstrates that the batter tracking performance, fast reaching phase and sliding motion is achieved by proposed control scheme.

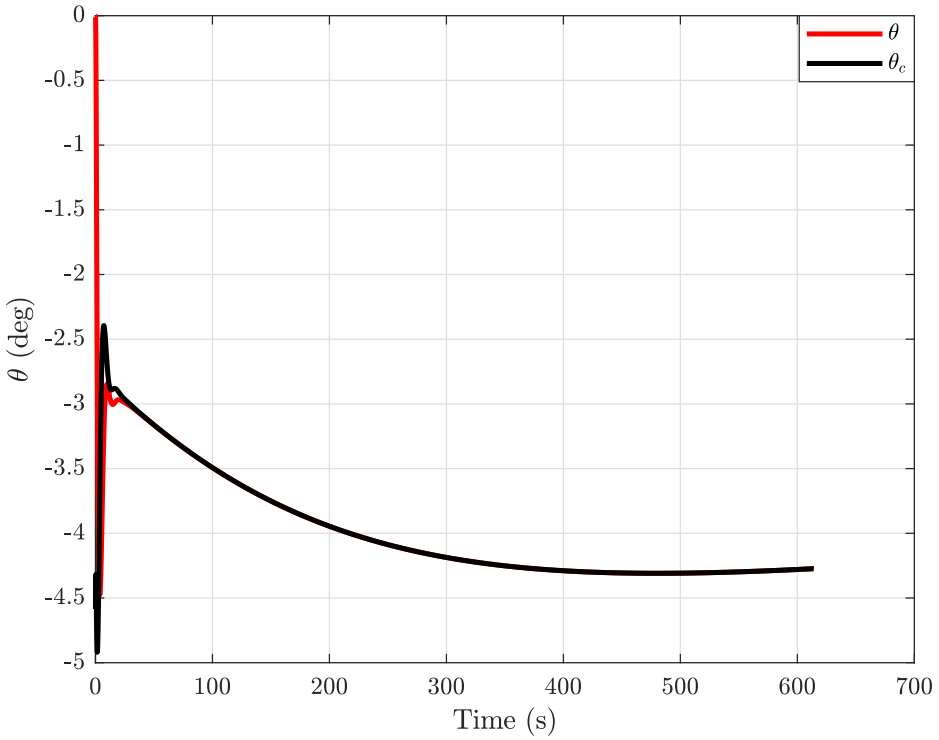

FIGURE 5.20: PID SMC tracking profile for 125 km range.

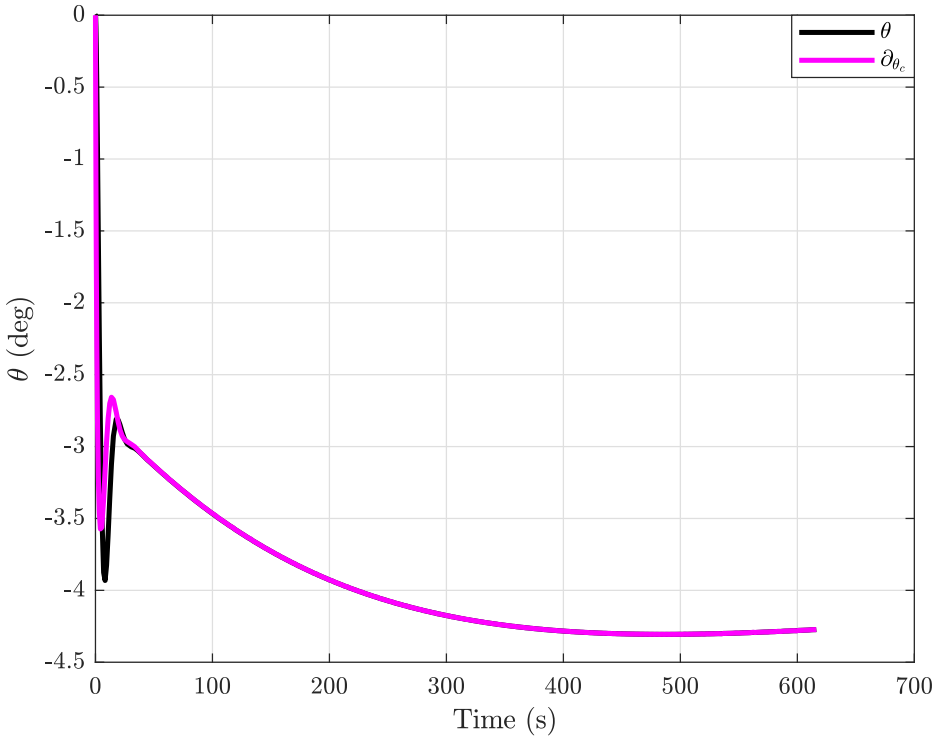

FIGURE 5.21: IA SMC tracking profile for 125 km range.

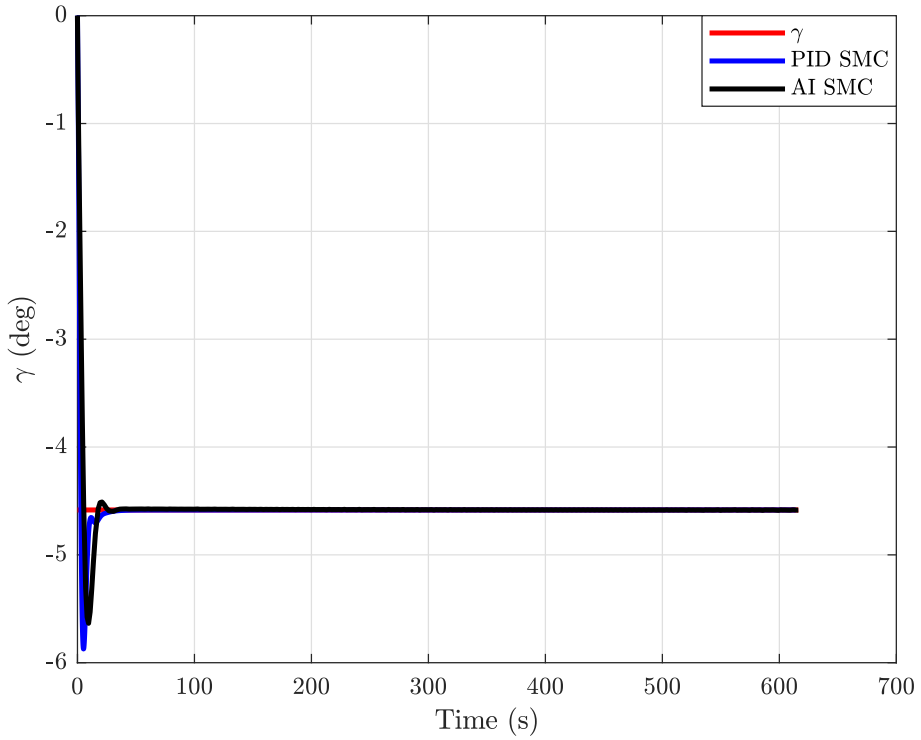

FIGURE 5.22: γ tracking for 125 km range.

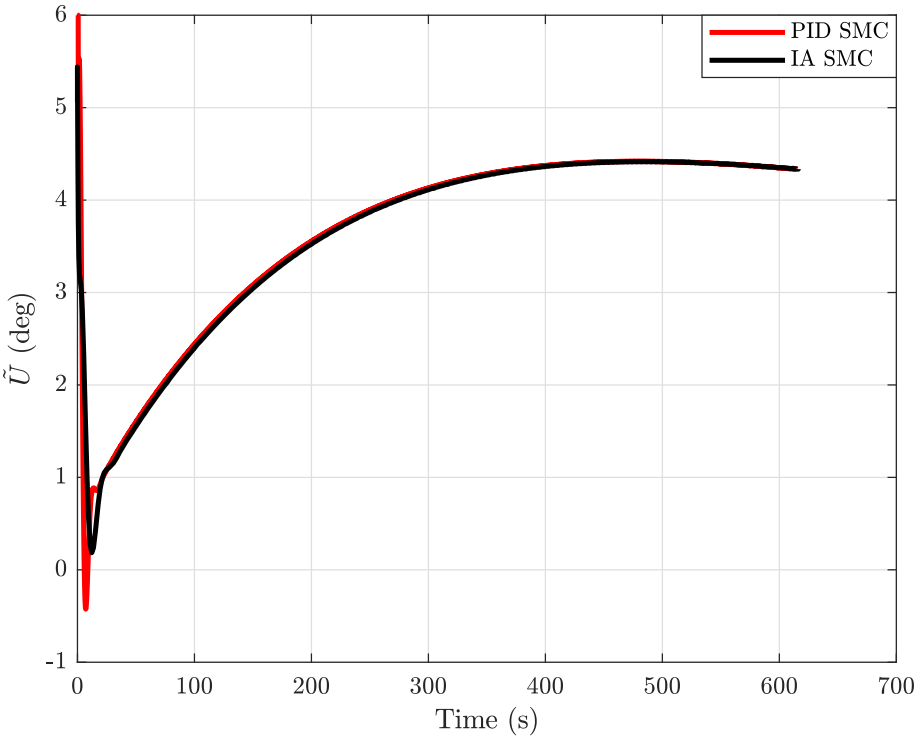

FIGURE 5.23: Control input profile for 125 km range.

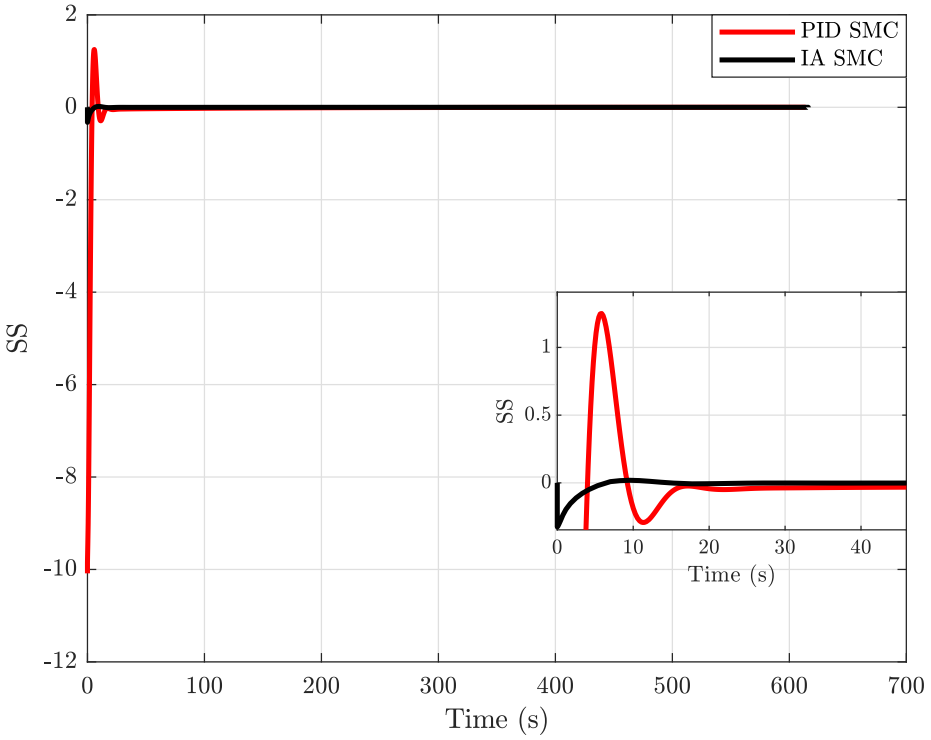

FIGURE 5.24: Sliding surface profile for 125 km range.

5.5.3 Quantitative Analysis

A terminal error (Difference between desired range and final range from controller) and quantitative analysis is performed to assess the superiority of proposed IA SMC controller.

Terminal error for both cases 120 km and 125 km are tabulated in Table 5.3. Comparison between terminal error explains that IA SMC performed very well as compared to PID SMC.

TABLE 5.3: Terminal error.

Controller	Case A	Case B
PID SMC	281.3 m	273.8 m
IA SMC	0.35 m	0.29 m

A quantitative analysis is also synthesized to judge the effectiveness of PID SMC and IA SMC. As judgement criteria for performance evaluation, Integral Square

Value (ISV) [131] of $\tilde{U}$ for energy consumption and Root Mean Square Error (RMSE) are used. RMSE is computed by

$$RMSE = \sqrt{\frac{1}{N}\sum_{m=1}^{N}|e(m)|^2} \tag{5.34}$$

where N is the number of total time samples. Furthermore, ISV of $\tilde{U}$ is defined by

$$\tilde{U}_{ISV} = \int_{t_0}^{t_s} \tilde{U}^2 \, dt \tag{5.35}$$

where t_s is stopping time and detail discussion about this is given in [92]. $\tilde{U}_{ISV}$ and the RMSE for both the controllers are tabulated in Table 5.4. The comparison demonstrates that IA SMC has better tracking performance and consumes less energy than PID SMC because IA SMC lowers the saturation effect.

TABLE 5.4: Quantitative analysis.

Controller	Case A		Case B	
	$\tilde{U}_{ISV}$	RMSE	$\tilde{U}_{ISV}$	RMSE
PID SMC	9189.5470	0.3935	8775.9829	0.3588
IA SMC	9129.1242	0.2683	8712.0024	0.2455

5.6 Summary

This chapter has focused on sliding mode control based non-linear technique for range guidance to extend the range of UGV. In the guidance problem, the desired range is considered to obtain the guidance command which depends on the dispersion points and the angle of attack. To eliminate the saturation effect in the control input and smooth guidance command, an IA SMC is proposed. To overcome the perturbation problem in SMC, a atan based strong exponential reaching law is also incorporated. Simulation tests are performed to evaluate the effectiveness of the control scheme, which shows promising results against the issue of saturation effect and non-smooth guidance command. Furthermore, by ensuring

smooth control actions, enhanced control leads to good trajectory tracking. Additionally, a terminal error and quantitative comparison are performed between the PID SMC and the AI SMC, demonstrating that the AI SMC uses less energy during range guidance law generation and offers superior tracking for range guidance command.

Chapter 6

Conclusion and Future Work

6.1 Conclusion

The conclusions drawn from the work presented in the previous chapters can be divided into two major groups. The grouping is based on trajectory optimization or optimal control formulation and range guidance and control formulation.

- **Chapter 4: Trajectory Optimization of SUGV**

  First, to avoid the time-scaling approach, especially in the scenario of UGVs, the stopping constraint-based notion is updated for the maximum stoppable time. Unpowered gliding is handled by a non-uniform CVP scheme to mitigate fluctuations and unsteadiness that cause range reduction.

  A proposed non-uniform CVP is modeled by the exponential spacing phenomenon. To perform the trajectory optimization, the DS Simulia Isight environment is simulated by employing the SQP algorithm in conjunction with MATLAB. To verify the effectiveness of the proposed non-uniform CVP approach and to achieve damped and steady gliding flight in the presence of constraints, a comparison is made with the classical CVP approach and uncontrolled gliding flight. However, analysis of the scheme for three different cases designed based on the number of nodes shows that damped and

steady gliding flight is successfully achieved and the results have been able to maximize the range but with the increase in the number of nodes, it has been observed that the complexity and computation have increased. Furthermore, the saturation effect has also been evaluated in constraints which may be a bed factor of non-uniform CVP.

A comparison is also conducted between the proposed CVP and GPOPS, and the GPOPS outcomes demonstrate that all the constraints are satisfied with a maximum horizontal range of 120.525 km, which is 331 meters less than the non-uniform CVP approach.

- **Chapter 5: Range Guidance and Control for SUGV**

  A closed-loop nonlinear control method is proposed to attain the intended range. A guidance scheme is developed for the range which depends on the dispersion points and the measured angle of attack. IA SMC is proposed to negotiate the saturation problem in commanded control and achieve smooth guidance command. Additionally, to reduce the chattering issue in SMC, a atan based strong exponential reaching law is employed.

  To cross-check the effectiveness of the proposed guidance command, simulations of PID SMC and IA SMC are also carried out and from these simulations, it is observed that the proposed control scheme produces smooth guidance and avoids the saturation problem. For the two cases of the 120 km and 125 km range, a quantitative analysis based on terminal error, root mean square of error, and energy dissipation of the range guidance law is also calculated.

  Therefore, the evaluation of both cases states that the proposed IA effectively tracks the range guidance command and generates the smooth command, and suppresses the saturation problems in the range guidance law, and according to the quantitative analysis, the IA SMC for the SUGV fulfills the range guidance acquisition to achieve the desired range.

6.2 Future Work

Based on the contributions and findings of the present study, several possible future avenues can be explored. Following are some proposed future directions.

- Exponential spacing in non-uniform CVP can be adaptively modified with the Hilbert-Huang transform.
- Range maximization can be studied by incorporating the proposed CVP approach with variable center of gravity, wind shear, wind gusts, ground effects, and constraints on wing sweep angle and dynamic pressure.
- The research problem of range maximization needs to be performed with Grasshopper Optimization Algorithm, Ant Colony Optimization Algorithm, Whale Optimization Algorithm, and Gray Wolf Optimization Algorithm.
- The proposed non-uniform CVP approach can be implemented in the 6-DoF model of SUGV, and the scheme can be tested on other UGVs.
- Trajectory optimization itself is not robust so the results of range maximization can be used to design a robust controller based on the optimal model reference.
- Altitude-based range guidance can be designed that will depend on altitude control in the presence of weather disturbances and ground effects.
- A scheduling-based model predictive control with sliding mode control to achieve robustness can be designed for a range guidance scheme in the presence of variable wing sweep angle.
- A 6-DoF model of SUGV is required to verify the proposed range guidance scheme and IA SMC controller.

This study's future directions are not confined to the points indicated above. There is no end to knowledge.

Bibliography

[1] W. Chen, H. Zhou, W. Yu, and L. Yang, *Steady Glide Dynamics and Guidance of Hypersonic Vehicle*. Springer, 2021.

[2] J. T. Correll, "The emergence of smart bombs," *Air Force Magazine*, vol. 1, 2010.

[3] E. Miasnikov, "Long-range precision-guided conventional weapons: Implications for strategic balance, arms control and non-proliferation," *paper commissioned by the International Commission on Nuclear Non-proliferation and Disarmament*, 2009.

[4] J. D. Anderson, *Aircraft performance & design*. McGraw-Hill Science Engineering, 1999.

[5] M. Eshelby, *Aircraft performance: Theory and practice*. American Institute of Aeronautics and Astronautics, Inc., 2000.

[6] M. Saarlas, *Aircraft performance*. John Wiley & Sons, 2006.

[7] W. A. Mair and D. L. Birdsall, *Aircraft performance*. Cambridge University Press, 1996, vol. 5.

[8] A. K. Kundu, M. A. Price, and D. Riordan, *Theory and practice of aircraft performance*. John Wiley & Sons, 2016.

[9] D. G. Hull *et al.*, *Fundamentals of airplane flight mechanics*. Springer, 2007, vol. 19.

[10] U. M. Norberg, *Vertebrate flight: mechanics, physiology, morphology, ecology and evolution*. Springer Science & Business Media, 2012, vol. 27.

[11] D. Bye and P. McClure, "Design of a morphing vehicle," in *48th AIAA/ASME/ASCE/AHS/ASC structures, structural dynamics, and materials conference*, 2007, p. 1728.

[12] M. Secanell, A. Suleman, and P. Gamboa, "Design of a morphing airfoil using aerodynamic shape optimization," *AIAA journal*, vol. 44, no. 7, pp. 1550–1562, 2006.

[13] S. V. Shkarayev, P. G. Ifju, J. C. Kellogg, and T. J. Mueller, *Introduction to the design of fixed-wing micro air vehicles including three case studies*. American Institute of Aeronautics and Astronautics, 2007.

[14] A. G. Escobar-Ruiz, O. Lopez-Botello, L. Reyes-Osorio, P. Zambrano-Robledo, L. Amezquita-Brooks, and O. Garcia-Salazar, "Conceptual design of an unmanned fixed-wing aerial vehicle based on alternative energy," *International Journal of Aerospace Engineering*, vol. 2019, pp. 1–13, 2019.

[15] B. L. Stevens, F. L. Lewis, and E. N. Johnson, *Aircraft control and simulation: dynamics, controls design, and autonomous systems*. John Wiley & Sons, 2015.

[16] R. Chai, A. Savvaris, A. Tsourdos, and S. Chai, *Design of Trajectory Optimization Approach for Space Maneuver Vehicle Skip Entry Problems*. Springer, 2019.

[17] M. V. Cook, *Flight dynamics principles: a linear systems approach to aircraft stability and control*. Butterworth-Heinemann, 2012.

[18] H. Wu and F. Mora-Camino, "Knowledge-based trajectory control for engine-out aircraft," in *2013 IEEE/AIAA 32nd Digital Avionics Systems Conference (DASC)*. IEEE, 2013, pp. 2B1–1.

[19] W. Bell, "Joint direct attack munition (jdam)," US Air Force Hill AFB United States, Tech. Rep., 2015.

[20] K. T. Turco, "Development of the joint stand off weapon (jsow) moving target capability: Agm-154 block three program," 2006.

[21] M. Costello, "Extended range of a gun launched smart projectile using controllable canards," *Shock and Vibration*, vol. 8, no. 3-4, pp. 203–213, 2001.

[22] M. Yeo, "Guided weapons: Stand off munitions-essential for raaf combat operations," *Asia-Pacific Defence Reporter (2002)*, vol. 45, no. 1, pp. 22–25, 2019.

[23] A. Elsherbiny, A. Bayoumy, A. Elshabka, and M. Abdelrahman, "Aerodynamic design optimization of range extension kit of a subsonic flying body," in *International Conference on Aerospace Sciences and Aviation Technology*, vol. 17. The Military Technical College, 2017, pp. 1–20.

[24] D.-C. Zhang, Q.-L. Xia, Q.-Q. Wen, and G.-q. Zhou, "An approximate optimal maximum range guidance scheme for subsonic unpowered gliding vehicles," *International Journal of Aerospace Engineering*, vol. 2015, 2015.

[25] H. Kelley, E. Cliff, and F. Lutze, "Boost–glide range-optimal guidance," *Optimal Control Applications and Methods*, vol. 3, no. 3, pp. 293–298, 1982.

[26] O. Von Stryk and R. Bulirsch, "Direct and indirect methods for trajectory optimization," *Annals of operations research*, vol. 37, pp. 357–373, 1992.

[27] D. Sheu, Y.-M. Chen, Y.-J. Chang, and J.-S. Chern, "Optimal glide for maximum range," in *23rd Atmospheric Flight Mechanics Conference*, 1998, p. 4462.

[28] W. E. Williamson, "Minimum and maximum endurance trajectories for gliding flight in a horizontal plane," *Journal of Guidance and Control*, vol. 2, no. 6, pp. 457–462, 1979.

[29] J. BenAsher and M. Dekel K, "Pseudo-spectral-method based optimal glide in the event of engine cut-off," in *AIAA Guidance, Navigation, and Control Conference*, 2010, p. 6596.

[30] C. Faulders, E. Lekawa, and R. McNary, "Aerodynamic requirements for flare and landing of low-l/d glide vehicles." *Journal of Spacecraft and Rockets*, vol. 5, no. 8, pp. 915–920, 1968.

[31] L. Geng and Z. Zheng, "A homotopy method for guided bomb's optimal glide problem," in *2009 Chinese Control and Decision Conference*. IEEE, 2009, pp. 1909–1912.

[32] J. Shi, S. Tang, and C.-l. Yang, "Trajectory optimization for unpowered gliding submissile," in *2009 International Conference on Intelligent Human-Machine Systems and Cybernetics*, vol. 2. IEEE, 2009, pp. 229–232.

[33] D. Sheu, Y.-M. Chen, and J.-S. Chern, "Optimal three-dimensional glide for maximum reachable domain," in *24th Atmospheric Flight Mechanics Conference*, 1999, p. 4245.

[34] I. Shapira and J. Z. Ben-Asher, "Singular perturbation analysis of optimal glide," *Journal of guidance, control, and dynamics*, vol. 27, no. 5, pp. 915–918, 2004.

[35] W. Qiu, Q. Jia, X. Meng, and Y. Sun, "Maximum range trajectory optimization for a boost-glide vehicle using adaptive mesh refinement pseudospectral methods," *Proceedings of the Institution of Mechanical Engineers, Part G: Journal of Aerospace Engineering*, vol. 231, no. 7, pp. 1171–1182, 2017.

[36] K. Guo and F. Xiong, "Gliding trajectory optimization based on hp-adaptive pseudospectral method," in *2013 International Conference on Quality, Reliability, Risk, Maintenance, and Safety Engineering (QR2MSE)*, 2013.

[37] Y. Yan-bo, Z. Ke, and X. Xiao-dong, "Optimization of glide trajectory of guided bombs using a radau pseudo-spectral method," *Acta Armamentarii*, vol. 35, no. 8, p. 1179, 2014.

[38] Q. Yang, P. Li, and Z. Zheng, "Design of the optimal glide scheme for the airdropped mine using gpops," in *2013 Chinese Automation Congress*. IEEE, 2013, pp. 98–103.

[39] J. J. Wang and J. Q. Yu, "Study of the optimal design for the gliding trajectory," in *Applied Mechanics and Materials*, vol. 568. Trans Tech Publ, 2014, pp. 1063–1067.

[40] W. Yu and W. Chen, "Guidance scheme for glide range maximization of a hypersonic vehicle," in *AIAA Guidance, Navigation, and Control Conference*, 2011, p. 6714.

[41] I. Shapira and J. Ben-Asher, "Range maximization for emergency landing after engine cutoff," *Journal of aircraft*, vol. 42, no. 5, pp. 1296–1306, 2005.

[42] X. Fang, N. Wan, H. Jafarnejadsani, D. Sun, F. Holzapfel, and N. Hovakimyan, "Emergency landing trajectory optimization for fixed-wing uav under engine failure," in *AIAA Scitech 2019 Forum*, 2019, p. 0959.

[43] D. Segal, A. Bar-Gill, and N. Shimkin, "Max-range glides in engine cutoff emergencies under severe wind," *Journal of Guidance, Control, and Dynamics*, vol. 42, no. 8, pp. 1822–1835, 2019.

[44] W. WILLIAMSON, JR, "A comparison of first and second order techniques for computing optimal horizontal gliding trajectories," in *18th Aerospace Sciences Meeting*, 1980, p. 61.

[45] N. X. Vinh, C.-Y. Yang, and J.-S. Chern, "Optimal trajectories for maximum endurance gliding in a horizontal plane," *Journal of Guidance, Control, and Dynamics*, vol. 7, no. 2, pp. 246–248, 1984.

[46] N. VINH, C.-Y. YANG, and J.-S. CHERN, "Optimal trajectories for maximum endurance gliding in a horizontal plane," in *7th Atmospheric Flight Mechanics Conference*, 1981, p. 1868.

[47] J.-S. Chern, D.-M. Ma, and N. Vinh, "Analytical solution for horizontal gliding flight," in *Atmospheric Flight Mechanics Conference*, 2000, p. 4113.

[48] A. M. Elsherbiny, A. M. Aly, A. Elshabka, and M. Abdelrahman, "Modeling, simulation and hyprid optimization method as design tools for range extension kit of a subsonic flying body," in *2018 AIAA Modeling and Simulation Technologies Conference*, 2018, p. 0429.

[49] J. D. Vasile, J. Bryson, and F. Fresconi, "Aerodynamic design optimization of long range projectiles using missile datcom," in *AIAA Scitech 2020 Forum*, 2020, p. 1762.

[50] J. Bryson, J. D. Vasile, I. Celmins, and F. Fresconi, "Approach for understanding range extension of gliding indirect fire munitions," in *2018 Atmospheric Flight Mechanics Conference*, 2018, p. 3158.

[51] J. D. Vasile, J. Bryson, B. C. Gruenwald, L. Fairfax, L. Strohm, and F. Fresconi, "A multi-disciplinary approach to design long range guided projectiles," in *AIAA Scitech 2020 Forum*, 2020, p. 1993.

[52] L. Juan-mian and W. Jia-sheng, "Aerodynamic configuration design of gliding extended range guided bomb," *Transactions of Beijing Institute of Technology*, no. 12, pp. 1387–1390, 2011.

[53] A. Kivaj, S. Ghasemloo, H. Parhizkar, and S. Sadati, "Multivariate conceptual design of a guided project using genetic algorithms," *Journal of Fundamental and Applied Sciences*, vol. 8, no. 3S, pp. 3009–3032, 2016.

[54] D. G. Hull, "Conversion of optimal control problems into parameter optimization problems," *Journal of guidance, control, and dynamics*, vol. 20, no. 1, pp. 57–60, 1997.

[55] Y. Kim, G. H. Kim, and J.-H. Choi, "Optimal guidance for range maximization of guided projectile: The effects of autopilot delay and fin deployment timing on the flight range," in *2019 International Conference on Unmanned Aircraft Systems (ICUAS)*. IEEE, 2019, pp. 1143–1152.

[56] D. Rivas, A. Franco, and A. Valenzuela, "Optimization of unpowered descents for commercial aircraft," in *11th AIAA Aviation Technology, Integration, and Operations (ATIO) Conference, including the AIAA Balloon Systems Conference and 19th AIAA Lighter-Than*, 2011, p. 7019.

[57] R. Bulirsch, E. Nerz, H. J. Pesch, and O. von Stryk, *Combining direct and indirect methods in optimal control: Range maximization of a hang glider*. Springer, 1993.

[58] J. A. Bryan, *Maximum-range trajectories for an unpowered reusable launch vehicle*. University of Missouri-Columbia, 2011.

[59] A. Nevrekar, A. Striz, and P. Vedula, "Maximum range glide of a supersonic aircraft in the presence of wind," in *12th AIAA Aviation Technology, Integration, and Operations (ATIO) Conference and 14th AIAA/ISSMO Multidisciplinary Analysis and Optimization Conference*, 2012, p. 5633.

[60] H. Liu, H. Teng, G. Qiu, P. Liu, and J. Yang, "Gaussian discretization-based non-uniform control vector parameterization for terminal constrained hypersonic unmanned system trajectory optimization," in *2020 Chinese Automation Congress (CAC)*. IEEE, 2020, pp. 1799–1804.

[61] K. Teo, G. Jepps, E. Moore, and S. Hayes, "A computational method for free time optimal control problems, with application to maximizing the range of an aircraft-like projectile," *The ANZIAM Journal*, vol. 28, no. 3, pp. 393–413, 1987.

[62] P. Liu, X. Liu, P. Wang, G. Li, L. Xiao, J. Yan, and Z. Ren, "Control variable parameterisation with penalty approach for hypersonic vehicle reentry optimisation," *International Journal of Control*, vol. 92, no. 9, pp. 2015–2024, 2019.

[63] H. Liu, P. Liu, X. Liu, and H. Huang, "Adaptive control arc length-based time grid refinement control parameterisation method for unmanned hypersonic vehicle reentry trajectory optimisation," *International Journal of Control*, pp. 1–11, 2022.

[64] X. Hui, C. Guangbin, Z. Shengxiu, Y. Xiaogang, and H. Mingzhe, "Hypersonic reentry trajectory optimization by using improved sparrow search algorithm and control parametrization method," *Advances in Space Research*, vol. 69, no. 6, pp. 2512–2524, 2022.

[65] K. Shahzad and H. Weiduo, "Design and simulation of range enhancement of reentry vehicle," in *2019 16th International Bhurban Conference on Applied Sciences and Technology (IBCAST)*. IEEE, 2019, pp. 444–451.

[66] G. N. Kumar, A. Sarkar, and S. Talole, "Dynamic pressure based mid-course guidance scheme for hypersonic boost-glide vehicle," *Proceedings of the Institution of Mechanical Engineers, Part G: Journal of Aerospace Engineering*, vol. 233, no. 9, pp. 3211–3222, 2019.

[67] S. Fok, E. H. Atta, and L. Eicher, "Simulation investigation on dynamic pressure in glide angle control," *Advances in Engineering Software*, vol. 23, no. 1, pp. 1–6, 1995.

[68] I. Mir, S. Akhtar, S. Eisa, and A. Maqsood, "Guidance and control of standoff air-to-surface carrier vehicle," *The Aeronautical Journal*, vol. 123, no. 1261, pp. 283–309, 2019.

[69] C. P. Phillips, "Guidance algorithm for range maximization and time-of-flight control of a guided projectile," *Journal of Guidance, Control, and Dynamics*, vol. 31, no. 5, pp. 1447–1455, 2008.

[70] H. Wu and F. Mora-Camino, "Glide control for engine-out aircraft," in *AIAA Guidance, Navigation, and Control Conference*, 2012, p. 4442.

[71] A. F. U. Din, I. Mir, F. Gul, M. R. Al Nasar, and L. Abualigah, "Reinforced learning-based robust control design for unmanned aerial vehicle," *Arabian Journal for Science and Engineering*, pp. 1–16, 2022.

[72] A. F. ud Din, I. Mir, F. Gul, S. Mir, N. Saeed, T. Althobaiti, S. M. Abbas, and L. Abualigah, "Deep reinforcement learning for integrated non-linear control of autonomous uavs," *Processes*, vol. 10, no. 7, p. 1307, 2022.

[73] A. F. U. Din, S. Akhtar, A. Maqsood, M. Habib, and I. Mir, "Modified model free dynamic programming: an augmented approach for unmanned aerial vehicle," *Applied Intelligence*, pp. 1–21, 2022.

[74] A. F. U. Din, I. Mir, F. Gul, and S. Akhtar, "Development of reinforced learning based non-linear controller for unmanned aerial vehicle," *Journal of Ambient Intelligence and Humanized Computing*, pp. 1–18, 2022.

[75] P. T. Hung, N. D. Cuong, and N. D. Thanh, "Optimization of long-range trajectory for an unpowered flight vehicle," *Vietnam Journal of Science and Technology*, vol. 57, no. 6A, pp. 43–51, 2019.

[76] I. K. Peddle, "Autonomous flight of a model aircraft," Ph.D. dissertation, Stellenbosch: Stellenbosch University, 2005.

[77] J. H. Blakelock, *Automatic control of aircraft and missiles.* John Wiley & Sons, 1991.

[78] J. Arora, *Introduction to optimum design.* Elsevier, 2004.

[79] A. V. Rao, "A survey of numerical methods for optimal control," *Advances in the Astronautical Sciences*, vol. 135, no. 1, pp. 497–528, 2009.

[80] T. J. Böhme, B. Frank, T. J. Böhme, and B. Frank, "Indirect methods for optimal control," *Hybrid systems, optimal control and hybrid vehicles: Theory, methods and applications*, pp. 215–231, 2017.

[81] I. M. Ross and F. Fahroo, "A direct method for solving nonsmooth optimal control problems," *IFAC Proceedings Volumes*, vol. 35, no. 1, pp. 479–484, 2002.

[82] R. Bellman, "Dynamic programming," *Science*, vol. 153, no. 3731, pp. 34–37, 1966.

[83] R. Paulen and M. Fikar, *Optimal operation of batch membrane processes.* Springer, 2016.

[84] M. R. Osborne, "On shooting methods for boundary value problems," *Journal of mathematical analysis and applications*, vol. 27, no. 2, pp. 417–433, 1969.

[85] H. G. Bock and K.-J. Plitt, "A multiple shooting algorithm for direct solution of optimal control problems," *IFAC Proceedings Volumes*, vol. 17, no. 2, pp. 1603–1608, 1984.

[86] G. T. Huntington and A. V. Rao, "A comparison between global and local orthogonal collocation methods for solving optimal control problems," in *2007 American Control Conference*. IEEE, 2007, pp. 1950–1957.

[87] M. Sniedovich, "A new look at bellman's principle of optimality," *Journal of optimization theory and applications*, vol. 49, pp. 161–176, 1986.

[88] D. E. Kirk, *Optimal control theory: an introduction*. Courier Corporation, 2004.

[89] C.-G. Jung, C.-H. Lee, and M.-J. Tahk, "Legendre pseudo-spectral method for missile trajectory optimization with free final time," in *The Proceedings of the 2021 Asia-Pacific International Symposium on Aerospace Technology (APISAT 2021), Volume 2*. Springer, 2022, pp. 569–581.

[90] F. Mazzia and G. Settanni, "Bvps codes for solving optimal control problems," *Mathematics*, vol. 9, no. 20, p. 2618, 2021.

[91] V. Quintana and E. Davison, "A numerical method for solving optimal control problems with unspecified terminal time," *International Journal of Control*, vol. 17, no. 1, pp. 97–115, 1973.

[92] A. Mahmood, F. u. Rehman, and A. I. Bhatti, "Trajectory optimization of a subsonic unpowered gliding vehicle using control vector parameterization," *Drones*, vol. 6, no. 11, p. 360, 2022.

[93] Q. Lin, R. Loxton, K. L. Teo, and Y. H. Wu, "Optimal control problems with stopping constraints," *Journal of Global Optimization*, vol. 63, pp. 835–861, 2015.

[94] R. Sargent and G. Sullivan, "The development of an efficient optimal control package," in *Optimization Techniques: Proceedings of the 8th IFIP Conference on Optimization Techniques Würzburg, September 5–9, 1977*. Springer, 1978, pp. 158–168.

[95] Y. Cai, "Dynamic programming and its application in economics and finance," *PhD diss., Stanford University*, 2009.

[96] F. Aràndiga, R. Donat, and M. Santágueda, "The pchip subdivision scheme," *Applied Mathematics and Computation*, vol. 272, pp. 28–40, 2016.

[97] J.-n. Chou, *Optimal turning maneuvers for six-degree-of-freedom high-angle-of-attack aircraft models*. Iowa State University, 1995.

[98] C. Rabbath and D. Corriveau, "A comparison of piecewise cubic hermite interpolating polynomials, cubic splines and piecewise linear functions for the approximation of projectile aerodynamics," *Defence Technology*, vol. 15, no. 5, pp. 741–757, 2019.

[99] B. C. Fabien, "Piecewise polynomial control parameterization in the direct solution of optimal control problems," *Journal of Dynamic Systems, Measurement, and Control*, vol. 135, no. 3, p. 034506, 2013.

[100] Z. Wang, "Optimal trajectories and normal load analysis of hypersonic glide vehicles via convex optimization," *Aerospace Science and Technology*, vol. 87, pp. 357–368, 2019.

[101] P. E. Gill, W. Murray, M. A. Saunders, and M. H. Wright, "User's guide for npsol (version 4.0): A fortran package for nonlinear programming." Stanford Univ CA Systems Optimization Lab, Tech. Rep., 1986.

[102] P. Gath and K. Well, "Trajectory optimization using a combination of direct multiple shooting and collocation," in *AIAA Guidance, Navigation, and Control Conference and Exhibit*, 2001, p. 4047.

[103] G. Lecohier and K. Mehlem, "A new trajectory optimisation tool (altos) applied to conventional launchers," *IFAC Proceedings Volumes*, vol. 25, no. 22, pp. 477–482, 1992.

[104] Z. Foroozandeh, M. Shamsi *et al.*, "On numerical methods for singular optimal control problems: An application to an auv problem." *Discrete & Continuous Dynamical Systems-Series B*, vol. 24, no. 5, 2019.

[105] C. L. Darby, W. W. Hager, and A. V. Rao, "An hp-adaptive pseudospectral method for solving optimal control problems," *Optimal Control Applications and Methods*, vol. 32, no. 4, pp. 476–502, 2011.

[106] M. A. Patterson and A. V. Rao, "Gpops-ii: A matlab software for solving multiple-phase optimal control problems using hp-adaptive gaussian quadrature collocation methods and sparse nonlinear programming," *ACM Transactions on Mathematical Software (TOMS)*, vol. 41, no. 1, pp. 1–37, 2014.

[107] V. I. Utkin, "Sliding modes and their applications in variable structure systems," *Mir, Moscow*, 1978.

[108] A. Mahmood, A. I. Bhatti, and B. A. Siddique, "Landing of aircraft using integral state feedback sliding mode control," in *2019 International Conference on Electrical, Communication, and Computer Engineering (ICECCE)*. IEEE, 2019, pp. 1–6.

[109] H. Sira-Ramírez, "On the sliding mode control of nonlinear systems," *Systems & control letters*, vol. 19, no. 4, pp. 303–312, 1992.

[110] M. Taleb, F. Plestan, and B. Bououlid, "An adaptive solution for robust control based on integral high-order sliding mode concept," *International Journal of Robust and Nonlinear Control*, vol. 25, no. 8, pp. 1201–1213, 2015.

[111] C. Edwards and S. Spurgeon, *Sliding mode control: theory and applications*. Crc Press, 1998.

[112] G. Bartolini, L. Fridman, A. Pisano, and E. Usai, *Modern sliding mode control theory: New perspectives and applications*. Springer, 2008, vol. 375.

[113] W. Perruquetti and J. P. Barbot, *Sliding mode control in engineering*. Marcel Dekker New York, 2002, vol. 11.

[114] S. E. Ryvkin and E. P. Lever, *Sliding mode control for synchronous electric drives*. CRC press, 2012.

[115] A. Ferrara, *Sliding mode control of vehicle dynamics*. IET, 2017, vol. 5.

[116] U. Ali, M. Z. Shah, R. Samar, and A. I. Bhatti, "Robust level flight control design for scaled yak-54 unmanned aerial vehicle using single sliding surface." in *2012 24th Chinese Control and Decision Conference (CCDC)*. IEEE, 2012, pp. 1209–1214.

[117] S. U. Ali, R. Samar, M. Z. Shah, A. I. Bhatti, and K. Munawar, "Higher-order sliding mode based lateral guidance for unmanned aerial vehicles," *Transactions of the Institute of Measurement and Control*, vol. 39, no. 5, pp. 715–727, 2017.

[118] J.-J. E. Slotine, W. Li *et al.*, *Applied nonlinear control*. Prentice hall Englewood Cliffs, NJ, 1991, vol. 199, no. 1.

[119] V. I. Utkin, *Sliding modes in control and optimization*. Springer Science & Business Media, 2013.

[120] S. Laghrouche, F. Plestan, and A. Glumineau, "Higher order sliding mode control based on integral sliding mode," *Automatica*, vol. 43, no. 3, pp. 531–537, 2007.

[121] V. Utkin, J. Guldner, and J. Shi, *Sliding mode control in electro-mechanical systems*. CRC press, 2017.

[122] G. Shen, Y. Xia, J. Zhang, and B. Cui, "Adaptive super-twisting sliding mode altitude trajectory tracking control for reentry vehicle," *ISA transactions*, 2022.

[123] A. Saeed, Y. Liu, M. Z. Shah, L. Wang, and Q.-G. Wang, "Sliding mode lateral guidance and control of finless airship," *Journal of Aerospace Engineering*, vol. 35, no. 2, p. 04021131, 2022.

[124] M. Herrera, O. Camacho, H. Leiva, and C. Smith, "An approach of dynamic sliding mode control for chemical processes," *Journal of Process Control*, vol. 85, pp. 112–120, 2020.

[125] I. M. Boiko, "Chattering in sliding mode control systems with boundary layer approximation of discontinuous control," *International Journal of Systems Science*, vol. 44, no. 6, pp. 1126–1133, 2013.

[126] H. Hassrizal and J. A. Rossiter, "Application of decaying boundary layer and switching function method thorough error feedback for sliding mode control on spacecraft's attitude," in *2017 25th Mediterranean Conference on Control and Automation (MED)*. IEEE, 2017, pp. 1250–1256.

[127] N. Mazhar, F. M. Malik, A. Raza, and R. Khan, "Predefined-time control of nonlinear systems: A sigmoid function based sliding manifold design approach," *Alexandria Engineering Journal*, vol. 61, no. 9, pp. 6831–6841, 2022.

[128] A. Najafi, M. T. Vu, S. Mobayen, J. H. Asad, and A. Fekih, "Adaptive barrier fast terminal sliding mode actuator fault tolerant control approach for quadrotor uavs," *Mathematics*, vol. 10, no. 16, p. 3009, 2022.

[129] M. Asad, M. Ashraf, S. Iqbal, and A. I. Bhatti, "Chattering and stability analysis of the sliding mode control using inverse hyperbolic function," *International Journal of Control, Automation and Systems*, vol. 15, no. 6, pp. 2608–2618, 2017.

[130] A. Isidori, *Nonlinear control systems: an introduction*. Springer, 1985.

[131] N. Xuan-Mung and M. Golestani, "Energy-efficient disturbance observer-based attitude tracking control with fixed-time convergence for spacecraft," *IEEE Transactions on Aerospace and Electronic Systems*, 2022.

Appendix A

A.1 Sequential Quadratic Programming

The NLP problem is broken into a sequence of QP subproblems. The QP subproblem's objective function is a quadratic approximation of the Lagrangian function, and its constraints are linearizations of the original constraints. To demonstrate the SQP method, the following NLP problem is defined as

$$\begin{aligned} &minf(x) \quad \text{for} \quad x \in \Re^n \\ &A_i(x) = 0 \quad \text{for} \quad i = 1, 2, ..., l \\ &B_j(x) \geq 0 \quad \text{for} \quad j = 1, 2, ..., m \end{aligned} \tag{1}$$

The problem's corresponding Lagrangian function is provided by

$$\mathcal{L}(x, \Phi, \Psi) = f(x) + \Phi^T A + \psi^T B$$

where vectors $\Phi \in \Re^l$ and $\Psi \in \Re^m$ are Lagrangian multipliers. A detailed conceptualization of SQP procedure to solve the optimal problem is given by the following algorithm.

1. Set $x = x^0$ (x^0 is initial guess), sequential variable as $k = 0$ and initialize the tolerance ϵ.

2. Determine the search direction d^0 by solving the QP subproblem.

3. Compute the step length C^0 by 1-D minimization of the cost function $\mathcal{M}(x^0 + C^0 d^0)$.

4. Evaluate $x^1 = x^0 + C^0 d^0$.

5. *While* $\|C^k d^k > \epsilon\|$

   (a) Set $k = k + 1$.

   (b) Evaluate d^k by solving the QP^k subproblem.

   (c) Determine C^k which minimizes $\mathcal{M}(x^k + C^k d^k)$.

   (d) Compute $x^{k+1} = x^k + C^k d^k$.

6. *end while*

7. Output: $x_{op} = x^{k+1}$

where the function $\mathcal{M}$ provides a suitable decrease in $f(x)$ as well as the fulfilment of the constraints with d^k with an proper C^k. The search direction d^k is the solution of the following QP^k subproblem.

$$\begin{aligned} &\min_d \left\{ \ 0.5 d^T \mathsf{H}_k d + \Delta f(x_k)^T d \right\} \\ &s.t. \ \Delta A_i(x_k)^T d + A_i(x_k), i = 1, 2, ..., m \\ &\qquad \Delta B_j(x_k)^T d + B_j(x_k) \leq 0, j \in \mathcal{A}(x^k) \\ &\qquad \mathcal{A}(x^k) = \{ j \in \{1, 2, ..., n\} \, | B_j(x_k) = 0 \} \end{aligned} \tag{2}$$

where H_k is the Hessian of the Lagrangian $\Delta_x^2 \mathcal{L}$ and $\mathcal{A}(x^k)$ refers to the set of active constraints at x^k.

A.2 GPOPS Mathematics

In order to employee the GPOPs, optimal problem is that tries to minimize the cost function, is configured as

$$J = \Phi[x_{t_o}, t_o, x_{t_f}, t_f] + \int_{t_0}^{t_f} \phi(x(t), u(t), t)dt \tag{3}$$

Subject to dynamic constraints are as

$$\dot{x} = f(x, u, t) \tag{4}$$

Subject to inequality path constraints are as

$$C_{min} \leq C(x, u, t) \leq C_{max} \tag{5}$$

Subject to boundary constraints are as

$$B_{min} \leq B(x_{t_o}, t_o, x_{t_f}, t_f) \leq B_{max} \tag{6}$$

To approximate the state variables, a $N + 1$ Lagrange interpolating polynomials is expressed as

$$x(\tau) \approx X(\tau) = \sum_{i=1}^{N} X_i \cdot V_i(\tau), \quad \tau \in [-1\ 1] \tag{7}$$

where V_i is

$$V_i(\tau) = \prod_{j=0, j\neq i}^{N} \frac{\tau - \tau_j}{\tau_i - \tau_j},\ i = 0, 1, ..., N$$

To estimate the control variables, an N Lagrange interpolating polynomials is expressed as

$$u(\tau) \approx U(\tau) = \sum_{i=1}^{N} X_i \cdot V_i^*(\tau), \quad \tau \in [-1\ 1] \tag{8}$$

where V_i^* is $\prod_{j=1, j\neq i}^{N} \frac{\tau - \tau_j}{\tau_i - \tau_j}$, $i = 1, 2, ..., N$. Time derivative of (7) is expressed as

$$\dot{x}(\tau) \approx \dot{X}(\tau) \tag{9}$$

The derivative of each Lagrange polynomial at the Legendre-Gauss points in a differential approximation matrix, $D \in \Re^{N\times(N+1)}$ are given as

$$D_{ki}(\tau) = \dot{V}_i(\tau_k) = \sum_{l=0}^{N} \frac{\prod_{j=0,j\neq i,k}^{N} \tau_k - \tau_i}{\prod_{j=0,j\neq i,k}^{N} \tau_i - \tau_i} \quad k = 1, 2, ..., N,\ i = 0, 1, 2...., N \tag{10}$$

The dynamic constraints $\dot{x}(\tau)$ are translated into algebraic constraints by $D_{ki}(\tau)$.

$$\sum_{l=0}^{N} D_{ki} X_i - \frac{t_f - t_o}{2} f(X_k, U_k, \tau_k; t_o, t_f) = 0, \quad k = 1, 2, ..., N \tag{11}$$

A continuous cost function using Gaussian quadrature is given as

$$J = \Phi[x_{t_o}, t_o, x_{t_f}, t_f] + \frac{t_f - t_o}{2} \sum_{k=1}^{N} G_k \cdot g(X_k, U_k, \tau_k; t_o, t_f) \tag{12}$$

where G_k are the Gaussian weights and the boundary constraint is denoted as

$$\Phi(X_o, t_o, X_f, t_f) = 0 \tag{13}$$

Furthermore, the path constraints at the Legendre-Gauss points are written as

$$C(X_k, U_k, t_k; t_o, t_f) \leq 0 \quad k = 1, 2, ..., N \tag{14}$$

The transformed problem is defined by Eqs. (11, 12, 13, 14), and its solution is the approximate solution of the original optimum problem from t_o to t_f.